From the Institute of Neuro- and Sensory Physiology
at Heinrich Heine University Düsseldorf

# Independent Modulation of AMPA Receptors by PORCN and Wnt: Dissecting Molecular Mechanisms and Functional Implications

Dissertation
to obtain the academic title of Doctor rerum medicarum (Dr. rer. med.)
from the Faculty of Medicine at Heinrich Heine University Düsseldorf

Submitted by
Naomi Mölders
2025

As an inaugural dissertation printed by permission of the Faculty of Medicine at Heinrich Heine University Düsseldorf

signed:
Dean: Prof. Dr. med. Nikolaj Klöcker
Examiners: Jun.-Prof. Dr. rer. nat. Nadine Erlenhardt
Prof. Dr. phil. Patrick Küry

To Max,

None of this would have been possible without you.

## Zusammenfassung

Ionotrope Glutamatrezeptoren vom AMPA-Subtyp (AMPARs) sind hauptverantwortlich für die exzitatorische Neurotransmission im zentralen Nervensystem. AMPAR-Multiproteinkomplexe bestehen aus vier porenbildenden Untereinheiten sowie teilweise transient assoziierten Hilfsproteinen. Zu diesen assoziierten Proteinen zählt die Protein-Serin-O-Palmitoleoyltransferase Porcupine (PORCN). PORCN ist ein multifunktionales Protein, das neben seiner Rolle bei der Biogenese von AMPARs im endoplasmatischen Retikulum (ER) auch eine kanonische Funktion bei der Palmitoylierung von Wnt-Proteinen im ER erfüllt. Frühere Arbeiten der Forschungsgruppe identifizierten zudem Wnt als einen neuartigen, von PORCN unabhängigen Interaktionspartner von AMPARs.

Ziel der vorliegenden Studie war es, die molekularen und funktionellen Zusammenhänge zwischen AMPARs, PORCN und Wnt aufzuklären. Untersucht wurden sowohl die Regulationsmechanismen, die die multifunktionale Rolle von PORCN modulieren, als auch die strukturellen Domänen, die die Interaktion mit AMPARs vermitteln. Zusätzlich wurde die molekulare Basis der Wnt-AMPAR-Interaktionen untersucht. Ein multidisziplinärer Ansatz kombinierte Methoden der Molekular- und Zellbiologie, immunfluoreszenzbasierte Analysen, Biochemie und Elektrophysiologie in heterologen Expressionssystemen und in primären murinen Hippocampusneuronen.

Es konnte gezeigt werden, dass bereits der Austausch einer einzelnen Aminosäure in PORCN (Serin zu Asparaginsäure an Position 297) ausreichte, um die AMPAR-Funktion zu beeinträchtigen und die dendritische Komplexität zu reduzieren, ohne die Protein-Protein-Interaktionen zu verändern. Dieses Ergebnis unterstreicht die Bedeutung spezifischer struktureller Merkmale und posttranslationaler Modifikationen für die Regulation der multifunktionellen Eigenschaften von PORCN. Der Vergleich der AMPAR-regulierenden Funktion von PORCN über verschiedene Spezies hinweg zeigte, dass diese zwischen Vertebraten und Invertebraten erhalten geblieben ist.

In HeLa-Zellen reduzierte Wnt5a die GluA1-Menge im ER, während dieser Effekt in primären hippocampalen Neuronen nicht beobachtet wurde. Stattdessen korrelierte die Akkumulation von Wnt5a im ER mit erhöhten GluA1-Leveln in Membranfraktionen, was auf eine direkte regulatorische Wirkung von Wnt auf AMPARs hinweist.

Zusammenfassend unterstreichen diese Ergebnisse die hohe Sensitivität von AMPARs gegenüber fein abgestimmter Regulation durch assoziierte Proteine und betonen die Notwendigkeit weiterführender Untersuchungen zur strukturellen Topologie von PORCN sowie zu den Mechanismen der Wnt-vermittelten Modulation von AMPARs in unterschiedlichen zellulären Kontexten.

## Summary

Ionotropic glutamate receptors of the AMPA subtype (AMPARs) are key mediators of excitatory neurotransmission. They assemble into multiprotein complexes composed of four pore-forming subunits and various associated proteins that interact with the receptor to modulate its function. Among these associated proteins is the protein-serine O-palmitoleoyltransferase Porcupine (PORCN), a multifunctional protein. In addition to supporting AMPAR biogenesis in the endoplasmic reticulum (ER), PORCN also performs a canonical enzymatic role in the palmitoylation of Wnt proteins. Previous work from the research group further identified Wnt as a novel, PORCN-independent interaction partner of AMPARs.

The present study aimed to elucidate the molecular and functional relationships between AMPARs, PORCN and Wnt. Specifically, the regulatory mechanisms underlying PORCN's multifunctionality and the structural domains mediating its interaction with AMPARs were examined, alongside the molecular basis of Wnt-AMPAR interactions. To address these objectives, a multidisciplinary approach was employed, integrating molecular and cell biology, advanced imaging, biochemistry and electrophysiology in both heterologous expression systems and primary murine hippocampal neurons.

A single amino acid substitution in PORCN (serine to aspartic acid at position 297) was sufficient to impair AMPAR function and reduce dendritic complexity without affecting protein–protein interactions. This finding highlights the importance of specific structural features and post-translational modifications in regulating PORCN's multifunctionality. Comparative analysis across species showed that PORCN's AMPAR-regulating function is evolutionarily conserved between vertebrates and invertebrates.

Moreover, Wnt5a reduced GluA1 levels in the ER of HeLa cells, whereas this effect was not observed in primary hippocampal neurons. In these neurons, ER-accumulation of Wnt5a correlated with increased amounts of GluA1 in membrane fractions, indicating a direct regulatory interaction between AMPARs and Wnt.

In summary, these results underscore the sensitivity of AMPARs to fine-tuned regulation by associated proteins and emphasize the need for further investigation into PORCN's structural topology and the mechanisms underlying Wnt-mediated modulation of AMPARs across diverse cellular contexts.

## List of abbreviations

Throughout the text, the standard abbreviations for amino acids are used with one letter according to the IUPAC conventions.

| | |
|---|---|
| Aβ | β-amyloid |
| ABHD6 | α/β-hydrolase domain-containing protein 6 |
| AHP | Adult hippocampal progenitor |
| AMPAR | α-Amino-3-hydroxy-5-methyl-4-isoxazole propionic acid receptor |
| ANOVA | Analysis of variance |
| APS | Ammonium persulfate |
| Ara-C | Cytosin β-D-Arabinofuranosid -hydrochlorid |
| ATD | Amino-terminal domain |
| bp | Base pairs |
| CaMKII | Calcium/calmodulin-dependent kinase II |
| cel | Caenorhabditis elegans |
| CNIH | Cornichon |
| co-IP | Co-immunoprecipitation |
| CPT1c | Carnitine palmitoyltransferase 1c |
| CTD | Carboxyl-terminal domain |
| DIV | Days in vitro |
| DKK-1 | Dickkopf-1 |
| dro | Drosophila melanogaster |
| DMEM | Dulbecco’s modified eagle medium |
| DMSO | Dimethyl sulfoxide |
| DNA | Deoxyribonucleic acid |
| dNTP | Deoxynucleotide triphosphates |
| DPBS | Dulbecco's phosphate-buffered solution |
| DTT | Diethiothreitol |
| EDTA | Ethylenediaminetetraacetic acid |
| EPSP | Excitatory postsynaptic potential |
| ER | Endoplasmic reticulum |
| Fig. | Figure |
| FBS/FCS | Fetal bovine serum/fetal calf serum |
| FDH | Focal dermal hypoplasia |
| FRRS1l | Ferric chelate reductase 1-like protein |
| fwd | Forward (primer) |
| Fzd | Frizzled receptor |
| GFP | Green fluorescent protein |
| GluA1 | Glutamate receptor ionotropic, AMPAR 1 |
| GluA2 | Glutamate receptor ionotropic, AMPAR 2 |
| GluK2 | Glutamate receptor ionotropic, kainate 2 |
| GluN1 | Glutamate receptor ionotropic, NMDAR 1 |
| GluN2 | Glutamate receptor ionotropic, NMDAR 2 |
| GSG1L | Germ cell-specific gene 1-like |
| h | Human |
| HBSS | Hank’s balanced salt solution |
| HCL | Hydrochloric acid |
| HCN2 | Hyperpolarization-activated cyclic nucleotide-gated channel 2 |
| HRP | Horseredish peroxidase |
| HS | Horse serum |
| IAA | Iodoacetamide |
| IF | Immunofluorescence |
| JNK | C-Jun N-terminal kinase |
| kDa | Kilodalton |
| Knockdown | KD |
| Knockout | KO |

| | |
|---|---|
| LBD | Ligand binding domain |
| LTD | Long term depression |
| LTP | Long term potentiation |
| m | Mouse |
| MBOAT | Membrane-bound O-acyltransferases |
| mEPSC | Miniature excitatory postsynaptic current |
| min | Minute(s) |
| NGS | Normal goat serum |
| NMDAR | N-methyl-D-aspartate receptor |
| P/S | Penicillin and streptomycin |
| PBS | Phosphate buffered saline |
| PCP | Planar cell polarity |
| PCR | Polymerase chain reaction |
| PDB | Protein data bank |
| PFA | Paraformaldehyde |
| PI-Mix | Protease inhibitor mix |
| PKC | Protein kinase C |
| PORCN | Porcupine |
| PTM | Post translational modifications |
| r | Rat |
| rb | Rabbit |
| Rac1 | Ras-related C3 botulinum toxin substrate 1 |
| rev | Reverse (primer) |
| RhoA | Ras homolog family member A |
| RM | Repeated measures |
| RNA | Ribonucleic acid |
| ROCK | RHO-associated coiled-coil-containing protein kinase 1 |
| S2 | Biosafety level 2 |
| SDS | Sodium dodecyl sulfate |
| sec | Second(s) |
| SEM | Standard error of the mean |
| Tab. | Table |
| TARP | Transmembrane AMPAR regulatory protein |
| TBS-T | Tris-buffered saline with Tween 20 |
| TCF | T-cell factor |
| TMD | Transmembrane domains |
| TRIS | Tris(hydroxymethyl)aminomethane |
| Wls | Wntless |
| WT | Wild type |

List of figures

List of tables

# 1 Introduction

## 1.1 AMPA Receptors

### 1.1.1 Structural Organization and Function of AMPA Receptors

In the mammalian central nervous system, fast excitatory synaptic transmission is primarily mediated by ionotropic glutamate receptors located in the postsynaptic membrane [1, 2]. These receptors are classified into three main types named after their respective agonists: α-amino-3-hydroxy-5-methyl-4-isoxazole propionic acid receptors (AMPARs), N-methyl-D-aspartate receptors (NMDARs) and kainate receptors [3, 4]. Among these, AMPARs play a crucial role due to their rapid activation kinetics, dynamic regulatory mechanisms and essential involvement in synaptic plasticity. These functions are shaped by adaptation of AMPAR synthesis, subunit assembly, auxiliary proteins, post translational modifications (PTMs) and subcellular trafficking [5-7]. Additionally, dysfunction of AMPAR complexes has been implicated in a range of neurological and psychiatric disorders, including Alzheimer's disease, Parkinson's disease, epilepsy and schizophrenia [8-10].

AMPARs are assembled from the pore-forming subunits GluA1 to GluA4, which initially form dimers that subsequently organize as dimers-of-dimers to generate functional homo- or heterotetrameric receptors required for physiological ion conduction [1, 10] (Figure 1B). The pore-forming AMPAR subunits differ in their kinetic properties and in their contribution to glutamate affinity and $Ca^{2+}$ permeability, thereby heteromerization further increases the functional diversity of these receptors [10, 11]. Each subunit consists of four major domains: an extracellular amino-terminal domain (ATD), an extracellular ligand-binding domain (LBD), transmembrane domains (TMDs) and an intracellular carboxyl-terminal domain (CTD) [10, 11] (Figure 1). The LBD is formed by two discontinuous segments, S1 and S2 [12]. The TMDs consist of three transmembrane segments (M1, M3, M4) and a re-entrant loop (M2), which forms the ion-conducting pore [13] (Figure 1A). AMPA receptor signaling is initiated by conformational changes in the LBD upon glutamate binding [10]. This induces a transition from the inactive resting state to an active, non-desensitized state, during which the ion channel opens, allowing the influx of sodium and calcium ions and the efflux of potassium [14]. The resulting ion flux induces an excitatory postsynaptic potential (EPSP). Due to the limited binding energy provided by glutamate, the active state is transient and the receptor quickly transitions into a desensitized state, wherein the LBD rearranges to prevent channel opening despite continued ligand presence [14].

The functional variability of AMPARs is further shaped by alternative splicing, mRNA editing, and PTMs like phosphorylation, which regulate synaptic plasticity, gating kinetics, subunit assembly and intracellular trafficking [15-19].

By alternative splicing of exon 14 and 15, two isoforms of the AMPAR LBD – flip and flop – occur [20] (Figure 1A). These isoforms of the AMPAR subunits differ in receptor function, particularly in properties such as desensitization and deactivation [10, 16, 21, 22]. Additional

functional diversity is provided by mRNA processing at the Q/R and R/G sites (Figure 1A). RNA editing at the Q/R site of the GluA2 subunit, which results in the substitution of glutamine (Q) with arginine (R), renders the subunit impermeable to $Ca^{2+}$ [15, 23]. Furthermore, Q/R editing also affects the endoplasmic reticulum (ER) exit of the GluA2 subunit and regulates AMPAR assembly [24].

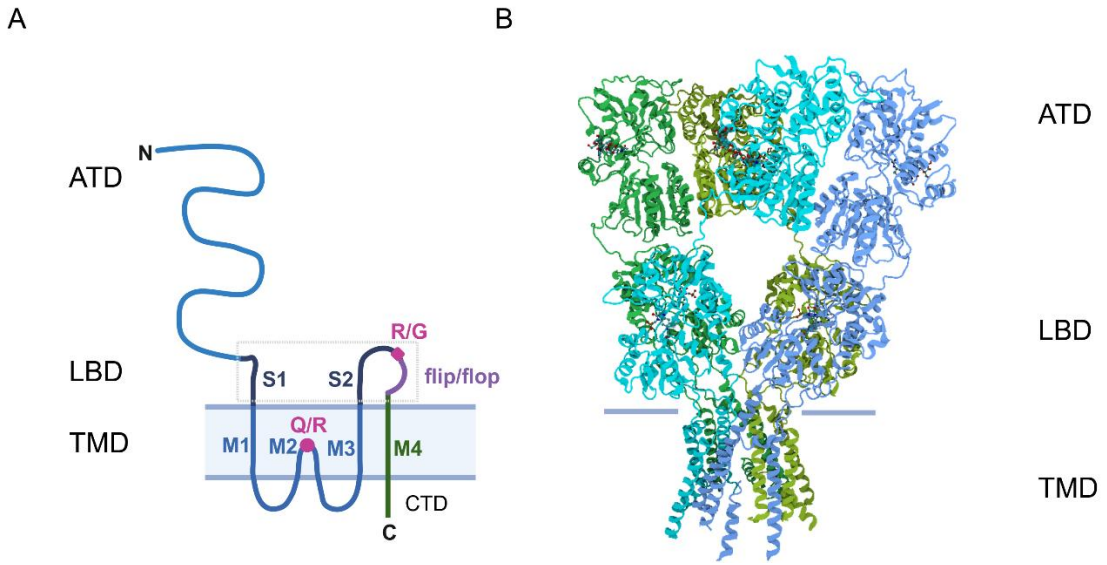


**Figure 1: Schematic and crystal structure of AMPAR.**
**A:** Schematic representation of a single AMPAR subunit. The subunit consists of an amino-terminal domain (ATD), a ligand-binding domain (LBD), transmembrane domains (TMD) and an intracellular carboxyl-terminal domain (CTD). The LBD is composed of two discontinuous segments, S1 and S2. The TMD comprises three transmembrane segments and a re-entrant pore loop (M2). Sites of mRNA editing and alternative splicing (Q/R site, R/G site, and flip/flop) are also indicated in the diagram. **B:** Crystal structure of a GluA2 homomeric AMPAR (PDB Code 3KG2). The four subunits are shown in different colors.
Illustration based on Greger at al. 2017 and created in BioRender.com by N. Mölders.
AMPAR = AMPA receptor; G = Glycine; M = Membrane segment; PDB = Protein data bank; Q = Glutamine; R = Arginine; S = Segment within the LBD.

Beyond these molecular modifications, the specific assembly of receptor subunits varies between cell types, brain regions and neuronal circuits. In the adult rat brain, GluA1 and GluA2 are the predominant subunits in the hippocampus [25]. In contrast, the cortex and striatum primarily express GluA2 followed by GluA1 and GluA3 [25]. Meanwhile, in the cerebellum and brainstem, GluA4 is the main subunit found, forming either GluA1/GluA4 heteromers or GluA4 homomers [25]. The function of the pore-forming AMPAR complexes is supported and expanded by a variety of auxiliary proteins.

### 1.1.2 Auxiliary and Associated Proteins in AMPAR Assembly and Function

A variety of auxiliary proteins are essential for the efficient biogenesis, trafficking and functional modulation of AMPARs [4, 26]. These proteins contribute significantly to the receptor's assembly within the ER, define subtype-specific properties and support receptor transport to the postsynaptic membrane, where they transiently participate in synaptic

transmission [26]. Given the broad range of AMPAR auxiliary and associated proteins, the following section will provide an overview of selected representatives with particular relevance to receptor assembly and synaptic function.

Within the ER, proteins such as ferric chelate reductase 1-like protein (FRRS1l), carnitine palmitoyltransferase 1c (CPT1c), α/β-hydrolase domain-containing protein 6 (ABHD6) and Porcupine (PORCN) contribute to the five-step assembly of AMPARs in the ER [27, 28]. In the first step, ABHD6 associates with GluA monomers, protecting them from ER-associated degradation and preventing their premature dimerization [28, 29]. These functions may also be carried out by PORCN, which could either replace or act in concert with ABHD6 [28]. Subsequently, ABHD6-bound GluA subunits interact with the FRRS1l–CPT1c complex, leading to the dissociation of ABHD6 and the formation of GluA–FRRS1l–CPT1c dimers [30]. Two such dimers then assemble to a GluA tetramer. After tetramer formation, FRRS1l and CPT1c dissociate from the complex and are replaced by cornichon homologs (CNIHs) and transmembrane AMPA receptor regulatory proteins (TARPs) [28, 30]. These auxiliary subunits are essential for the maturation of a fully functional AMPAR complex that is capable of leaving the ER [28]. In the final step, the assembled AMPAR complex is packaged into transport vesicles and shuttled to the cell membrane. Notably, CNIHs and TARPs remain associated with AMPARs at the plasma membrane, where they regulate receptor function [30].

The TARPs belong to the calcium channel γ subunit family and are well-characterized auxiliary subunits of AMPA receptors [31]. Based on sequence homology and functional properties, TARPs are classified into type I (including γ2 [Stargazin], γ3, γ4, and γ8) and type II (γ5 and γ7) [32]. The classification mirrors their differential expression across brain regions and developmental stages [33]. Given their broad regulatory influence on AMPAR function and trafficking, TARPs are emerging as critical modulators of both physiological synaptic signaling and pathological processes, including those implicated in neurodevelopmental and neurodegenerative disorders [31]. For example, TARPγ8 modulates AMPAR function by anchoring AMPARs at the postsynaptic membrane and acting as a transporter that regulates their surface expression levels [34]. In *Tarpγ8* knockout (KO) mice, AMPAR expression is decreased [34].

The protein CNIH2 was identified through proteomic analyses as an auxiliary subunit of AMPA receptors [35]. CNIHs are essential for AMPAR trafficking and kinetics [36]. AMPAR surface levels are increased by CNIHs in both cultured cells and *Xenopus* oocytes [35]. By slowing AMPAR deactivation and desensitization, CNIHs influence excitatory glutamate-mediated neurotransmission [35, 37]. Loss of CNIH2 reduces AMPAR-mediated miniature excitatory postsynaptic current (mEPSC) amplitudes and accelerates deactivation and desensitization kinetics [38]. In addition, CNIH2 regulates the composition of the AMPAR complex in conjunction with TARPγ8 and is incorporated into the receptor complex only in

the presence of TARPγ8 [39, 40]. Both CNIH2 and CNIH3 interact with the LBD and TMD of AMPARs [41].

The Germ Cell-Specific Gene 1-Like protein (GSG1L) belongs to the tetraspanin superfamily, similar to the TARPs [42]. In contrast to TARPs, GSG1L slows AMPAR recovery from desensitization, thereby limiting the ability of associated receptors to respond to high-frequency synaptic transmission [42]. Overexpression of GSG1L reduces both amplitude and frequency of AMPAR-mediated mEPSCs and impairs AMPAR trafficking to the plasma membrane in neurons [43]. The Loop1 domain of GSG1L is essential for the modulation of AMPAR function [43].

While several AMPAR-associated proteins, such as the TARPs, are well characterized, others - like PORCN - remain less understood. Further research is needed to elucidate how these less-characterized proteins contribute to the structural diversity and dynamic regulation of AMPAR complexes and how they may influence synaptic plasticity under both physiological and pathological conditions.

## 1.2 Porcupine

### 1.2.1 Structure and Function of PORCN

The multifunctional protein PORCN is a member of the membrane-bound O-acyltransferases (MBOATs) family [44-46]. MBOATs can be classified into two distinct groups: those that acylate small-molecule acceptors and those that acylate proteins [47]. PORCN belongs to the latter group of protein-acylating MBOATs, along with the Hedgehog acyltransferase and the ghrelin O-acyltransferase [48-50]. Due to alternative splicing, four isoforms of PORCN (A–D) have been described, all of which localize in the ER [51, 52]. Among these, isoform D is predominantly expressed in the brain, reflecting a tissue-specific expression pattern [51, 52]. Based on sequence analysis and a manually curated annotation according to UniProt (entry number: Q9H237), PORCN is predicted to contain eight TMDs, with both N- and C-termini facing the cytosol. The catalytically active site is located within the seventh TMD (Figure 2). But the membrane topology of PORCN has been subject of ongoing discussion, particularly with regard to the orientation of the N-terminus - whether it resides in the ER lumen or the cytoplasm - as well as the organization and length of the loops [53, 54] (Figure 2). The active site contains a conserved histidine residue (H341 in human PORCN isoform D), which plays a pivotal role in enzymatic activity [55].

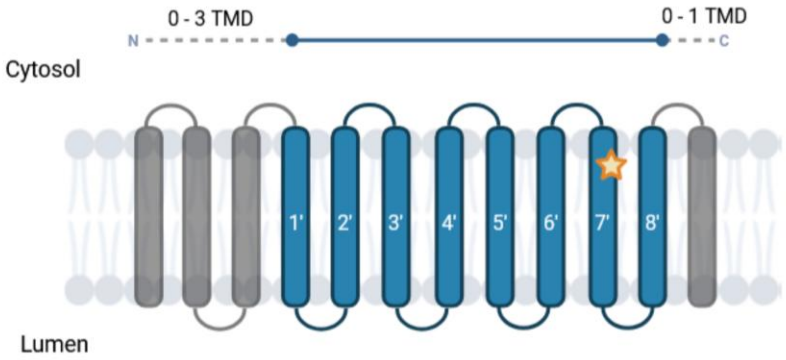


**Figure 2: Schematic representation of PORCN topology.**
The topology of PORCN remains incompletely resolved, with reports describing eight to eleven TMDs. The presented topology is derived from sequence-based predictions and reflects a manual assertion provided by UniProt (blue; entry number: Q9H237), along with possible variations in the number of TMDs and the orientation of the N- and C-termini (grey). The star marks the location of the proposed catalytic center. For clarity, potential re-entrant loops are not depicted.
Illustration based on Coupland et al. 2023 and created in BioRender.com by N. Mölders.
TMD = Transmembrane domain.

PORCN is characterized by its multifunctionality. It was initially identified as a key factor in the post-translational processing of Wnt proteins [44]. PORCN catalyzes the palmitoylation of Wnt within the ER, a modification that enables Wnt to leave the ER and to get subsequently transported along the secretory pathway [55-57]. Independent from its enzymatic function, PORCN also fulfils distinct moonlighting functions. The multifunctionality of PORCN is further underscored by its discrete role in tumorigenesis, evidenced by the growth inhibition of epithelial cancer cell lines upon PORCN knockdown (KD) [58]. In addition, proteomic analyses identified PORCN as an AMPAR-interacting protein restricted to the ER, indicating that it does not associate with surface-expressed AMPAR complexes [26, 27].

### 1.2.2 The Role of PORCN in AMPAR Physiology

Independent of its canonical function in Wnt signaling, PORCN has been identified as a moonlighting protein involved in the regulation of AMPAR physiology [28, 59]. Functional KD of PORCN in rat hippocampal neurons revealed a critical role in maintaining AMPAR complex stability [59]. Its absence results in destabilization of the AMPAR complex, characterized by a depletion of the auxiliary subunit TARPγ8 from the AMPAR complexes and a marked decrease in both total and surface-expression of AMPARs [59]. In addition, PORCN KD leads to a significant reduction in AMPAR-mediated synaptic currents and an acceleration of receptor desensitization kinetics [59]. Complementary electrophysiological analyses of HEK293T cells demonstrated that PORCN attenuates glutamate-induced currents mediated via GluA1-containing AMPARs, without affecting GluK2-mediated currents [59]. PORCN exerts an inhibitory effect on AMPAR function that appears to be independent of the receptor's subunit composition [60]. While accumulating evidence

indicates a regulatory function of PORCN in AMPAR physiology, the exact molecular mechanisms through which this modulation occurs have yet to be fully characterized. Biochemical analyses excluded both the N- and C-termini of the receptor as interaction sites, implicating either the LBD or TMD as the most likely domains mediating the interaction [60]. Nevertheless, the regulation of PORCN's multifunctionality remains poorly understood.

### 1.2.3 Medical Significance of PORCN

An X-linked mutation in the *PORCN* gene is associated with focal dermal hypoplasia (FDH), also known as Goltz syndrome [61]. This loss-of-function mutation abolishes the enzymatic activity of PORCN as an O-acyltransferase, thereby disrupting Wnt signaling - a pathway essential for embryonic development and adult tissue homeostasis [46]. In male embryos, the mutation is typically lethal, whereas affected females commonly exhibit severe abnormalities [46]. The phenotypic spectrum includes skin abnormalities, malformations of the skeletal system, ocular anomalies and craniofacial dysmorphisms [62]. Additionally, FDH has been reported to occur with neurological manifestations, including epilepsy, developmental delay, intellectual disability and microcephaly [63-65]. Neurological abnormalities are a rarely diagnosed but documented feature of the highly variable clinical presentation of FDH. Nevertheless, the literature highlights the importance of thorough neurological evaluation in patients affected by the disease [64].

## 1.3 Wnt

### 1.3.1 Wnt Signaling Pathways

Wnt proteins were first identified in *Drosophila* and have since been implicated in a wide range of cellular processes during development [66]. In humans, 19 Wnt ligands have been described, interacting with various transmembrane receptors, most notably members of the Frizzled (Fzd) receptor family [67]. PORCN is essential for the acylation of Wnt in the ER, a modification required for their interaction with the cargo transporter Wntless (Wls). Wls facilitates the transport of Wnt ligands to the cell surface and promotes their efficient binding to Fzd receptors [68]. Following post-translational processing in the Golgi apparatus, Wnt ligands are secreted and activate both canonical and non-canonical intracellular signaling pathways [69].

The canonical or β-catenin-dependent, pathway relies on the stabilization and nuclear translocation of β-catenin, which interacts with the T-cell factor (TCF) family of transcription factors to regulate Wnt target gene expression [69]. Non-canonical Wnt signaling comprises primarily the planar cell polarity (PCP) pathway and the Wnt/calcium pathway. In the Wnt/PCP pathway, activation of Ras homolog family member A (RhoA) and Ras-related C3 botulinum toxin substrate 1 (Rac1) leads to stimulation of stress-activated protein kinases such as c-Jun N-terminal kinase (JNK) and RHO-associated coiled-coil-containing protein kinase 1 (ROCK), resulting in cytoskeletal reorganization and alterations in cell adhesion

and motility [67, 70]. In the Wnt/calcium pathway, heterotrimeric G proteins and phospholipases mediate an increase in intracellular calcium, which in turn activates protein kinase C (PKC), calcium/calmodulin-dependent kinase II (CaMKII) and the phosphatase calcineurin [70-72]. Wnt proteins are also modified by N-linked glycosylation, which can enhance their stability and solubility depending on the specific ligand [73]. For Wnt3a and Wnt5a, glycosylation is important for secretion but does not influence Wnt signaling efficiency [74, 75].

Dysregulation of the Wnt signaling pathway is associated with a wide spectrum of endocrine, metabolic, inflammatory and neurodegenerative disorders, as well as oncogenic transformation [76-78]. In this context, inhibition of PORCN-mediated Wnt ligand acylation has emerged as a promising strategy in cancer research. One such inhibitor, Wnt-C59 (2-(4-(2-methylpyridin-4-yl)phenyl)-N-(4-(pyridin-3-yl)phenyl)acetamide), is known to inhibit all murine PORCN isoforms [79].

### 1.3.2 Wnt in Synaptic Function

In addition to its role in various developmental and homeostatic processes, Wnt signaling also plays a crucial role in neurophysiological functions such as synaptic differentiation and synaptic plasticity. Inhibition of Wnt signaling by the PORCN inhibitor Wnt-C59 impairs neurite outgrowth, an effect that can be rescued by the extracellular application of recombinant Wnt3a, Wnt5a and Wnt7a [67, 80]. Wnt7a/b and Wnt3a have been shown to promote the formation of presynaptic sites and to enhance the pool of recycling synaptic vesicles [81, 82]. Furthermore, Wnt7a is capable of modulating dendritic spine growth and synaptic strength [83]. Wnt7a, along with the postsynaptic Frizzled-7 receptor (Fz7), has been shown to regulate AMPAR localization and function [84]. Loss of Wnt7a or Fz7 impairs LTP-dependent synaptic potentiation and dendritic spine growth, accompanied by disrupted AMPAR distribution at synaptic sites [84]. Another Wnt ligand, Wnt5a, regulates the distribution of PSD-95 and thereby influences the organization of the postsynaptic compartment via the Wnt5a/JNK signaling cascade [85]. Wnt5a is also known to promote the differentiation and maturation of adult hippocampal neurons, as its KD impairs dendritic development in adult mice [86, 87]. The presence of Wnt5a is essential for the neuronal differentiation of adult hippocampal progenitor (AHP) cells and for the neurogenic potential of AHP-derived cells *in vivo* [87]. Wnt5a has been shown to potentiate excitatory synaptic transmission by increasing the mEPSC amplitude of both AMPAR- and NMDAR-mediated responses, with a notably stronger modulatory effect on NMDAR function in cultured hippocampal neurons [88]. Previous work from the working group identified Wnt as a novel AMPAR-interacting partner. Independent from its established interaction with PORCN, Wnt5a reduced total and surface expression of AMPARs in heterologous cell culture.

## 1.4 Research Objectives

Reflecting its multifunctionality, PORCN functions both as an essential acyltransferase for Wnt modification in the ER and, independently of Wnt signaling, as an auxiliary factor that regulates AMPAR stability and trafficking. Recent findings indicate that Wnt may directly interact with AMPARs, yet the functional significance of this potential interaction has not been elucidated.

This study aims to dissect the molecular and functional relationship between AMPARs, PORCN and Wnt. To this end, the following research questions will be examined:

- How is the multifunctionality of PORCN functionally regulated?
- Which domains of PORCN mediate its interaction with AMPARs?
- How does Wnt interact with AMPARs at the molecular level?

To address the research questions, the study will investigate the influence of possible phosphorylation sites in PORCN on dendritic architecture and subsequently examine how these changes affect synaptic transmission and subcellular localization. Disease-associated and region-specific mutations will be analyzed to uncover potential structure-function relationships. The role of PORCN's enzymatic activity on AMPARs will be evaluated, before extending the analysis to PORCN's evolutionary conservation. Additionally, the independent interaction of AMPARs with Wnt ligands will be examined.

A multidisciplinary approach will be employed, combining molecular biology (cloning and site-directed mutagenesis), cell biology (surface expression assay and morphological reconstruction), imaging (fluorescence and confocal laser scanning microscopy), biochemistry (membrane preparation and co-immunoprecipitation (co-IP)), and electrophysiology (patch-clamp recordings) in heterologous expression systems and primary murine hippocampal neurons.

# 2 Materials and Methods

## 2.1 Materials

All consumables were sourced from the companies Greiner Bio-One (Frickenhausen, Germany), Eppendorf (Hamburg, Germany), Sigma-Aldrich (via Merck, Darmstadt, Germany), Starlab (Hamburg, Germany), VWR (Darmstadt, Germany) and Thermo Fisher Scientific (Schwerte, Germany). Exceptions will be specified separately.

### 2.1.1 Chemicals and Reagents

**Table 1: List of chemicals and reagents used.**

| Name | Company and Catalog No. |
|---|---|
| 30% Acrylamide/Bis Solution 37.5:1 | Bio-Rad 1610158 |
| Agar-agar | Roth 2266.2 |
| Agarose | Invitrogen 16500-500 |
| 6-Aminohexanoic acid | Sigma-Aldrich 07260 |
| Ampicillin | Sigma-Aldrich A0166 |
| Amphotericin B | Gibco 15290026 |
| Ampuwa® | Fresenius Kabi 1080181 |
| Aprotinin | Roth A162.2 |
| Ammonium persulfate | Sigma-Aldrich A3678 |
| Ara-C | Sigma-Aldrich C6645 |
| B-27® Supplement | Gibco 17504044 |
| Bacto™ Tryptone | Gibco 211705 |
| Boric acid | Sigma-Aldrich B0394 |
| Bromphenol blue | Sigma-Aldrich 114405 |
| Chymotrypsin | Sigma-Aldrich C4129 |
| Dimethyl pimelidat dihydrochloride | Sigma-Aldrich D8388 |
| DMEM (1x) | Gibco 41966029 |
| DMEM (1x) + GlutaMax™ | Gibco 10566016 |
| DMSO | Invitrogen D12345 |
| n-Dodecanoylsucrose | Millipore 324374 |
| DPBS | Gibco 14190094 |
| DTT | AppliChem A1101.0025 |
| EDTA | Roth 8040.2 |
| Ethanol 70% | Technisolv 85825.360 |

| | |
|---|---|
| Ethanol absolut | VWR 20821.330 |
| Ethanolamine hydrochloride | Sigma-Aldrich E6133 |
| FastDigest Green Buffer (10x) | Thermo Scientific B72 |
| FBS Superior | Sigma-Aldrich S0615 |
| FuGENE® HD Transfection Reagent | Promega E2312 |
| Glycerin | Sigma-Aldrich G2025 |
| Glycine | Roth 3908,3 |
| HBSS (10x) | Gibco 14185045 |
| HEPES Buffer Solution (1M) | Gibco 15630056 |
| HI Horse Serum | Gibco 26050088 |
| Iodoacetamide | Sigma-Aldrich I6125 |
| Isoflurane | Piramal 09714675 |
| Kohrsolin® FF | Hartmann 9804314 |
| Korsolex® med AF | Roth KY66.1 |
| Leupeptin | Roth CN33.1 |
| Lipofectamine™ 2000 Reagent | Invitrogen 100014469 |
| MEM (1x) + GlutaMAX™ | Gibco 41090036 |
| Neurobasal® Medium (1x) | Gibco 12348017 |
| Normal Goat Serum | Biowest S2000 |
| Opti-MEM® I (1x) | Gibco 31985047 |
| Paraffin | Merck 1.07158.1000 |
| Paraformaldehyde | Sigma-Aldrich 441244 |
| Penicillin Streptomycin | Gibco 15140122 |
| Pepstatin A | Roth 2936.2 |
| Phenylmethylsulfonyl fluoride | Roth 6367.3 |
| Phusion HF Buffer (5x) | Thermo Scientific F-518 |
| Poly-D-lysine hydrobromide | Sigma-Aldrich P7886 |
| Polyethylenimine, Linear | Polysciences 23966100 |
| Potassium chloride | Roth HN02.3 |
| Potassium hydrogen phosphate | Roth 60220 |
| 2-Propanol | GPR Rectapur 20839.297 |

| | |
|---|---|
| Recovery™ Cell Culture Freezing Medium | Gibco 12648-010 |
| ROTIPHORESE®50x TAE Buffer | Roth CL86.1 |
| SDS | Roth 2326,2 |
| Skim Milk Powder | Sigma-Aldrich 70166 |
| Sodium chloride | Roth 3957.1 |
| Sodium dihydrogen phosphate | Roth 2370.3 |
| di-Sodium hydrogen phosphate anhydrous | Roth P030.1 |
| Sodium hydroxide solution | Roth K021.1 |
| Sodium pyruvate 100 mM (100x) | Gibco 11360039 |
| Sodium tetraborate decahydrate | Sigma-Aldrich B9876 |
| Sucrose | AppliChem A3935 |
| Restore™ PLUS Western Blot Stripping Buffer | Thermo Scientific 46430 |
| T4 DNA Ligase Buffer (10x) | Thermo Scientific B69 |
| TEMED | Roth 2367.1 |
| Tricine | Sigma-Aldrich T0377 |
| TRIS Base | Sigma-Aldrich T1503 |
| TRIS HCl | Sigma-Aldrich T5941 |
| Triton™ X-100 | Sigma-Aldrich T8787 |
| Trypan Blue | Sigma-Aldrich T8154 |
| 0.25% Trypsin (1x) | Gibco 25050014 |
| 2.5% Trypsin (10x) | Gibco 15090046 |
| Tween® 20 | Sigma-Aldrich P7949 |
| Water sterile | Sigma-Aldrich W3500 |
| Wnt-C59 | Tocris 5148 |
| Yeast Extract | Roth 2363.2 |

### 2.1.2 Buffers and Solutions

The buffers and solutions used are listed in table 2. Unless otherwise indicated, dilutions of stock solutions were prepared using deionised water.

**Table 2: List and composition of the buffers and solutions used.**

| Purpose | (Stock) solutions | Composition |
|---|---|---|
| | 10x PBS; pH 7.4 | 137 mM Sodium chloride<br>27 mM Potassium chloride<br>80 mM Sodium dihydrogen phosphate<br>15 mM Potassium hydrogen phosphate |
| **Primary Cell Culture** | Borate Buffer; filtrated; pH 8.4 | 50 mM Boric acid<br>12,45 mM Sodium tetraborate decahydrate |
| | HBSS solution; pH 7,3 | 1x HBSS<br>1 mM Hepes |
| | PDL Stock Solution; filtrated | 10 mg/ml PDL in Borat buffer |
| **Protein analysis** | 10x TBS-T; pH 7.6 | 200 mM TRIS Base<br>137 mM Sodium chloride<br>1% Tween® 20 |
| | 5x Laemmli buffer | 312.5 mM TRIS HCl<br>10% SDS<br>0.05% Bromphenol blue<br>50% Glycerin |
| | 4x Separating gel buffer; pH 8.8 | 1.5 M TRIS HCl<br>0.4% SDS |
| | 4x Stacking gel buffer; pH 6.8 | 0.5 M TRIS-HCl<br>0.4% SDS |
| | 10x SDS running buffer | 250 mM TRIS Base<br>1.9 M Glycine<br>1% SDS |
| | Anode buffer; pH 8.8 | 300 mM TRIS Base<br>100 mM Tricine |
| | Cathode buffer; pH 8.7 | 300 mM 6-Aminohexanoic acid<br>30 mM TRIS Base |
| | PI-Mix | 10 mg/ml Aprotinin<br>10 mg/ml Leupeptin<br>10 mg/ml Pepstatin A |
| **Co-IP** | Washing solution; pH 7.4 | 1x PBS<br>0.05% Tween-20 |
| | Coupling solution; pH 9.0 | 100 mM Sodium tetraborate decahydrate<br>0.05% Tween® 20 |
| | Crosslinker solution; pH 9.0 | 20 mM Dimethyl pimelidat dihydrochloride<br>100 mM Sodium tetraborate decahydrate<br>0.05% Tween® 20 |
| | Blocking solution; pH 8.0 | 200 mM Ethanolamine hydrochloride<br>0.05% Tween® 20 |
| | Cleansing solution; pH 3.0 | 100 mM Glycine<br>0.05% Tween® 20 |

| | | |
|---|---|---|
| **Fixation** | Sorensen's phosphate buffer; pH 7.4 | 200 mM Sodium dihydrogen phosphate<br>200 mM di-Sodium hydrogen phosphate anhydrous |
| | 4% PFA/120 mM Sucrose; filtrated; pH 7.0 | 3,33 M Paraformaldehyde (20g in 200 ml $H_2O$)<br>3–4 drops 5M Sodium hydroxide solution (to solve PFA)<br>250 ml Sorensen's phosphate buffer<br>50 ml Ampuwa $H_2O$<br>120 mM Sucrose |

### 2.1.3 Culture Media

**Table 3: List and composition of culture media used.**

| Media | Composition |
|---|---|
| BHK-21 cell culture medium | MEM (1x) + Glutamax<br>5% FBS<br>1% P/S |
| Glial cell culture medium | DMEM (1x) + Glutamax<br>10% Horse Serum<br>1% Sodium pyruvate 100 mM<br>1% Amphotericin B<br>1% P/S |
| HeLa cell culture medium | DMEM (1x) + Glutamax<br>10% FBS<br>1% HEPES<br>1% P/S |
| HEK293T cell culture medium | DMEM (1x)<br>10% FBS<br>1% P/S |
| Hippocampal neurons cell culture medium | *NB/FCS*<br>Neurobasal medium<br>5% FBS<br>1% Sodium pyruvate 100 mM<br>1% Amphotericin B<br>1% P/S |
| | *NB/B-27*<br>Neurobasal medium<br>2% B-27<br>1% Sodium pyruvate 100 mM<br>1% Amphotericin B<br>1% P/S |
| LB-Medium for bacterical culture | 10 g/l Bacto-Trypton<br>5 g/l Yeast Extract<br>10 g/l Sodium chloride |
| LB-Agar for bacterial culture | 10 g/l Bacto-Trypton<br>5 g/l Yeast Extract<br>10 g/l Sodium chloride<br>15 g/l Agar-Agar |

### 2.1.4 Antibodies

**Table 4: List of primary antibodies**.

| Primary Antibody | Company and Catalog No. | Species | Purpose |
|---|---|---|---|
| Anti-β actin | Abcam ab8227 | rabbit | Western Blot |
| Anti-Flag M2 | Sigma-Aldrich F3165 | mouse | Western Blot |
| Anti-GluR1-NT (NT), clone RH95 | Sigma-Aldrich MAB2263 | mouse | Staining<br>IP |
| Anti-Glutamate receptor 1 | Sigma-Aldrich AB1504 | rabbit | Western Blot<br>IP |
| Anti-GluA1 | Synaptic Systems 182003 | rabbit | Western Blot |
| Anti-GluR2 | Sigma-Aldrich AB1768-I | rabbit | Western Blot |
| Anti-HA-tag (F-7) | Santa Cruz sc-7392 | mouse | Surface expression staining |
| Anti-HCN2 | Alomone labs APC-030 | rabbit | Western Blot |
| Anti-MAP2 | Abcam ab5392 | chicken | Staining |
| Anti-NMDAR1 | Abcam ab68144 | rabbit | Western Blot |
| Anti-TARPγ8 | Cosmobio NMD-MSFR105820 | rabbit | Western blot |
| Anti-V5 tag | Invitrogen R960-25 | mouse | Western blot<br>IP |
| Anti-V5 tag (D3H8Q) | Cell Signaling Technology 13202 | rabbit | IF |
| Anti-Wnt5a | Thermo Scientific MA5-15502 | mouse | Western blot |

**Table 5: List of secondary antibodies.**

| Secondary Antibody | Company and Catalog No. | Species | Purpose |
|---|---|---|---|
| Goat Anti-Mouse IgG (H&L), HRP | Abcam ab205719 | goat | Western blot |
| Goat Anti-Rabbit IgG (H+L), HRP | Invitrogen ab16110 | goat | Western blot |
| Goat Anti-Chicken IgG (H+L), Alexa Fluor 647 | Jackson ImmoResearch 103-605-155 | goat | IF |
| Goat Anti-Mouse IgG (H+L), Alexa Fluor 555 | Invitrogen A-21424 | goat | IF |
| Goat Anti-Rabbit IgG (H+L), Alexa Fluor 488 | Invitrogen A-11008 | goat | IF |

### 2.1.5 Vectors

**Table 6: List of used vectors.**

| Name | Origin |
|---|---|
| pcDNA3.1 + | Invitrogen |
| pEGFP-C1 | Clontech |

| | |
|---|---|
| pCMV | Cooperation Pfeiffer |
| pRSV-Rev | Addgene |
| pMD2.G | Addgene |
| pMDLg/pRRE | Addgene |
| pHelper | Cooperation Stein |
| pSFV | Cooperation Stein |
| pNLF1-C | Promega |

### 2.1.6 Constructs

**Table 7: List of already existing and newly cloned constructs.**

| Species | Name | Plasmid | Cloned by me |
|---|---|---|---|
| r | GluA1-HAex flip | pcDNA3.1+ | - |
| h | GluA1 flip | pcDNA4/TO | - |
| h | GluA1-V5 flip | pcDNA4/TO | - |
| h | GluK2-Flag | pcDNA4/TO | + |
| r | GluN1-1a | pcDNA1-Amp | - |
| r | GluN2B | pcDNA1-Amp | - |
| m | HCN2-HAex | pEGFP-N1 | - |
| m | PORCN D | N-term FLAG pCI-neo | - |
| cel | PORCN N-term Flag | pcDNA3.1 + | - |
| dro | PORCN N-term Flag | pcDNA3.1 + | - |
| m | PORCN D N-term V5 | pcDNA3.1 + | - |
| m | PORCN D N-term V5 | pSFV | + |
| m | PORCN D S92A N- term V5 | pcDNA3.1 + | - |
| m | PORCN D S186A N- term V5 | pcDNA3.1 + | - |
| m | PORCN D S297A N- term V5 | pcDNA3.1 + | - |
| m | PORCN D Y430F N- term V5 | pcDNA3.1 + | - |
| m | PORCN D S92D N- term V5 | pcDNA3.1 + | + |
| m | PORCN D S186D N- term V5 | pcDNA3.1 + | + |
| m | PORCN D S297D N- term V5 | pcDNA3.1 + | + |
| m | PORCN D Y430E N- term V5 | pcDNA3.1 + | + |
| m | PORCN D S297L N- term V5 | pcDNA3.1 + | + |

| | | | |
|---|---|---|---|
| m | PORCN D H341D N-term V5 | pcDNA3.1+ | + |
| m | PORCN D S297G N-term V5 | pcDNA3.1+ | + |
| m | PORCN D S297K N-term V5 | pcDNA3.1+ | + |
| m | PORCN R228C N-term V5 | pcDNA3.1+ | + |
| m | PORCN D ∆285 N-term V5 | pcDNA3.1+ | + |
| m | PORCN D S297A | N-term FLAG pCI-neo | - |
| m | PORCN D S297D | N-term FLAG pCI-neo | - |
| m | PORCN D S297L | N-term FLAG pCI-neo | - |
| m | PORCN D S297E | N-term FLAG pCI-neo | - |
| m | PORCN D S297T | N-term FLAG pCI-neo | - |
| m | PORCN D Y430F | N-term FLAG pCI-neo | - |
| m | PORCN D Y430E | N-term FLAG pCI-neo | - |
| m | PORCN D S136F | N-term FLAG pCI-neo | + |
| m | PORCN D D283H | N-term FLAG pCI-neo | + |
| h | TARPg8 | pcDNA3.1+ | - |
| r | Wnt5a | pNLF1-C | - |
| r | Wnt5a-V5 | pcDNA3.1+ | - |
| r | Wnt5a-V5 C240A | pcDNA3.1+ | - |
| r | Wnt5a-V5 WT | pCMV | - |
| r | Wnt5a-V5 C240A | pCMV | - |
| r | Wnt5a-V5 WT | pSFV | + |

### 2.1.7 Enzymes

All FastDigest restriction enzymes used were supplied by Thermo Fisher Scientific. The other enzymes used for molecular biological methods are specified in the following table (Table 8).

**Table 8: List of enzymes used.**

| Name | Company and Catalog No. |
|---|---|
| FastAP Thermosensitive Phosphatase | Thermo Scientific EF0651 |
| Phusion™ High-Fidelity DNA-Polymerase | Thermo Scientific F-E30L |
| T4 DNA Ligase | Thermo Scientific EL0011 |

### 2.1.8 Primer

Oligonucleotide primers were designed using *benchling.de* or *nebasechanger.neb.com* and ordered at *biomers.net.* The sequences of the primer are mentioned in Table 9.

**Table 9: List of primers used.**

| Name | | Sequence | Purpose |
|---|---|---|---|
| GluK2-Flag F1 | fwd | 5'- agctcgtttagtgaaccgtcag-3' | Overlap PCR GluK2-Flag |
| GluK2-Flag R1 | rev | 5'- cttatcgtcgtcatccttgtaatcggttccttgagaatatccaatcc-3' | |
| GluK2-Flag R2 | rev | 5'- gagagttaacaccactgtatcggtag-3' | |
| GluK2-Flag F2 | fwd | 5'- gattacaaggatgacgacgataagacacatgtattaagatttggtg g-3' | |
| EcoRI_V5-PORCN | fwd | 5'-gagagaattcgccaccatgggaaagcctatcccaaatcca cttcttggacttgattctactgccaccttcagccgccagg-3' | PCR V5-Tag in PORCN constructs |
| NotI_PORCN | rev | 5'-gagagcggccgctcagcctatgagacggtagaag-3' | |
| T7 | fwd | 5'- taatacgactcactataggg-3' | Overlap PCR PORCN Mutation S136F |
| PORCN_S136F | rev | 5'- gaagcccagaaacaccgccttcatggccac-3' | |
| BGH | rev | 5'- tagaaggcacagtcgagg-3' | |
| PORCN_S136F | fwd | 5'- aggcggtgtttctgggcttcgacctggac-3' | |
| T7 | fwd | 5'- taatacgactcactataggg-3' | Overlap PCR PORCN Mutation D283H |
| PORCN_D283H | rev | 5'- gactgtcaggtgccattccaggtggtcctt -3' | |
| BGH | rev | 5'- tagaaggcacagtcgagg-3' | |
| PORCN_D283H | fwd | 5'- ctggaatggcacctgacagtctctagaccg -3' | |
| PORCN_R228C | fwd | 5'-ccgactcctttgcaacaagaaac-3' | Mutagenesis PORCN Mutation R228C |
| PORCN_R228C | rev | 5'-tcaccgtcgaggggg-3' | |
| PORCN_ Δ285 | fwd | 5'- gtctctagaccgttgaatg-3' | Mutagenesis PORCN Deletion T285 |
| PORCN_ Δ285 | rev | 5'- caggtcccattccag-3' | |
| PORCN_ S297G | fwd | 5'- gctgccccggggcatggtggaag-3' | Mutagenesis PORCN Mutation S297G |
| PORCN_ S297G | rev | 5'- tccacattcaacggtctagag-3' | |
| PORCN_ S297K | fwd | 5'- gctgccccggaaaatggtggaag-3' | Mutagenesis PORCN Mutation S297G |
| PORCN_ S297K | rev | 5'- tccacattcaacggtctag-3' | |

### 2.1.9 Kits

**Table 10: List of kits used.**

| Name | Company and Catalog No. | Purpose |
|---|---|---|
| mMESSAGE mMACHINE™ SP6 Transcription Kit | Invitrogen AM1340 | In vitro transcription |

| | | |
|---|---|---|
| Q5® Site-Directed Mutagenesis Kit | New England Biolabs E054 | Mutagenesis |
| QIAquick® Gel Extraction Kit | Quiagen 28704 | Gel extraction |
| QIAGEN® Plasmid Plus Midi Kit | Quiagen 12945 | Purification of plasmid DNA (up to 10 mg) |
| QIAprep® Spin Miniprep Kit | Quiagen 27106 | Purification of plasmid DNA (up to 20 µg) |

### 2.1.10 Equipment

**Table 11: List of devices used.**

| | Device | Manufacturer |
|---|---|---|
| Clean bench | Heraguard™ ECO | Thermo Scientific, Langenselbold, Germany |
| Biological safety cabinet | Safe 2020 | Thermo Scientific, Langenselbold, Germany |
| Electroporation system | GenePulser Xcell | Bio-Rad, Feldkirchen, Germany |
| Gel documentation chamber | UVsolo TS Imaging System | Biometra, Göttingen, Germany |
| Thermoshaker/Incubator | Thermomixer compact | Eppendorf, Hamburg, Germany |
| | Thriller | peqlab, Erlangen, Germany |
| Incubators | Heracell™ VIOS 250i $CO_2$ | Thermo Scientific, Langenselbold, Germany |
| | Heratherm™ | Thermo Scientific, Langenselbold, Germany |
| | GFL3031 | GFL, Burgwedel, Germany |
| Micropipettes | Research plus™ | Eppendorf, Hamburg, Germany |
| Photometer | NanoDrop™ 2000c | Thermo Scientific, Langenselbold, Germany |
| Pipette | Accu-jet® pro | Brand, Wertheim, Germany |
| Shakers and rotators | PTR-35 | Grant-bio, Cambridge, UK |
| | Rocking plattform | VWR, Darmstadt, Germany |
| | Duomax 1030 | Heidolph, Schwarbach, Germany |
| | SB3 Rotator | Stuart, Loughborough, UK |
| Voltage transmitters | PowerPac™ HC High-Current Power Supply | Bio-Rad, Feldkirchen, Germany |
| | Electrophoresis Power Supply EPS 301 | GE Healthcare, Solingen, Germany |

| | | |
|---|---|---|
| Thermocyclers | Mastercycler pro S | Eppendorf, Hamburg, Germany |
| | Mastercycler epgradient S | Eppendorf, Hamburg, Germany |
| Transilluminator | Safe Imager™ 2.0 | Thermo Scientific, Langenselbold, Germany |
| Ultrasonic probe | Branson Sonifier 250 | Emerson, Saint Louis, USA |
| Vortex mixer | Vortex Mixer | VWR, Darmstadt, Germany |
| Western blot documentation chamber | FusionFx | Vilber, Eberhardzell, Deutschland |
| Western blot systems | Mini-PROTEAN Tetra Vertical Electrophoresis Cell System | Bio-Rad, Feldkirchen, Germany |
| | Trans-Blot® Turbo™ Transfer System | Bio-Rad, Feldkirchen, Germany |
| Centrifuges | Mini Star | VWR, Darmstadt, Germany |
| | MiniSpin plus | Eppendorf, Hamburg, Germany |
| | 5424 R | Eppendorf, Hamburg, Germany |
| | 5804 | Eppendorf, Hamburg, Germany |
| | 5810 R | Eppendorf, Hamburg, Germany |
| | Optima™ MAX-XP Ultracentrifuge | Beckman Coulter, Krefeld, Germany |
| | Optima™ L-80 XP | Beckman Coulter, Krefeld, Germany |
| Luminometer | GloMax 2031-001 | Turner BioSystems, Sunnyvale, USA |
| Water bath | GFL 1003 | GFL, Burgwedel, Germany |
| Microscope | Axiovert 40 CFL | Zeiss, Oberkochen, Germany |
| | BZ-X800 | Keyence, Neu-Isenburg, Germany |
| | LSM 710 | Zeiss, Oberkochen, Germany |
| | Stemi 305 | Zeiss, Oberkochen, Germany |
| pH meter | SevenEasy pH | Mettler-Toledo, Schwerzenbach, Switzerland |
| Microwave | MG5887U | LG, Eschborn, Germany |

### 2.1.11 Software

The statistical analysis was conducted using either PRISM 10.0.2 (GraphPad, Boston, USA) or OriginPro 2021b (OriginLab Corporation, Northampton, USA). The reconstruction of

hippocampal neurons was performed using the Neurolucida system 11 (MBF Bioscience, Williston, USA), while the electrophysiological measurements were analyzed using the Clampfit 11.2.2.17 software program (Molecular Devices, San Jose, USA). The analysis of immunofluorescence images and the quantification of Western blot band intensity was conducted using ImageJ software 1.54p (NIH, Bethesda, USA).

### 2.1.12 Animals

All animal experimentation procedures conducted in this study comply with the European Union Directive 2010/63/EU on the ethical treatment of animals used in scientific research. In this study, E16 embryos of C57BL/6J mice were used for primary cell culture. The animal test authorization G 389/18 with the designation “In Vitro-Kultivierung hippocampaler und kortikaler Nervenzellen und Gliazellen aus Mäusegehirn” was approved on 17.06.2019 (LANUV file reference: 81-02.04.2018.A389) and expired on 31.07.2024. The new authorization with the name „In vitro Kultivierung von Neuronen und Gliazellen aus embryonalem Mäusegehirn" has the project number VG633/24 (LANUV file reference: 2024-633-Grundantrag (VG)) and was approved on 14.10.2024. The FELASA Accredited Course F048/16 ‘Versuchstierkundliche Einführung zur Erlangung des Fachkundenachweises gemäß § 9 des geltenden Tierschutzgesetzes“ has been successfully completed (FELASA Certificate ID: F048/16_#_0406).

## 2.2 Cell Biological Methods

### 2.2.1 Cultivation of Immortalized Cell Lines

Three immortalized cell lines were used: HeLa cells (human cervical carcinoma), HEK293T cells (human embryonic kidney, SV40 T-antigen-expressing) and BHK-21 cells (fibroblasts from baby hamster kidney). HeLa cells were used for protein analysis, HEK293T for lentivirus production and BHK-21 for Semliki Forest virus (SFV) production. All were cultured under the same conditions, except for media, as described in Chapter 2.1.3.

#### 2.2.1.1 Cultivation

The cells were cultured at 37°C with 5% $CO_2$. When reaching approximately 85–90% confluency, they were passaged or seeded. Prior to passaging, culture medium, DPBS and 1x trypsin (0.25%) were pre-warmed to 37°C. Cells were washed with 10 ml of DPBS, treated with 3 ml of 1x trypsin for three minutes and the reaction was stopped by adding 7 ml fresh medium. After resuspension, cells were centrifuged at 1,000 rpm for two minutes and the pellet was resuspended in 10 ml medium before transferring the solution to new flasks at the required dilution.

#### 2.2.1.2 Cryopreservation

For cryopreservation, the cell pellet was resuspended in 1.5 ml of freezing medium (Thermo fisher scientific 12648010) and transferred to a cryogenic storage tube. Using "Mr.Frosty"

(Thermo fisher scientific 10110051), the cells were stored at -80°C for two days before being transferred to a liquid nitrogen tank for long-term storage.

#### 2.2.1.3 Counting and Seeding

The following protocols specifically apply to HeLa cells. The handling of HEK293T and BHK-21 cells is described in the virus preparation protocols below. The process of counting cells was always carried out using a Neubauer counting chamber, as described in the following section.

A 1.5 ml reaction tube was prepared with 450 µl medium and 50 µl of the cell suspension (1:10 dilution). 10 µl of this diluted suspension was applied to the chamber. Under a microscope, the cells were counted in four corner squares of the chamber and the average cell count per corner square was calculated. Given that the area of one square is 1 mm² and the chamber depth is 0.1 mm, the total volume per square corresponds to 0.1 µl.

The total cell number was then calculated using the following formula:

$$\frac{number\ of\ cells}{number\ of\ counted\ corner\ squares} \times 10^4 \times 10 = number\ of\ cells\ in\ 1000\ \mu l$$

To obtain the specific cell count required for experiments, the calculated total cell number was scaled to the volume corresponding to 1000 µl. The appropriate volume for seeding was calculated as:

$$\frac{specific\ cell\ count}{number\ of\ cells\ in\ 1000\ \mu l} = specific\ volumina\ in\ ml$$

The adjusted cell suspension was then added to the cell culture dishes as specified in Table 12.

**Table 12: Cell count of HeLa cells for cell culture experiments.**

| Cell culture dish | Volume | Cell count |
|---|---|---|
| 6-well plate/30 mm dish | 2 ml | 500,000 |
| 24-well plate | 500 µl | 50,000 |

The following day, cell adhesion and density were evaluated to ensure suitability for further experiments.

### 2.2.2 Transfection of HeLa cells

To overexpress the proteins of interest, the respective DNA was transfected into HeLa cells using FuGENE® HD as the transfection reagent. The protocols described in Tables 13 and 14 were designed for transient transfections, performed solely for experimental purposes and the cells were not passaged further.

**Table 13: Procedure for HeLa cell transfection.**

| Step | Procedure |
|---|---|
| 1. Prepare transfection mixture | Add the appropriate amount of DNA and the transfection reagent to transfection medium and vortex the mixture |
| 2. Incubation | Incubate the mixture at RT for 15 minutes |
| 3. Add to cells | Carefully add the transfection solution to the cells |
| 4. Incubation and medium change | After 4 hours, replace culture medium with fresh medium |

**Table 14: Standard transfection protocol for HeLa cells.**

| Cell culture dish | Purpose | Replicates | Opti-MEM | DNA | Fugene |
|---|---|---|---|---|---|
| 1 well/6-well plate | Protein analysis | 3 | 300 µl | 5 µg | 15 µl |
| 35 mm dish | Surface expression assay | 3 | 600 µl | 6 µg | 36 µl |
| 24-well plate | Wnt secretion assay | 6 | 150 µl | 1.5 µg | 7.5 µl |

The cells were incubated overnight at 37°C with 5% $CO_2$ in an incubator and used for subsequent experiments on the following day.

### 2.2.3 Preparation, Cultivation and Seeding of Glial cells

During hippocampal neuron preparation, the remaining brain tissue was used to establish glial cell cultures. Tissues were collected in 1x HBSS/Hepes solution, then incubated with 0.05% trypsin at 37°C for 15 minutes. After trypsinization, tissues were washed with glial medium twice, resuspended and dissociated. Large clumps were removed using a filter and the cell suspension was diluted and transferred to a T75 flask, with cells from four to seven brains per flask. Glial cells were maintained by washing with DPBS and changing the medium twice a week. After 14 days, cells were either used as a feeder layer or cryopreserved. To prepare the glial feeder layer, cells were seeded six days before neuron preparation (Table 15).

**Table 15: Cell count of glial cells.**

| Cell culture dish | Volume | Cell count |
|---|---|---|
| 6-well plate | 2 ml | 70,000 |
| 12-well plate | 1 ml | 35,000 |
| 24-well plate | 1 ml | 17,500 |

Two days before the preparation, the glial medium was replaced with NB/B27 medium, with 3 ml for 6-well plates, 1.5 ml for 12-well plates and 1 ml for 24-well plates.

### 2.2.4 Preparation of Cell Culture Plates for Primary Cell Culture

Hippocampal neurons were cultured in a high-density sandwich co-culture system. Coverslips were prepared with wax spots and coated with poly-D-lysine (PDL) to promote neuronal adhesion. Neurons were seeded onto the PDL-coated coverslips with wax spots, using 30 mm coverslips for 6-well plates, 18 mm for 12-well plates and 12 mm for 24-well plates. After seeding, the coverslips were inverted and placed into culture plates with a glial feeder layer. The wax spots maintained a defined distance between the glial layer and the neurons. For wax preparation, paraffin was melted and applied to the coverslips using a 100 µl pipette for large coverslips and a 10 µl pipettes for small ones. The paraffin-dotted coverslips were placed in sterile culture plates and treated with UV light for 30 minutes. PDL stock solution was diluted 1:100 in borate buffer (0.1 mg/ml) and applied to the coverslips (2 ml for 6-well plates, 1 ml for 12-well plates and 500 µl for 24-well plates). The plates were incubated for 2.5 days. After incubation, coverslips were washed three times with sterile water, then left in water in the incubator until further use.

### 2.2.5 Preparation of Hippocampal Neurons

Hippocampal neurons and glial cells were isolated from E16 mouse embryos. The workbench was cleaned with 70% ethanol and sterilized under UV light for 30 minutes, while dissecting tools were disinfected in 3% Korsolex Basic for 30 minutes. Glia medium, NB/FCS medium and 0.05% trypsin solution were prewarmed to 37°C. Ice-cold 1x HBSS/Hepes solution was prepared for storing the dissected hippocampi and handling the embryos. The pregnant mouse was anesthetized with isoflurane and euthanized by decapitation. The abdominal wall was sterilized with 70% ethanol and opened laterally to expose the embryos. The embryos were removed, instantly placed into ice-cold HBSS/Hepes and decapitated. The heads were transferred to a separate dish with ice-cold HBSS/Hepes. An incision was made in the skull to detach the brain, which was then placed into a clean dish. Under a dissecting microscope, the hemispheres were separated from the brainstem and the meninges, which were discarded. The hippocampi were dissected and transferred into a tube containing HBSS/Hepes. After collecting all hippocampi, the HBSS/Hepes solution was removed and 2 ml of 0.05% trypsin solution was added. The hippocampi were incubated for 15 minutes at 37°C to dissociate the cells. After incubation, the trypsin solution was removed and the hippocampi were washed three times with 10 ml of NB/FCS medium. After the final wash, 3 ml of NB/FCS medium was added and the tissue was dissociated by pipetting. For cell counting, 70 µl NB/FCS medium, 20 µl Trypan Blue and 10 µl of the cell suspension was mixed and cell density was determined as detailed in Chapter 2.2.1.

**Table 16: Cell count of hippocampal neurons for primary cell culture experiments.**

| Cell culture dish | Volume | Cell count |
|---|---|---|
| 6-well plate | 2 ml | 400,000 |
| 12-well plate | 1 ml | 150,000 |
| 24-well plate | 1 ml | 50,000 |

The cell count specified in table 16 was applied to the coverslips in the appropriate volume and the cells were cultured at 37°C with 5%$CO_2$. After four hours, the cells were transferred to the glia-co-culture plate.

### 2.2.6 Transfection of Hippocampal Neurons

To investigate the effect of protein overexpression, hippocampal neurons were transfected with DNA at five days in vitro (DIV) and stained at 20–22 DIV. Two mixtures were prepared to transfect four coverslips with neurons: MIX1 (4 µg DNA + 100 µl Opti-MEM) and MIX2 (4 µl Lipofectamine 2000 + 100 µl Opti-MEM). Both mixtures were incubated separately for 5 minutes, then combined and incubated for 20 minutes. The transfection mixture was added to the neurons on coverslips which were placed in a new plate with conditioned medium. The cells were incubated in the transfection solution at 37°C with 5%$CO_2$ for two hours. After incubation, the coverslips were transferred back to the glial feeder layer, where fresh medium containing Ara-C (1:5,000 dilution) was added. Ara-C was also added on day five to non-transfected neurons during a partial medium change to inhibit glial proliferation.

### 2.2.7 Preparation and Transduction of Lentivirus

Lentivirus and SFV were used to transduce hippocampal neurons, with transduction rates exceeding 75%. Due to low transfection rates (<1%), transfection is unsuitable for protein analysis in primary neuronal cell cultures.

For lentivirus preparation, HEK293T cells were cultured and split into six T175 flasks three days before preparation. On the first day, 12.1 x $10^6$ cells were seeded in 150 mm dishes and incubated overnight. The following day, the cell density (70–80%) was checked and the cells were transfected. The transfection solution was prepared, vortexed, incubated for 30 minutes at room temperature and added to the cells (Table 17). The following day, the old medium was aspirated and 16 ml of fresh, pre-warmed medium was added to each plate. Two days after transfection, the virus was harvested.

**Table 17: Standard scheme of transfection solution for lentivirus preparations.**

| | Volume/plate | Volume/sample |
|---|---|---|
| Cell culture medium | 0.8 ml | 5 ml |
| Plasmid of interest | 22.5 µg | 135 µg |
| pRSV-Rev | 6.4 µg | 38.4 µg |
| pMD2.G(CMVvsvg) | 6.1 µg | 36.6 µg |
| pMDLg/pRRE | 14.6 µg | 87.6 µg |
| Polyethylenimine (1mg/ml; pH 7) | 200 µl | 1.2 ml |

For virus harvesting, the supernatant was filtered through a 0.45 µm filter (Thermo Scientific 1210045) and transferred into ultracentrifuge tubes (Beckman Coulter 344058); three tubes per sample, topped up with 1x HBSS. The filtrate was centrifuged at 64,200 g at 17°C for two hours using the SW 32Ti rotor. The cells were replenished with 16 ml of fresh medium and returned to the incubator. After centrifugation, the supernatant was discarded and the virus pellet was resuspended in 100 µl 1x HBSS in each tube. An additional 100 µl of 1x HBSS was used to wash each sample. The virus solution from all tubes was combined and stored at 4°C overnight. A second harvest was then performed the following day according to the same protocol. To concentrate the virus solution, a sucrose gradient was prepared by adding 3 ml of 20% sucrose to the bottom of an ultracentrifuge tube (Beckman Coulter 326819). The virus solution was carefully layered on top of the sucrose and the tubes were centrifuged at 53,500 g for two hours using the MLS 50 rotor. After centrifugation, the pellet was resuspended in 60 µl of 1× HBSS and shaken at 1,400 rpm at 16°C for 45 minutes. Finally, the tube was centrifuged for 15 seconds at 13,000 g and the supernatant was aliquoted and stored at -80°C.

For transduction, the virus was added to the neurons at 14 DIV, with 3 µl per well for 12-well plates and 5 µl per well for 6-well plates. Before adding the virus, the medium was removed (500 µl per well for 12-well plates, 1 ml per well for 6-well plates) and stored in the incubator overnight. The medium was then returned to the plates the next day. Neurons were incubated for seven days post-transduction.

### 2.2.8 Preparation and Transduction of Semliki Forest Virus

SFV preparation requires BHK cells, which were cultured as described previously. Cells were seeded four days prior to electroporation in one T75 flask per sample. Having been washed with DPBS and treated with 1x trypsin, detached cells were resuspended in cold DPBS and centrifuged at 1,000 g for two minutes. The wash step was repeated twice to remove residual trypsin. The final cell pellet was resuspended in 10 ml DPBS. For cell counting, 495 µl DPBS was mixed with 5 µl of the cell suspension and the required amount of 17 million cells per sample was collected in a tube and centrifuged. The pellet was resuspended in an appropriate volume of 500 µl per virus sample. RNA (pHelper and pSFV) was prepared by in vitro transcription (Chapter 2.3.10), mixed with the cell suspension and

transferred to a sterile 2-mm cuvette. Electroporation was performed using a BioRad system with 1.5 kV, 25 µF and infinite resistance, applying two pulses with a 10-second interval. After electroporation, cells were left at room temperature for 10 minutes. During this time, 10 ml of medium was prepared in a new 150-mm dish and the electroporated cells were transferred into the dish. The cells were incubated for 48 hours; the medium was changed the following morning. After the incubation, the viral supernatant was collected and centrifuged at 3,000 g for 15 minutes. The virus was further concentrated by centrifugation at 50,000 g at 4°C for 90 minutes using a SW32Ti rotor. The pellet was resuspended in 60 µl DPBS and stored at – 80°C.

Hippocampal neurons were transduced at 20 DIV. To activate the virus, chymotrypsin was added at a 1:20 dilution and incubated for 45 minutes. Aprotinin was then added at a 1:15 dilution and after 10 minutes, 3 µl of virus (for 12-well plates) or 6 µl (for 6-well plates) was added to the neurons. The neurons were incubated in the S2 incubator for 24 hours.

### 2.2.9 Inhibition of PORCN Enzymatic Activity

The PORCN inhibitor Wnt-C59 was used to inhibit PORCN enzymatic activity in hippocampal neurons at 19–21 DIV. The inhibitor prevents the palmitoylation of Wnt in the ER, thereby halting Wnt secretion.

The experimental setup included two groups: DMSO (control) and 100 nM Wnt-C59, with four wells per group in a 12-well plate. Each group received 500 µl of the old medium and 500 µl of fresh NB/B27 per tube, resulting in a total volume of 1 ml per well. A 100 nM Wnt-C59 solution was prepared by diluting the 100 µM stock solution (stored at -20°C) at a 1:1,000 ratio, while the control group received an equivalent volume of DMSO. The medium was added to a new 12-well plate, into which the neurons were transferred. The plates were incubated for 48 hours in a $CO_2$ incubator. After incubation, the cells were harvested and membrane preparation was performed.

### 2.2.10 Immunofluorescence Staining of Hippocampal Neurons

Immunofluorescence (IF) staining of hippocampal neurons was performed at 20–22 DIV. Before staining, 4% PFA in 120 mM sucrose/PBS was defrosted and a 120 mM sucrose solution in DPBS was pre-warmed to 37°C. The coverslips, with the cell side facing up, were transferred into a new well plate containing 1 ml of warm sucrose-solution per well and washed twice with the same solution. Then, 4% PFA with 120 mM sucrose was added (500 µl per well) and the coverslips were incubated at room temperature for ten minutes. After fixation, the fixative was removed and the coverslips were washed three times with PBS. Immunostaining was either performed immediately or the plate was stored at 4°C for later processing. For intracellular targets, permeabilization was done with 0.25% Triton X-100 at room temperature for ten minutes (500 µl per well), followed by two washes with

PBS. Blocking was done using 10% NGS-PBS at room temperature for 45 minutes. The cells were incubated with the primary antibody (diluted in 10% NGS-PBS) at room temperature for one hour or at 4°C overnight. After incubation, the antibody solution was decanted and the cells were washed three times with PBS. The secondary antibody, diluted in 1% NGS-PBS, was added in the dark at room temperature for one hour. Afterwards, the secondary antibody solution was removed and the cells were washed three times with PBS. If the cell nuclei were to be stained, Hoechst was added during the second washing step and the neurons were incubated in the solution for 20 minutes before being washed twice again.

To mount the coverslips a drop of ProLong™ Diamond Antifade Mountant was added to the slide and the coverslip was carefully positioned with the cell side down. Slides were allowed to dry for 24 hours in the dark and sealed with nail polish. The mounted slides were stored in the dark at 4°C.

Confocal images were captured with the Zeiss LSM 710 equipped with a 63x oil immersion objective at the Center of Advanced Imaging at HHU.

### 2.2.11 Reconstruction of Hippocampal Neurons

To investigate hippocampal neuron morphology, cells were transfected with the respective DNA constructs at 5 DIV and subjected to immunofluorescence staining at 19–22 DIV. Following staining, hippocampal neurons exhibiting morphological features characteristic of pyramidal neurons were selected for imaging using a Keyence BZ-X800 microscope (Institute of Anatomy II, Faculty of Medicine, HHU). Neuronal reconstructions were performed manually with Neurolucida software, focusing on the soma, apical dendrites and basal dendrites. A Sholl analysis was conducted to quantify the branching of the dendrites, using concentric spheres at 25 µm intervals, which was carried out using Neurolucida Explorer.

Morphological characteristics, particularly the total lengths of basal and apical dendrites, were compared and statistically analyzed. The statistical analysis was performed using a two-way repeated measures (RM) ANOVA to assess differences between groups, followed by a Bonferroni correction for pairwise comparisons to account for multiple testing. It is important to note that comparisons between dendrite lengths were made for each group as a whole and not for the individual intervals from the Sholl analysis.

### 2.2.12 Electrophysiological Measurements

AMPAR-mediated mEPSCs were recorded by Kelvin Tofan (Institute of Anatomy II, Heinrich Heine University Düsseldorf) following a protocol established in our lab [89]. Deviating from the protocol, the used extracellular solution contained 0.5 µM TTX, 1 µM strychnine and

6.25 µM gabazine. The analysis of the mEPSCs was performed by me using the Clampfit software and included the parameters frequency, amplitude, rise time and decay time constant.

## 2.3 Assays

### 2.3.1 Surface Expression Staining of HeLa Cells

Surface expression staining was performed to quantify receptor surface expression. For GluA1 surface expression analysis, GluA1 was conjugated with an extracellular HA epitope (HA-tag; YPYDVPDYASL) between amino acids 19 and 20.

HeLa cells were seeded two days prior to the experiment in 35 mm dish plates and transfected the following day. Each sample was prepared in triplicate. First, the cell culture medium was discarded and the cells were fixed with 4% PFA for 20 minutes. After fixation, the cells were washed three times with 1x PBS and blocked with 10% NGS-PBS for one hour. The cells were incubated with the primary antibody (HA-tag antibody (Santa Cruz), 1:100 in PBS) for one hour, followed by four 15-minutes-washes. Secondary antibody (goat-anti-mouse IgG (Abcam), 1:10,000 in 10% NGS-PBS) was applied for an additional hour. Cells were then washed extensively four times for 15 minutes each. Chemiluminescence measurement was performed as follows: PBS was removed and replaced with 900 µl of chemiluminescence reagent (SuperSignal™ ELISA Femto Substrate; Thermo Scientific 37074). The dish was placed in a luminescence reader and luminescence was measured at 15, 30, 45 and 60 seconds with an integration time of one second. For GluA1 surface expression analysis, the luminescence value recorded at 30 seconds was used.

### 2.3.2 Wnt Secretion Assay

Wnt secretion was measured in the supernatant of HeLa cells and hippocampal neurons. Wnt5a was fused to NanoLuc at its C-terminus using the pNLF1 NanoLuc® Protein Fusion Vectors (Promega; N1361). HeLa cells were transfected one day after seeding. Four hours post-transfection, the medium was replaced with fresh medium containing 100 nM Wnt-C59 to inhibit endogenous PORCN. The cells were then incubated for an additional 24 hours.

Hippocampal neurons were transduced with Wnt5a-NanoLuc lentivirus at 14 DIV and maintained in culture for an additional seven days prior the experiment. The supernatant of the neurons was transferred into a 24-well plate.

Following the incubation, the plates were centrifuged at 1,000 rpm for three minutes. 50 µl of the supernatant was transferred to a new well in a 96-well plate and 50 µl of NanoGlo Luciferase substrate solution was added. After shaking for 30 seconds, the plate was incubated for two minutes before luminescence was measured using the GloMax Discover System.

## 2.4 Molecular Biological Methods

### 2.4.1 Polymerase Chain Reaction

Polymerase chain reaction (PCR) is a method for amplifying specific DNA sequences. The process involves three steps: denaturation, annealing and elongation. In the first step, the hydrogen bonds between DNA strands are broken at 98°C, resulting in single-stranded DNA (denaturation). Next, specific oligonucleotide primers bind to the single strand and frame the target sequence for amplification (annealing). The annealing temperature depends on the primers' G/C content and length. In this study, Phusion™ High-Fidelity DNA Polymerase was used, which has an optimal temperature of 72°C. The polymerase binds to the primers and synthesizes complementary strands using the single-strand template and free nucleotides (elongation). The elongation time depends on the expected product length, with a recommended time of 0.5–1 minute per kb. These steps were repeated multiple times to ensure sufficient amplification. The PCR mixture was prepared in a 0.2 ml reaction tube on ice, following the standard pipetting scheme (Table 18). The specific protocol for PCR with Phusion DNA polymerase is outlined in table 19.

**Table 18: Standard pipetting scheme of a PCR with Phusion DNA polymerase.**

| Reagents | Volume |
|---|---|
| DNA | 10 ng |
| Primer fwd (5 µM) | 3 µl |
| Primer rev (5 µM) | 3 µl |
| 5x Phusion HF Buffer | 10 µl |
| dNTPs | 1 µl |
| Phusion DNA Polymerase | 0.5 µl |
| $H_2O$ | ad 50 µl |

**Table 19: Standard scheme for a PCR run with Phusion DNA polymerase.**

| Stage | Temperature | Time | Cycle |
|---|---|---|---|
| Initial Denaturation | 98°C | 30 sec | - |
| Denaturation | 98°C | 15 sec | 35 |
| Annealing | specific | 30 sec | 35 |
| Elongation | 72°C | specific | 35 |
| Final Elongation | 72°C | 2 min | - |
| End | 4°C | ∞ | |

### 2.4.2 Overlap Extension Polymerase Chain Reaction

Overlap extension polymerase chain reaction (Overlap PCR) was used to introduce point mutations into the DNA constructs. Initially, two DNA fragments were amplified using standard PCR protocols with two distinct primer pairs. The first primer pair consisted of a forward primer, binding at least 100 base pairs upstream of the protein-coding region and a reverse primer that bound to the mutation site, incorporating the desired mutation as an overhang. The second primer pair included a forward primer binding to the mutation site, incorporating the mutation sequence as an overhang and a reverse primer binding to a

downstream restriction site. The overlap PCR reaction was prepared as specified in the following table (Table 20).

**Table 20: Standard pipetting scheme of an Overlap PCR.**

| Reagents | Volume |
|---|---|
| PCR product | 5 µl each |
| 5x HF Puffer | 10 µl |
| dNTPs | 1 µl |
| Phusion Polymerase | 0.5 µl |
| $H_2O$ | ad 50 µl |

Following amplification of the two DNA fragments, the PCR products were purified from an agarose gel and used as templates for the overlap PCR, which was carried out according to the standard protocol (Table 21).

**Table 21: Standard scheme for an overlap PCR.**

| Stage | Temperature | Time | Cycle |
|---|---|---|---|
| Denaturation | 98°C | 5 min | 3 |
| Annealing | specific | 5 min | 3 |
| Elongation | 72°C | 5 min | 3 |

After the overlap PCR run, 3 µl of the undiluted forward and reverse primers were added to the sample. Subsequently, a standard PCR run was performed to amplify the full-length mutated construct (Table 22).

**Table 22: Standard scheme for a PCR following the overlap PCR**.

| Stage | Temperature | Time | Cycle |
|---|---|---|---|
| Initial Denaturation | 98°C | 5 min | - |
| Denaturation | 98°C | 10 sec | 35 |
| Annealing | specific | 30 sec | 35 |
| Elongation | 72°C | specific | 35 |
| Final Elongation | 72°C | 2 min | - |
| End | 4°C | ∞ | |

### 2.4.3 Agarose Gel Electrophoresis and Gel Extraction

The analysis of DNA on 1% agarose gel was performed after PCR and restriction digestion. The gel was prepared by boiling agarose in 1x TAE buffer until fully dissolved. After cooling briefly, SYBR™ Safe DNA Gel Stain (Invitrogen S33102) was added (Table 23). The gel was then poured while warm and hardened under the fume hood.

**Table 23: Preparation of a 1% agarose gel with SYBR™ Safe™.**

| Reagents | Volume |
|---|---|
| Agarose | 30 g |
| 1x TAE Buffer | 30 ml |
| SYBR™ Safe | 1 µl (1:30.000) |

Following PCR and overlap PCR, 10 µl of 6x loading dye was added to the (overlap) PCR product and the sample was loaded onto the 1% agarose gel. For restriction digestion with Fast Digest buffer, samples could be loaded directly. A DNA ladder was included to verify fragment size. Electrophoresis was performed for 35 minutes at 130 volts in 1x TAE buffer. The bands were visualized under blue light and DNA fragments were excised for gel extraction if necessary.

To extract the DNA, the gel was placed on a clear plate illuminated with blue light. Goggles with a blue light filter were worn for eye protection. The desired bands were excised using a scalpel and transferred to a 1.5 ml tube. The gel was photographed under UV light. DNA extraction was carried out using the QIAquick Gel Extraction Kit. 450 µl of QG buffer was added to the gel fragments, which were incubated at 50°C with shaking for 10 minutes. After adding 150 µl isopropanol, the remaining steps followed the manufacturer's protocol. Finally, the DNA was eluted in 30 µl $H_2O$ and stored at -20°C.

### 2.4.4 Restriction Enzyme Digestion

After DNA fragment extraction, restriction digestion was performed to determine fragment sizes and prepare plasmids for cloning. FastDigest enzymes were chosen because of their quick digestion time and universal buffer compatibility. The digestion was carried out as follows.

#### 2.4.4.1 PCR Product and Vector Digestion

The PCR product and vector were combined in a 1.5 ml reaction tube (Table 24), along with the appropriate restriction enzymes and buffer and incubated at 37°C for 30 minutes. Phosphatase was added to prevent self-ligation in the vector plasmid digest, followed by a ten minute incubation at 37°C. After digestion, the fragments were analyzed on a 1% agarose gel and those of the desired size were extracted and ligated.

**Table 24: Standard pipetting scheme for a restriction digest after PCR.**

| | PCR product | Vector |
|---|---|---|
| DNA | 16 µl | 1 µg |
| Fast Digest Buffer | 2 µl | 2 µl |
| Restriction enzyme | 1 µl each | 1 µl each |
| $H_2O$ | ad 20 µl | ad 20 µl |

#### 2.4.4.2 Mini/Midi Preps Digestion

A restriction digest was also performed after mini or midi preparations to verify the success of transformations (Table 25). The digest was incubated at 37°C for 30 minutes and the fragment sizes were checked on a 1% agarose gel.

**Table 25: Standard pipetting scheme for a restriction digest after mini/midi preparation.**

| | Mini | Midi |
|---|---|---|
| DNA | 5 µl | 1 µl |
| Fast Digest Buffer | 2 µl | 2 µl |
| Restriction enzyme | 1 µl each | 1 µl each |
| $H_2O$ | ad 20 µl | ad 20 µl |

#### 2.4.4.3 Cloning without PCR Amplification

When suitable restriction sites were available, cloning could be performed without prior PCR amplification. Both the target plasmid and the plasmid containing the insert were digested with the same restriction enzymes (Table 26). Phosphatase was added to the target plasmid to prevent self-ligation. After digestion, the fragment sizes were confirmed on a 1% agarose gel, followed by gel extraction and ligation.

**Table 26: Standard pipetting scheme for a restriction digest for cloning.**

| | Vector/Insert |
|---|---|
| DNA | 1 µg |
| Fast Digest Buffer | 2 µl |
| Restriction enzyme | 1 µl each |
| $H_2O$ | ad 20 µl |

### 2.4.5 Ligation

Ligation is the process of joining a DNA fragment, such as a PCR product, to a vector. Prior to ligation, restriction digestion was performed to expose the necessary interfaces for precise joining. A negative control was included by replacing the PCR product with water. The ligation mixture was prepared in a 1.5 ml reaction tube and incubated overnight at 16°C (Table 27).

**Table 27: Standard pipetting scheme for a ligation approach.**

| Reagents | Volume |
|---|---|
| Vector DNA | 1 µl |
| PCR product or $H_2O$ | 16 µl |
| T4 Ligase Buffer | 1 µl |
| T4 Ligase | 1 µl |

### 2.4.6 (Re-)Transformation

The ligation of the PCR product and vector was introduced into chemically competent XL1-Blue Escherichia coli (Agilent). The bacteria were thawed on ice and 70 µl were added to 3 µl of the ligation mixture. The mixture was incubated on ice for 20 minutes, followed by 50 seconds at 42°C and then on ice for two minutes. Afterward, 400 µl of LB medium (without antibiotic) was added and the mixture was incubated for 60 minutes at 37°C with agitation. The solution was spread onto agar plates containing the appropriate antibiotic and then incubated overnight at 37°C. Transformation efficiency was assessed by

comparing the number of colonies on the experimental plate to the negative control plate. To amplify DNA from a miniculture sample, a re-transformation procedure was performed. The DNA was diluted to 1:1,000 and the transformation was carried out as previously described.

### 2.4.7 Insertion of Point Mutations Using Q5® Site-Directed Mutagenesis Kit

In addition to conventional cloning methods such as PCR and overlap PCR, the Q5® Site-Directed Mutagenesis Kit was used to introduce point mutations. The mutagenesis process was carried out in two stages: PCR amplification followed by a Kinase-Ligase-DPnl (KLD) reaction.

#### 2.4.7.1 PCR Amplification

The first stage involved PCR amplification using primers designed specifically for the targeted mutations. The PCR reaction was carried out with Q5® High-Fidelity DNA Polymerase, following the standard pipetting scheme and PCR run protocol (Tables 28 and 29).

**Table 28: Standard pipetting scheme of a PCR with Q5 High-Fidelity DNA Polymerase.**

| Reagents | Volume |
|---|---|
| DNA 10 ng/µl | 1 µl |
| Primer fwd (10 µM) | 1.25 µl |
| Primer rev (10 µM) | 1.25 µl |
| Q5 Hot Start High-Fidelity 2x Master Mix | 12.5 µl |
| Ad $H_2O$ | ad 25 µl |

**Table 29: Standard scheme for a PCR run with Q5 High-Fidelity DNA Polymerase.**

| Stage | Temperature | Time | Cycle |
|---|---|---|---|
| Initial Denaturation | 98°C | 30 sec | - |
| Denaturation | 98°C | 10 sec | 25 |
| Annealing | 64°C | 30 sec | 25 |
| Elongation | 72°C | 2 min | 25 |
| Final Elongation | 72°C | 2 min | - |
| End | 4°C | ∞ | |

#### 2.4.7.2 KLD Reaction

The KLD reaction was incubated at room temperature for five minutes to facilitate the ligation process (Table 30). The reaction mixture (5 µl) was then added to 70 µl of chemically competent bacteria. After an initial incubation on ice for five minutes, the mixture was heat-shocked at 42°C for 45 seconds and returned to ice for five minutes. The bacterial solution was spread onto agar plates and colonies were allowed to grow. If successful colonies appeared, the bacterial culture was propagated for further analysis.

**Table 30: Standard pipetting scheme for a KLD-Reaction.**

| Reagents | Volume |
|---|---|
| PCR product | 1 µl |
| 2x KLD Reaction Buffer | 5 µl |
| 10x KLD Enzyme Mix | 1 µl |
| Ad $H_2O$ | ad 10 µl |

### 2.4.8 Cultivation of Bacterial Cultures and DNA purification

For the mini culture, a colony from the agar plate was transferred into 3 ml of LB medium with antibiotic and incubated overnight shaking at 37°C. DNA was prepared using the QIAprep® Spin Miniprep Kit: 2 ml of bacterial culture was centrifuged at 13,000 rpm for 60 seconds. Following the kit protocol, the DNA was eluted in 50 µL of EB buffer and the fragment sizes were verified by a test digest.

For the midi culture, 100 ml of LB medium with antibiotic was inoculated with the colony and incubated overnight at 37°C. DNA extraction was performed using the QIAGEN® Plasmid Plus Midi Kit, following the protocol and the DNA was eluted in 100 µl EB buffer. The concentration was measured with a Nanodrop and adjusted to 1 µg/µl. After sequencing, the DNA was entered into the institute database and stored at 4°C.

### 2.4.9 Sequencing of DNA Samples

DNA from mini and midi preparations was sequenced and the sequences were compared to those in the *Benchling.de* database. Sequencing was performed using standard primers and Sanger sequencing (TubeSeq Supreme) by Eurofins Genomics Europe Shared Services GmbH, Anzinger Straße 7a, 85560 Ebersberg, Germany (Table 31).

**Table 31: List of standard primer from Eurofins Genomics used for DNA sequencing.**

| Name | Sequence |
|---|---|
| CMVfor | 5'-cgcaaatgggcggtaggcgtg-3' |
| pCR3.1-BGHrev | 5'-tagaaggcacagtcgagg-3' |
| T7 | 5'-taatacgactcactataggg-3' |

### 2.4.10 In Vitro Transcription

To generate SFV, RNA from the pHelper plasmid and the plasmid carrying the coding sequence of the respective protein of interest was prepared. The plasmid DNA was linearized overnight at 37°C using SpeI (except for PORCN WT, which was linearized with AanI) as detailed in the following table (Table 32).

**Table 32: Standard pipetting scheme for the linearization of plasmid DNA.**

| Reagents | Volume |
|---|---|
| DNA 1 µg/µl | 20 µl |
| Fast Digest Buffer | 5 µl |
| Restriction enzyme | 5 µl |
| Ad $H_2O$ | ad 50 µl |

After incubation, the reaction was verified on a 1% agarose gel. In vitro transcription was performed using the mMessage mMachine SP6 Kit (Table 33), with the reaction incubating for three hours at 37°C, followed by adding 1 µl of Turbo DNase and a 10-minute incubation. Afterwards, 30 µl lithium chloride and 30 µl sterile water were added to the reaction mix and incubated overnight at -20°C.

**Table 33: Standard pipetting scheme for an in vitro transcription reaction.**

| Reagents | Volume |
|---|---|
| DNA (linear) | 6 µl |
| 2x NTP/CAP | 10 µl |
| Buffer | 2 µl |
| Enzyme mix | 2 µl |

The RNA was centrifuged at 4°C for 30 minutes and the pellet washed with 1 ml of 70% ethanol. After centrifuging again for 15 minutes, the pellet was dried and dissolved in 30 µl of water. RNA concentration was measured and the correct size was verified on 1% agarose gel. The RNA was aliquoted and stored at -80°C.

## 2.5 Protein Analysis

### 2.5.1 Membranepreparation of HeLa Cells and Hippocampal Neurons

Membrane preparation was used to separate the soluble and membrane fractions of HeLa cells and hippocampal neurons, following similar steps unless stated otherwise. HeLa cells were seeded in 6-well plates and transfected one day prior to preparation. Hippocampal neurons were transduced with lentivirus at 14 DIV or with Semliki Forest virus at 20 DIV. Three 6-well or six 12-well plates were used for protein analysis.

For both cell types, cells were washed with warm DPBS, detached with a scraper and transferred to a 15 ml tube. After centrifugation at 1,000 rpm for two minutes, the supernatant was discarded and cells were resuspended in 500 µl homogenization buffer (Table 34). Cells were lysed by ultrasound (HeLa: 4–5 output control; hippocampal neurons: 3, 50% duty cycle) with twelve initial and eight subsequent pulses. The cell suspension was pelleted at 1,000 rcf at 4°C for ten minutes. For whole-cell lysates, 75 µl lysate was mixed with 20 µl 5x Laemmli buffer and 5 µl 2 M DTT and heated at 37°C for ten minutes.

The membrane fraction was isolated by ultracentrifugation in ultracentrifugation tubes (Beckman Coulter 357448) at 125,000 g at 4°C for 35 minutes. The supernatant (soluble

fraction) was discarded and the membrane pellet was resuspended in 100 µl 1x Laemmli buffer with 100 mM DTT, followed by heating at 37°C for ten minutes.

**Table 34: Composition and concentration of the homogenization buffer.**

| | Stock | Final concentration |
|---|---|---|
| TRIS HCL pH 7.5 | 1 M | 20 mM |
| IAA | 100 mM | 1 mM |
| EDTA | 500 mM | 1 mM |
| NaCl | 2 M | 150 mM |
| PI-Mix | 1,000x | 1x |

For co-IP, the pellet was resuspended in 350 µl solubilization buffer (Table 35) and incubated on ice for 30 minutes with repeated vortexing. The sample was then ultracentrifuged at 131,000 g and 4°C for 25 minutes, resulting in a membrane-enriched fraction for co-IP with magnetic beads.

**Table 35: Composition and concentration of the solubilization buffer.**

| | Stock | Final concentration |
|---|---|---|
| TRIS HCL pH 7.5 | 1 M | 20 mM |
| IAA | 100 mM | 1 mM |
| EDTA | 500 mM | 1 mM |
| NaCl | 2 M | 150 mM |
| PI-Mix | 1,000x | 1x |
| Dodecanoylsucrose | 10% | 1% |

### 2.5.2 Coupling of Magnetic Beads

Magnetic beads (Dynabeads™ G, Invitrogen 10004D, for mouse antibodies; Dynabeads™ A, Invitrogen 10002D, for rabbit antibodies) were used for the co-IP. The composition of the coupling solutions is listed in Chapter 2.1.2. The required amount of beads was transferred into a Protein LoBind® Tube (Eppendorf 0030108116), washed twice with PBS-T and incubated with antibody loading solution on a rotating wheel (0.1 mg/ml in PBS-T) for 60 minutes (Dynabeads™ A) or 100 minutes (Dynabeads™ G). Following incubation, the beads were washed twice with washing solution, then equilibrated with coupling solution. Next, Crosslinker solution was added and the beads were incubated for 30 minutes. The beads were blocked by incubation in blocking solution for 120 minutes, then washed twice with cleansing solution and twice with washing solution. Finally, the beads were resuspended in PBS-T to a concentration of 0.25 µg antibody/ml and stored at 4°C until use.

### 2.5.3 Co-Immunoprecipitation

The antibody-coupled Dynabeads were sedimented in a magnetic stand and the supernatant discarded. The beads were resuspended in 1 ml solubilization buffer and divided into new tubes. From the membrane-enriched fraction, 30 µl of the sample were

mixed with 8 µl 5x Laemmli buffer and 2 µl 2M DTT (Load). The remaining solubilized sample was incubated with the beads at 4°C for two hours. After sedimenting the beads, 30 µl of the supernatant (unbound proteins) was mixed with 8 µl 5x Laemmli buffer and 2 µl 2M DTT (Unbound).

The beads were washed twice with 1 ml wash buffer (1:10 dilution of solubilization and homogenization buffers), each time on a rotating wheel for five minutes. After each wash, the supernatant was discarded. To elute bound proteins, the beads were incubated with 40 µl 1x Laemmli buffer at 37°C for ten minutes. The supernatant (eluate) was transferred to a new tube. A second elution was performed by adding 17 µl 1x Laemmli buffer and incubating at 37°C for five minutes. The eluates were combined and supplemented with 3 µl 2M DTT, then denatured at 37°C, together with the load and unbound samples, for ten minutes. The samples were either used for Western blot analysis or stored at -20°C.

### 2.5.4 SDS-PAGE

SDS gels consisted of a separating gel to separate proteins by size and a stacking gel for sample loading. The gels, containing 30% acrylamide, were prepared under the fume hood. Typically, a 10% separating gel and a 5% stacking gel were prepared (Tables 36 and 37). To prepare the gel, 5 ml of separating gel solution was poured between two glass plates with spacers and the surface was coated with isopropanol to prevent bubbles. After 30 minutes of polymerization, the isopropanol was discarded and the plates were rinsed with deionized water. A 2 ml stacking gel solution was then added and a 15 mm comb was inserted to create wells. The stacking gel polymerized for 25 minutes. The gel was used immediately for electrophoresis or stored at 4°C for later use.

**Table 36: Pipetting scheme for four 10% separating gels.**

| Reagents | Volume |
|---|---|
| 30% Acrylamide | 6.66 ml |
| 4x Separating gel buffer | 5 ml |
| TEMED | 8 µl |
| 10% APS | 200 µl |
| $H_2O$ | 8.32 ml |

**Table 37: Pipetting scheme for four 5% stacking gels.**

| Reagents | Volume |
|---|---|
| 30% Acrylamide | 1.34 ml |
| 4x Stacking gel buffer | 2 ml |
| TEMED | 8 µl |
| 10% APS | 80 µl |
| $H_2O$ | 4.6 ml |

SDS-PAGE was performed using the Mini-PROTEAN Tetra Vertical Electrophoresis Cell System (Bio-Rad). Samples were thawed if necessary. The gel plates were inserted into

the module, sealed and 1x SDS running buffer was added. The module was placed into the buffer tank and the comb was removed. The Precision Plus Protein™ Dual Color Standard (Bio-Rad 1610394) was loaded into the first well with a volume of 7 µl, followed by 10 µl of each sample into the remaining wells. The tank was filled with 1x SDS running buffer and the system was connected to the PowerPac™ HC High-Current Power Supply. The gel was first operated at a voltage of 80 V for ten minutes and then at 100 V for 110 minutes. After the run, the gel was transferred to deionized water for further processing.

### 2.5.5 Western Blotting

Proteins separated by SDS-PAGE were transferred to a PVDF membrane for antibody detection using the TransBlot Turbo System. The PVDF membrane was activated by immersion in ethanol, washed with deionized water and stored in water. The transfer setup included three layers of filter paper (Merck WHA10427818), soaked in anode or cathode buffer. The filter papers soaked in anode buffer were placed first in the TransBlot Turbo Cassette, followed by the PVDF membrane, the SDS-PAGE gel and finally, the filter papers soaked in cathode buffer. The blotting was performed at 25 V for 30 minutes. After transfer, the membrane was air-dried or blocked immediately.

Membrane blocking and antibody incubation used milk powder-TBS-T solutions: 5% for blocking and secondary antibody incubation, 2% for primary antibody incubation. The 5% solution was prepared by dissolving 2.5 g milk powder in 50 ml 1x TBS-T and the 2% solution was made by diluting it 1:2.5. Membranes were blocked for one hour at room temperature. Primary antibody was applied and incubated overnight at 4°C. After primary antibody incubation, the membrane was washed multiple times with 1x TBS-T while shaking. It was then incubated with secondary antibody for one hour at room temperature, followed by multiple washes with 1x TBS-T while shaking.

For detection, the Fusion Fx camera was used with freshly prepared developer solution (ECL™ Prime Western Blotting Detection Reagent, Amersham™ RPN2236). The membrane was dried, placed on a board, where developer solution was then applied. After adjusting the camera settings for chemiluminescence, the exposure time was optimized based on the protein and antibody used.

The membrane was stored in 1x TBS-T at 4°C for further experiments. To re-incubate with another antibody, the membrane was stripped with stripping buffer for 20 minutes, then blocked again.

## 2.6 Statistical Analysis

Statistical analyses were conducted using PRISM or Origin software. Data were normalized to the control specified in the corresponding results section and normality was tested with the Shapiro-Wilk test. For parametric data, an unpaired t-test was used for two group

comparisons and an one-way ANOVA for larger group sizes. For non-parametric data, the Mann-Whitney U test was applied for two-group comparisons and the Kruskal-Wallis test for larger groups. A two-way ANOVA on ranks was used for reconstruction data. Post hoc tests and exact p-values are provided in the results section. A significance threshold of $p < 0.05$ was applied, with no distinction made between different significance levels. P-values are presented with three decimal places and rounded where appropriate.

# 3 Results

## 3.1 PORCN Mutations Differentially Affect Dendritic Architecture

PORCN has a canonical function, as it palmitoylates Wnt in the ER and a moonlighting function as a modulator of AMPAR physiology [44, 59, 90]. PTMs have the capacity to extend the functional scope of proteins [91] and may serve as a molecular switch between PORCN's two independent functions. Potential phosphorylation sites in PORCN were previously identified in the working group using the NetPhos 3.1 prediction algorithm. Based on high prediction scores (>0.85) and presumed cytoplasmic localization, four candidate residues (S92, S186, S297, Y430) were selected and mutated in PORCN WT to mimic either a dephosphorylated (A/F) or phosphorylated (D/E) state (Figure 3A). The selection of candidate phosphorylation sites in PORCN and the generation of corresponding phospho-mutants were carried out prior to this study by members of the working group. Two of these sites (S297 and Y430) correspond to known mutation sites in FDH patients [46, 92]. Although FDH is primarily characterized by skin, skeletal and craniofacial abnormalities, neurological symptoms have also been reported in some cases [64, 65]. However, for the mutations at S297 and Y430, no neurological phenotypes have been described to date.

As a first step, the expression of PORCN WT and its mutant variants in primary hippocampal neurons was assessed to confirm successful transfection and protein production prior to subsequent functional analyses. To this end, immunofluorescence staining was performed on neurons overexpressing V5-tagged PORCN constructs. No differences in the expression were observed between PORCN WT and the respective mutants. All variants displayed a comparable expression throughout the soma and dendrites ($n \geq 3$) (Figure 3B). Interestingly, overexpression of different PORCN variants appeared to result in distinct morphological differences in hippocampal neurons.

Hippocampal neurons overexpressing the phosphomimetic mutant PORCN S297D (S/D) appeared to have fewer dendrites compared to neurons overexpressing the dephosphorylated mutant PORCN S297A (S/A) and PORCN WT (Figure 3B). Furthermore, PORCN Y430 mutations in both variants seemed to result in a smaller overall dendritic arbor compared to PORCN WT overexpressing neurons (Figure 3B).

Subsequent experimentation in heterologous systems conducted within the working group yielded no discernible impacts pertaining to the alternate potential phosphorylation sites S92X and S186X. Consequently, the focus of this study was directed solely towards a more comprehensive exploration of the amino acids S297 and Y430 in PORCN.

**A**

| AA | Context | Score | Kinase | Known FDH mutation | Reference |
|---|---|---|---|---|---|
| S92 | LCRH**S**SHRG | 0.993 | unsp. | - | |
| S186 | GRPL**S**RRWL | 0.989 | unsp. | - | |
| S297 | ELPR**S**MVEV | 0.865 | unsp. | S297L | Maas et al. 2009 |
| Y430 | EEQG**Y**GMAY | 0.956 | unsp. | Y430* | Bornholdt et al. 2009 |

**B**

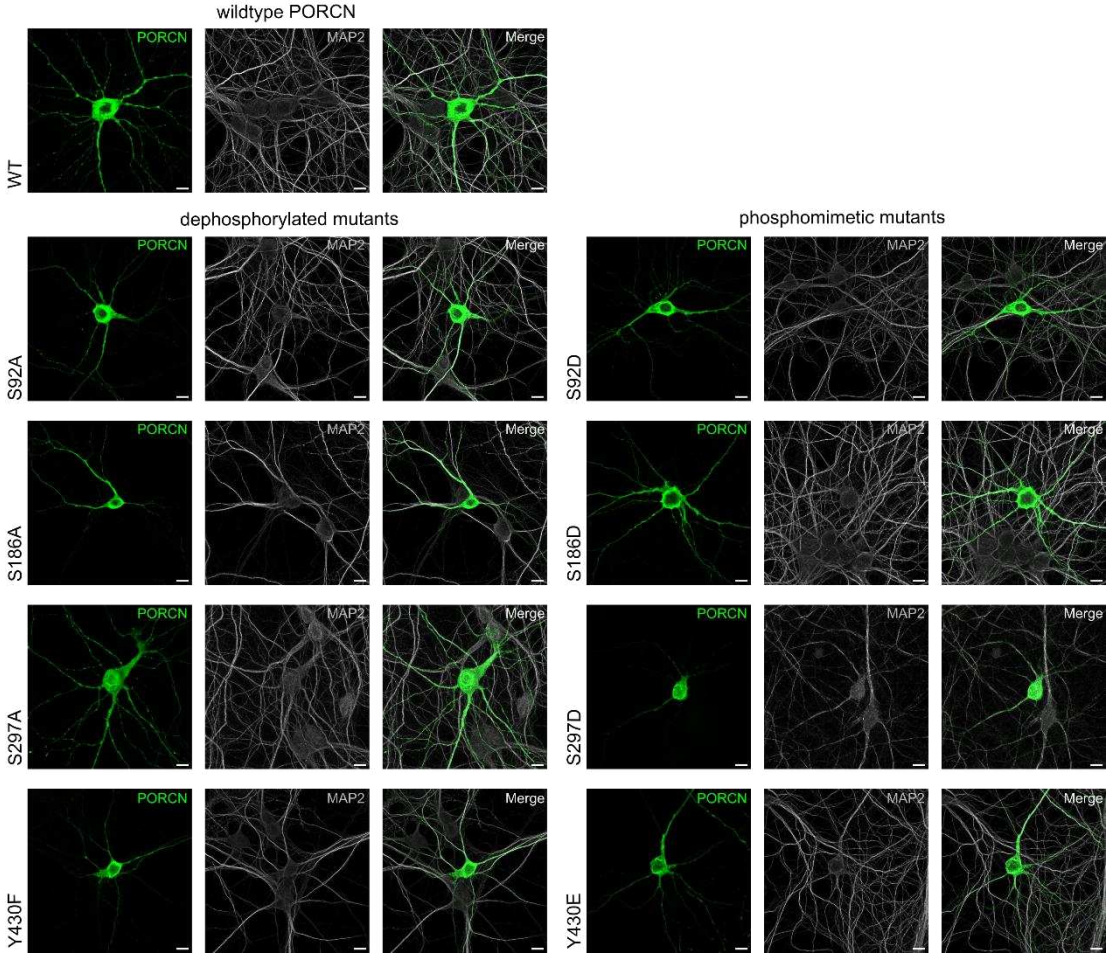


**Figure 3: Possible phosphorylation sites in PORCN affect the morphology of hippocampal neurons.**

**A:** Phosphorylation sites were predicted using NetPhos3.1. Four phosphorylation sites meet the criteria of a prediction score above 0.85 and localization in the cytoplasm. Two possible phosphorylation sites (S297 and Y430) are known as FDH mutation sites. **B:** Immunofluorescence staining of hippocampal neurons overexpressing PORCN WT and PORCN mutants that mimic a dephosphorylated (S→A/ Y→F) or a phosphorylated (S→D/ Y→E) state. PORCN-overexpressing neurons were identified using a rabbit anti-V5 antibody and dendrites were stained using an anti-MAP2 antibody. Hippocampal neurons overexpressing the phosphomimetic mutant PORCN S297D show fewer dendrites compared to PORCN S297A and PORCN WT overexpressing mutants. The mutations at Y430 both lead to smaller dendritic trees compared to PORCN WT.
Z-stack immunofluorescence images of hippocampal neurons were acquired on an LSM710 confocal microscope using a 63x objective (n ≥ 3). Bar represents 10 µm.
A= Alanine; D = Aspartic acid; E = Glutamic acid; F = Phenylalanine; FDH = Focal dermal hypoplasia; MAP2 = Microtubule-associated protein 2; PORCN = Porcupine S = Serine; unsp. = unspecific; WT = Wild type; Y= Tyrosine.

## 3.2 Phosphomimetic Mutant PORCN S297D Reduces Neuronal Outgrowth and Synaptic Transmission

The analysis of the expression of PORCN variants in hippocampal neurons revealed distinct qualitative differences in the morphology of hippocampal neurons overexpressing PORCN S/D and neurons overexpressing PORCN S/A or PORCN WT.

### 3.2.1 PORCN S297D Alters Dendritic Complexity in Hippocampal Neurons

To achieve a more precise quantification of these differences, reconstructions of PORCN overexpressing hippocampal neurons were performed and dendritic length was determined using Sholl analysis. The reconstruction of neurons provides important insight into structural features such as dendritic length and complexity, which are key determinants of neuronal functional capacity [93].

Overlaying of all reconstructed neurons revealed that overexpression of the PORCN S/D (n = 23) variant led to reduced dendritic arborization compared to neurons expressing PORCN WT (n = 20) or the PORCN S/A (n = 25) variant (Figure 4A). Density plots were used to visualize the distribution of dendritic length per 25 µm² based on the overlay of all reconstructed neurons. In regions proximal to the soma, dendritic length per 25 µm² was comparable across all three groups (Figure 4B). The plots demonstrated that neurons transfected with PORCN S/D exhibited a reduced distal dendritic span and lower distal complexity compared to neurons expressing PORCN WT or PORCN S/A (Figure 4B). Sholl analysis of apical dendrites revealed a significant reduction in dendritic length in hippocampal neurons overexpressing PORCN S/D compared to those expressing PORCN WT or PORCN S/A ($p_{(WT\_S/D)} < 0.001$; $p_{(S/A\_S/D)} < 0.001$) (Figure 4C). The apical dendritic length of neurons overexpressing PORCN S/A was significantly increased compared to those expressing PORCN WT ($p_{(WT\_S/A)} = 0.002$) (Figure 4C). Neurons overexpressing PORCN S/D displayed a significant reduction in basal dendritic length compared to those expressing either PORCN WT or PORCN S/A ($p_{(WT\_S/D)} < 0.001$; $p_{(S/A\_S/D)} < 0.001$) (Figure 4D). Overexpression of PORCN S/A did not alter the basal dendritic outgrowth of neurons compared to PORCN WT ($p_{(WT\_S/A)} > 0.999$) (Figure 4D). Overall, total dendritic length per cell was significantly reduced in neurons overexpressing PORCN S/D compared to those expressing PORCN WT or PORCN S/A (WT = 84.41 ± 4.5 µm; S/A = 95.9 ± 7.0 µm; S/D = 37.7 ± 3.7 µm; $p_{(WT\_S/A)} > 0.999$; $p_{(WT\_S/D)} < 0.001$; $p_{(S/A\_S/D)} < 0.001$). These results confirm that overexpression of the phosphomimetic mutant PORCN S/D negatively affects neuronal outgrowth compared to both the dephosphorylated mutant PORCN S/A and PORCN WT.

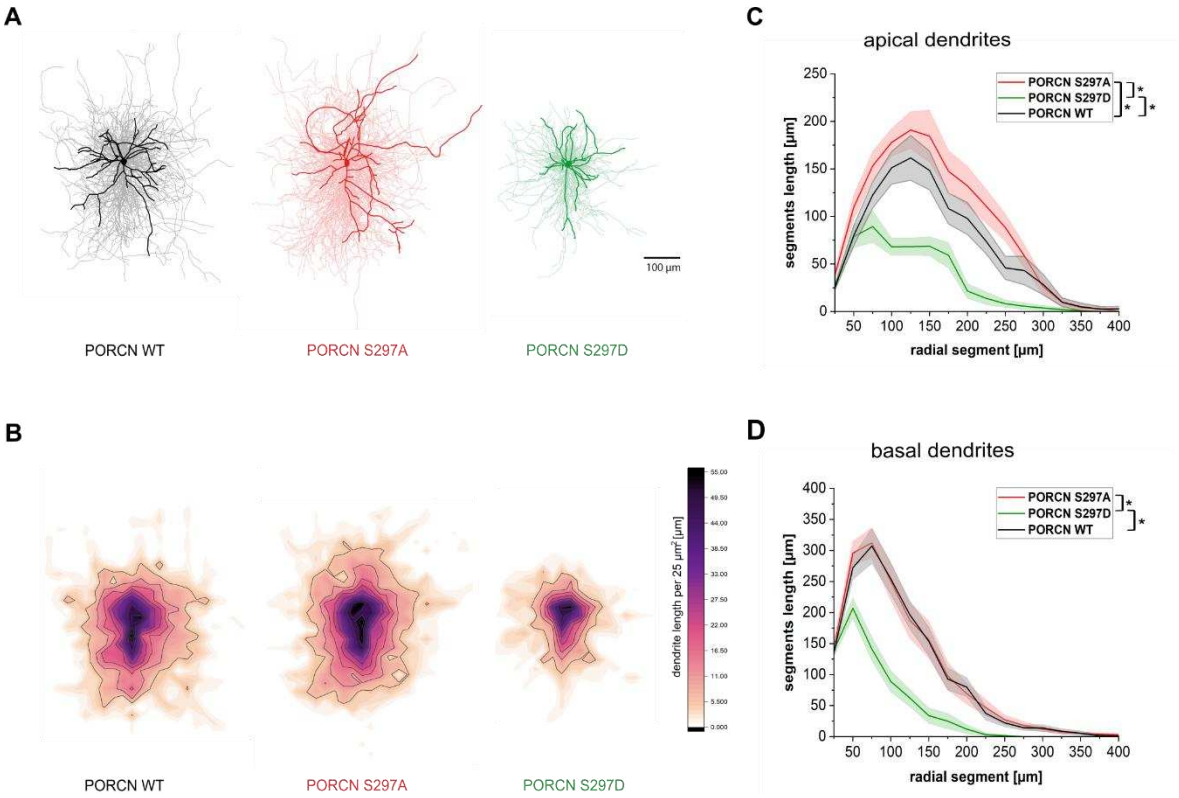


**Figure 4: The overexpression of PORCN S297D results in a decrease in the lengths of apical and basal dendrites in hippocampal neurons.**
**A:** Overlap of all manually reconstructed hippocampal neurons overexpressing PORCN WT (black; n = 20), PORCN S297A (red, S/A; n = 25) or PORCN S297D (green, S/D; n = 23). Hippocampal neurons were transfected with the respective V5-tagged PORCN and stained using rabbit anti-V5 tag antibody and anti-MAP2 antibody. Overexpression of PORCN S/D reduces the size of the dendritic tree. **B:** Density plots of PORCN WT, PORCN S/A and PORCN S/D overexpressing hippocampal neurons. Density was determined from the total number of reconstructed hippocampal neurons in 25 µm$^2$ squares. Transfection of hippocampal neurons with PORCN S/D leads to a smaller span and a lower distal complexity of the dendritic trees compared to PORCN WT and PORCN S/A expressing neurons. **C, D:** Sholl analysis of the reconstructed hippocampal neurons. Overexpression of PORCN S/D in hippocampal neurons leads to a significant reduction in the length of apical and basal dendrites compared to PORCN WT and PORCN S/A overexpressing hippocampal neurons (apical: $p_{(WT\_S/D)} < 0.001$; $p_{(S/A\_S/D)} < 0.001$; basal: $p_{(WT\_S/D)} < 0.001$; $p_{(S/A\_S/D)} < 0.001$). The length of apical dendrites of hippocampal neurons overexpressing PORCN S/A is significantly reduced, while the length of basal dendrites remains unchanged compared to neurons overexpressing PORCN WT (apical: $p_{(WT\_S/A)} = 0.002$; basal: $p_{(WT\_S/A)} > 0.999$).
Data are presented as mean ± SEM. Statistics: Two-way RM ANOVA + Bonferroni correction; significance shown for group comparisons only. Density plots were created by Prof. Dr. Max Anstötz. A= Alanine; D = Aspartic acid; PORCN = Porcupine; RM = repeated measures; S = Serine; WT = Wild type.

### 3.2.2 Functional Consequences of PORCN S297X Mutations on AMPAR-Mediated Synaptic Transmission

Following the observed reduction in dendritic length in hippocampal neurons overexpressing PORCN S/D, the effect of PORCN WT and its mutants on AMPA receptor-mediated synaptic transmission was investigated. This approach was motivated by evidence suggesting that reduced dendritic complexity is often associated with decreased

AMPAR expression and synaptic efficacy, whereas enhanced dendritic arborization supports higher AMPAR-mediated transmission [94, 95]. To determine whether the observed morphological alterations were accompanied by corresponding functional changes at the synapse, AMPAR-mediated mEPSCs were recorded by Kelvin Tofan (Institute of Anatomy II, Heinrich Heine University Düsseldorf). The mEPSC frequency was significantly reduced in PORCN S/D-overexpressing neurons (3.5 ± 0.6 Hz; n = 17), compared to PORCN WT (5.9 ± 1.2 Hz; n = 21) and PORCN S/A (5.1 ± 0.7 Hz; n = 26) ($p_{(WT\_S/D)}$ = 0.045; $p_{(S/A\_S/D)}$ = 0.045) (Figure 5B). No significant differences were detected between neurons overexpressing PORCN WT and PORCN S/A (p > 0.999). The current amplitude of recorded mEPSCs was significantly reduced in neurons overexpressing either PORCN S/A (11.47 ± 0.9 pA) or PORCN S/D (11.67 ± 0.6 pA), compared to PORCN WT (14.72 ± 1.1 pA) ($p_{(WT\_S/A)}$ = 0.041; $p_{(WT\_S/D)}$ = 0.046) (Figure 5C). No significant difference in amplitude was observed between PORCN S/A- and S/D-expressing neurons (p > 0.999).

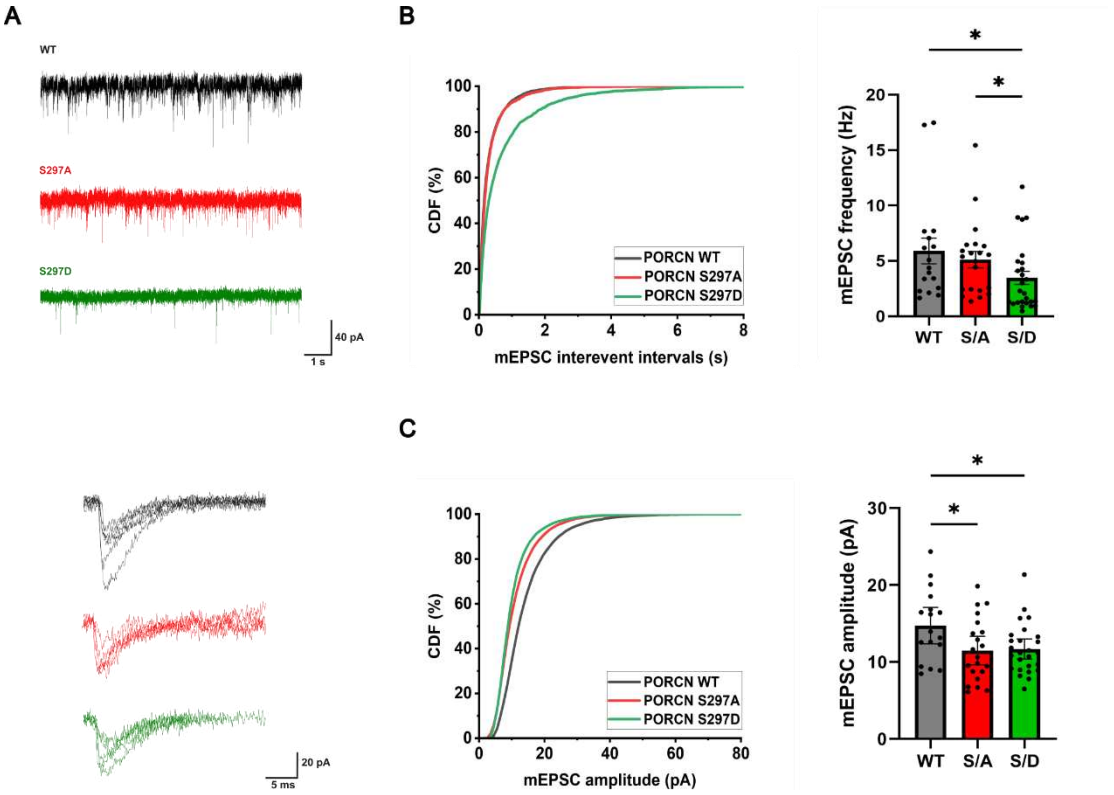


**Figure 5: Overexpression of PORCN S297D reduces the frequency and amplitude of AMPAR-mediated mEPSCs.**
**A:** Representative recordings from AMPAR-mediated mEPSCs are shown, along with an overlay of five individual mEPSCs for each experimental condition. **B:** Frequencies of mEPSCs from hippocampal neurons overexpressing PORCN WT (grey, WT; n = 17), PORCN S297A (red, S/A; n = 21) and PORCN S297D (green, S/D; n = 26). The frequencies were presented as cumulative distribution functions (CDFs) and additionally as mean ± SEM in bar graphs. Hippocampal neurons were transfected with the respective V5-tagged PORCN and subjected to electrophysiological measurements. It is remarkable that there is a significant reduction in the frequency of mEPSCs in hippocampal neurons transfected with PORCN S/D (3.5 ± 0.6 Hz), in comparison with both PORCN WT (5.9 ± 1.2 Hz; p = 0.045) and PORCN S/A (5.1 ± 0.7 Hz; p = 0.045). There is no significant difference in the frequency of PORCN WT and PORCN S/A overexpressing neurons (p > 0.999). **C:** Amplitudes of mEPSCs from hippocampal neurons overexpressing PORCN WT, PORCN S/A

and PORCN S/D presented as CDF and bar graph with mean ± SEM. The amplitudes of the mEPSCs in these neurons are significantly diminished in the case of PORCN S/D overexpression at 11.7 ± 0.6 pA ($p = 0.046$) and PORCN S/A overexpression at 11.5 ± 0.9 pA ($p = 0.041$), in contrast to PORCN WT (14.7 ± 1.1 pA). The amplitude does not significantly differ between PORCN S/A and PORCN S/D overexpressing neurons ($p > 0.999$).
Data are shown as mean ± SEM. Statistics: Kruskal-Wallis test + Dunn's multiple comparisons test (frequency); one-way ANOVA + Bonferroni correction (amplitude).
A = Alanine; D = Aspartic acid; mEPSCs = Miniature excitatory postsynaptic currents; PORCN = Porcupine; S = Serine; WT = Wild type.

Dendritic length correlates with the frequency of mEPSC events [94]. Consistent with the morphological data (Figure 4), the frequency of AMPAR mediated mEPSCs was significantly reduced in PORCN S/D overexpressing hippocampal neurons. The amplitudes of PORCN S/A and PORCN S/D overexpressing cells were lower than the WT amplitude. To investigate why PORCN S/A overexpression resulted in reduced mEPSC amplitude despite unchanged neuronal morphology, rise time and decay kinetics were examined, with particular attention to their variability. Analyzing the coefficient of variation (CV) provides insights into the heterogeneity of AMPAR-mediated responses, which may reflect changes in receptor dynamics or synaptic integration (Figure 6).

The rise time (10% to 90%) was significantly increased in PORCN S/A-expressing neurons (3.5 ± 0.3 ms; $n = 21$) compared to PORCN WT (2.4 ± 0.2 ms; $n = 17$; $p = 0.015$). There were no differences in the rise time between PORCN S/A and PORCN S/D overexpressing cells observed, with a value of 2.7 ± 0.2 ms ($n = 26$; $p = 0.240$). Also, no difference between PORCN WT and PORCN S/D was detected ($p = 0.241$) (Figure 6A). Moreover, PORCN S/A overexpression was associated with a significant increase in the rise time variability, as indicated by a higher CV (0.14 ± 0.01), compared to PORCN WT (0.11 ± 0.01) and PORCN S/D (0.12 ± 0.01) ($p_{(WT\_S/A)} = 0.016$; $p_{(S/D\_S/A)} = 0.032$) (Figure 6A). The CV of rise time did not significantly differ between neurons expressing PORCN WT and those expressing PORCN S/D ($p > 0.999$). The decay time constant ($\tau_{decay}$) was significantly increased in neurons overexpressing PORCN S/A (10.8 ± 0.8 ms) compared to PORCN WT (7.9 ± 0.7 ms) and PORCN S/D (8.5 ± 0.5 ms) ($p_{(WT\_S/A)} = 0.020$; $p_{(S/D\_S/A)} = 0.048$) (Figure 6B). No significant difference in $\tau_{decay}$ was observed between PORCN WT and PORCN S/D ($p > 0.999$). The CV of $\tau_{decay}$ was not significantly different across all groups (WT = 0.3 ± 0.02; PORCN S/A = 0.2 ± 0.02; PORCN S/D = 0.2 ± 0.01; ($p_{(WT\_S/A)} = 0.446$; $p_{(WT\_S/D)} = 0.901$; $p_{(S/A\_S/D)} > 0.999$) (Figure 6B). In PORCN S/A-overexpressing neurons, both the rise time and its CV were increased, indicating a greater heterogeneity in AMPAR activation. Additionally, the decay time constant was prolonged, while the CV of decay time constant remained unchanged. These changes in AMPAR kinetics occurred despite a reduction in mEPSC amplitude. The data suggest that altered receptor properties, possibly related to subunit composition or differential interaction with AMPAR auxiliary proteins may underlie the observed functional effects.

It has been shown previously, that PORCN KD leads to a depletion of TARPγ8 from the AMPAR complexes, which in turn reduces mEPSC amplitude and frequency, accompanied by faster desensitization kinetics [59]. To determine whether the observed changes in mEPSCs in neurons overexpressing PORCN mutants result from a dissociation of TARPγ8 from the AMPAR complexes, co-IPs were performed (n = 4). HeLa cells were transfected with PORCN variants, TARPγ8 and GluA1 to determine if PORCN WT and TARPγ8 interact with each other independently and if the PORCN mutants also interact with TARPγ8 and GluA1. PORCN WT interacted with TARPγ8 independently (Figure 6C). The mutants PORCN S/A and PORCN S/D interacted with GluA1 and TARPγ8 in HeLa cells (Figure 6C). The results suggest that the reduced mEPSC amplitude and frequency do not appear to result from a loss of TARPγ8 association with the AMPAR complexes.

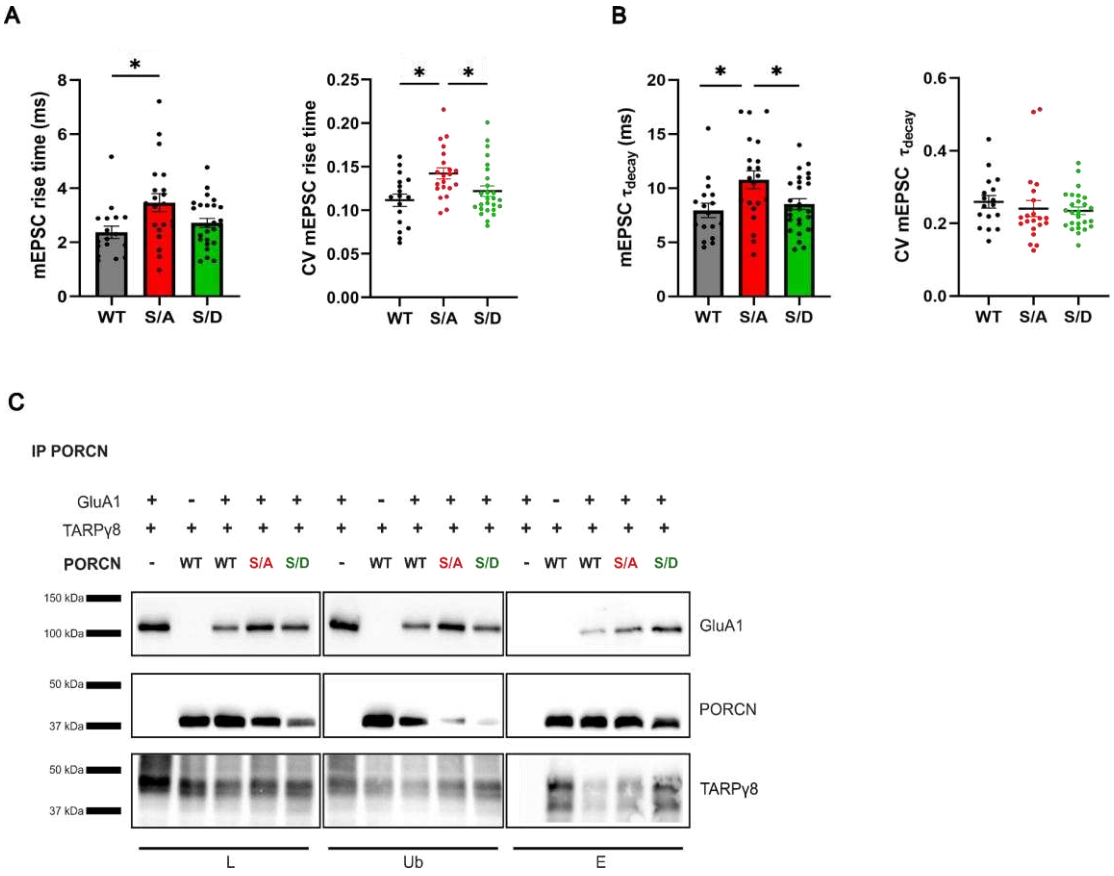


**Figure 6: Overexpression of the phosphodeficient PORCN S297A mutant increases the rise time and decay time constant of AMPAR-mediated mEPSCs in hippocampal neurons.**
**A**: The rise time (10% to 90%) and coefficient of variation (CV) of rise time of AMPAR-mediated mEPSCs of hippocampal neurons overexpressing PORCN WT (grey, WT; n = 17), PORCN S297A (red, S/A; n = 21) and PORCN S297D (green, S/D; n = 26). The overexpression of PORCN S/A (3.5 ± 0.3 ms) has been observed to result in a notable increase in mEPSC rise time when compared to PORCN WT (2.4 ± 0.2 ms) in hippocampal neurons (p = 0.015). PORCN S/A rise time does not significantly differ from PORCN S/D rise time (2.7 ± 0.2 ms; p = 0.240). Also, no difference between PORCN WT and PORCN S/D is detected (p = 0.241). The CV of the rise time is markedly elevated to 0.14 ± 0.01 in neurons exhibiting PORCN S/A overexpression in comparison to PORCN WT (0.11 ± 0.01; p = 0.016) and PORCN S/D overexpressing cells (0.12 ± 0.01; p = 0.032). The CV of the rise time does not significantly change between PORCN WT and PORCN S/D (p > 0.999). **B**: AMPAR-mediated mEPSC decay time constant ($\tau_{decay}$) and CV of $\tau_{decay}$. The overexpression of PORCN S/A results in a significant increase to 10.8 ± 0.8 in $\tau_{decay}$ in hippocampal neurons when

compared to PORCN WT at 7.9 ± 0.7 ($p = 0.020$) and PORCN S/D at 8.5 ± 0.5 ($p = 0.048$). The $\tau_{decay}$ is not different between PORCN WT and PORCN S/D overexpressing neurons ($p > 0.999$). The CV of $\tau_{decay}$ is identical across all three groups (WT = 0.3 ± 0.02; S/A = 0.2 ± 0.02; S/D = 0.02 ± 0.01; $p_{(WT\_S/A)} = 0.446$; $p_{(WT\_S/D)} = 0.901$; $p_{(S/A\_S/D)} > 0.999$). **C:** Representative Western blot of co-IPs of HeLa cells co-transfected with PORCN WT or mutants alongside with GluA1 and TARPγ8 (n = 4). The sample without PORCN serves as a negative control, while the sample without GluA1 serves as a positive control for the independent interaction between PORCN and TARPγ8. PORCN WT as well as PORCN S/A and PORCN S/D interact with GluA1 and TARPγ8.
Data are presented as mean ± SEM. Statistics: One-way ANOVA + Bonferroni multiple comparisons test ($\tau_{decay}$); Kruskal-Wallis test + Dunn's multiple comparisons test (rest).
A = Alanine; D = Aspartic acid; E = Eluate; GluA1 = Glutamate receptor ionotropic, AMPA 1; co-IP = Co-immunoprecipitation; kDa = Kilodalton; L = Load; mEPSCs = Miniature excitatory postsynaptic currents; PORCN = Porcupine; S = Serine; Ub = Unbound; WT = Wild type.

### 3.2.3 PORCN S297X Mutants Show ER Localization Similar to Wild Type

The initial analysis focused solely on the expression of PORCN variants within neurons, without resolving specific subcellular compartments. To verify and refine these findings, co-staining with the ER marker Calnexin was performed to determine whether PORCN mutants localize to the ER as PORCN WT. The immunofluorescence staining revealed that the cell compartments of the wild type and the mutants exhibit identical staining for Calnexin and PORCN, thereby indicating their localization within the ER ($n \geq 5$) (Figure 7). Differences in subcellular localization between wild type and mutant PORCN variants can therefore be excluded as the cause of the observed phenotypic effects. Furthermore, the staining revealed no aggregation of the respective proteins, ruling out altered stability or folding of PORCN as a potential source of the observed effects.

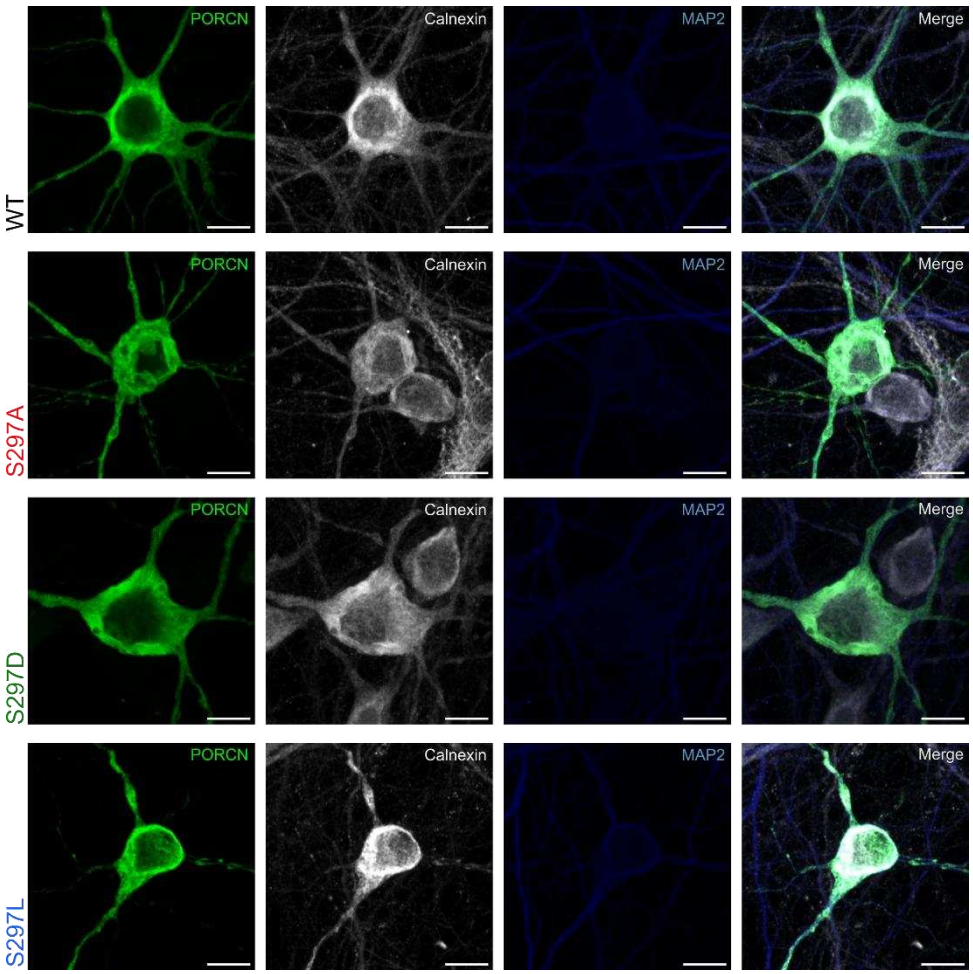


**Figure 7: PORCN WT and PORCN S297X mutants are localized in the ER.**
Representative images of hippocampal neurons overexpressing the respective PORCN variant. Cells were transfected with V5-tagged PORCN variants and stained using mouse anti-V5 antibody PORCN, anti-Calnexin antibody and anti-MAP2 antibody. Calnexin served as an ER marker, while MAP2 served as a vitality control for neuronal networks. PORCN WT as well as PORCN S297X mutants are located in the ER of hippocampal neurons.
Z-stacks were acquired with an 63x objective using an LSM710 confocal microscope (n ≥ 5). Bar represents 10 µm.
A = Alanine; D = Aspartic acid; L = Leucine; MAP2 = Microtubule-associated protein 2; PORCN = Porcupine; S = Serine; WT = Wild type.

### 3.2.4 PORCN S297D Increases GluA1 Surface Levels While Reducing Wnt5a Secretion in HeLa Cells

Given that morphological changes may account for the observed reduction in mEPSC frequency, the underlying cause of the decreased mEPSC amplitude remained unclear. Considering the dual function of PORCN in AMPAR regulation and Wnt signaling, the study aimed to determine whether the functional alterations arise from changes in GluA1 (surface) expression or from impaired Wnt secretion.

To evaluate the impact of PORCN variants on AMPAR expression, total GluA1 levels were analyzed in whole-cell lysates of HeLa cells overexpressing PORCN WT or mutants, in the presence or absence of co-transfected GluA1 (n = 3). Cells transfected with GluA1 alone served as a control to represent baseline GluA1 expression in HeLa cells. Both, the PORCN

variants and β-actin, were expressed at comparable levels across all samples, confirming equal protein loading and expression. Notably, total GluA1 levels were reduced in HeLa cells co-expressing PORCN WT, PORCN S/A and PORCN S/D compared to cells transfected with GluA1 alone, with no differences between the different PORCN variants (Figure 8A).

The surface expression assay employed in this study was based on a chemiluminescent detection method. HeLa cells were co-transfected with GluA1 and the respective PORCN constructs to evaluate GluA1 surface expression in the presence of PORCN mutants. In heterologous cell systems, PORCN decreases GluA1 surface expression, as reported by Erlenhardt et al. in HEK293T cells [59]. In this study, HeLa cells were used, where GluA1 surface levels were reduced to less than 5% in the presence of PORCN WT compared to its absence.

Normalized to PORCN WT co-expression with 100.0 ± 3.0%, the relative GluA1 surface expression was slightly increased at 116.6 ± 7.8% in PORCN S/A co-expressing cells and significantly increased at 130 ± 4.3% in PORCN S297D co-expressing cells ($p_{(WT\_S/A)}$ = 0.100; $p_{(WT\_S/D)}$ = 0.002) (Figure 8B). There was no significant difference between PORCN S/A and PORCN S/D co-expressing cells in the relative GluA1 surface expression (p = 0.211). The phosphomimetic mutant S297D attenuated the negative effect of PORCN on surface GluA1 levels relative to PORCN WT.

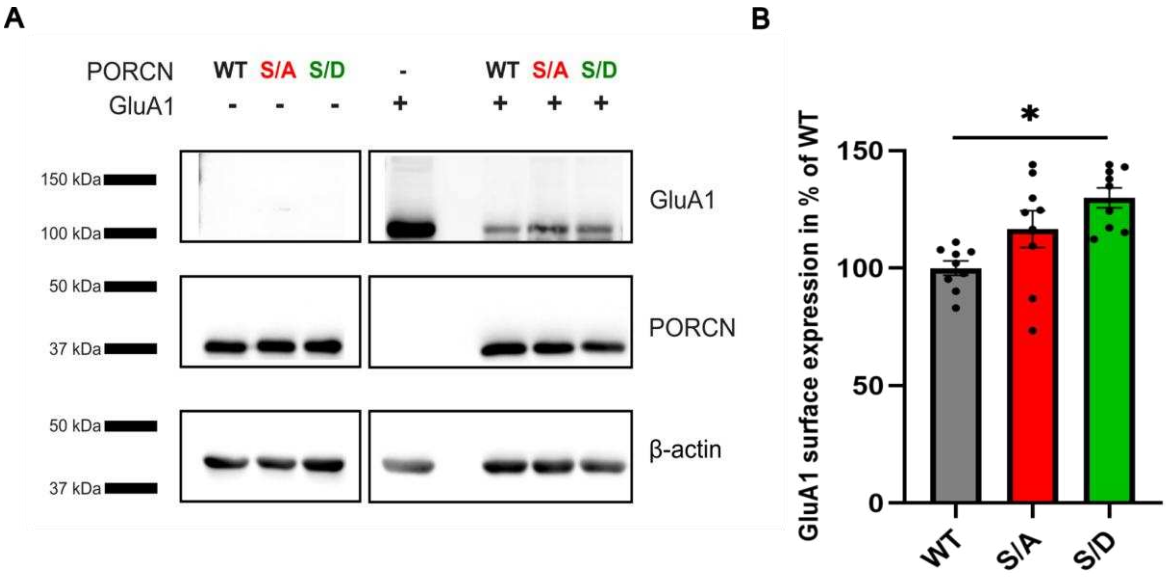


**Figure 8: Phosphomimetic mutant PORCN S297D attenuates the PORCN effect on GluA1 surface expression in HeLa cells.**
**A:** Representative Western blot of whole-cell lysates of HeLa cells transfected with PORCN WT (grey, WT), PORCN S297A (red, S/A) or PORCN S297D (green, S/D) alone or together with GluA1 (n = 3). GluA1 was detected at 102 kDa using anti-GluA1 antibody and V5-tagged PORCN was detected at 38 kDa using mouse anti-V5 antibody. The loading control was β-actin, detected at 42 kDa. All PORCN variants are equally expressed. Total GluA1 levels are decreased when PORCN variants are co-transfected with GluA1. **B:** Surface expression of GluA1 in HeLa cells was detected using a chemiluminescence approach where an extracellular HA-tag on GluA1 was detected using

anti-HA antibody. The data were normalized to GluA1 co-transfected with PORCN WT. Compared to a relative GluA1 surface expression of 100.0 ± 3.0% in HeLa cells co-transfected with GluA1 and PORCN WT, PORCN S/D co-transfection significantly increases the relative GluA1 surface expression to 130 ± 4.3% ($p = 0.002$), whereas the co-transfection of PORCN S/A results in a relative GluA1 surface expression of 116.6 ± 7.8% with no significant difference to the WT ($p = 0.100$) and to S/D ($p = 0.211$).
Original full-length blots in supplementary (Figure 24). Data are shown as mean ± SEM with n = 9 for all data. Statistics: One-way ANOVA + Tukey's multiple comparisons test.
A = Alanine; D = Aspartic acid; GluA1 = Glutamate receptor ionotropic, AMPA 1; kDa = Kilodalton; PORCN = Porcupine; S = Serine; WT = Wild type.

The next step involved investigating whether the observed effects could be attributed to altered Wnt secretion. Since the interaction between Wnt and PORCN is essential for Wnt secretion, it was first examined whether the PORCN mutants retained the ability to interact with Wnt using co-IPs in HeLa cells (n = 3). Although expression levels of the PORCN variants varied, all variants retained the ability to interact with Wnt5a (Figure 9A). Wnt5a was expressed equally throughout all samples (Figure 9A).

Since all PORCN variants were shown to interact with Wnt5a, the amount of Wnt5a secreted in the presence of each variant was quantified next. The Wnt5a secretion was normalized to cells co-expressing PORCN WT and Wnt5a (n = 14; relative Wnt5a secretion = 100.0 ± 4.8%) (Figure 9B). As controls, cells were transfected either with a pcDNA3.1+ vector (no Wnt5a) or with Wnt5a without PORCN co-expression (no PORCN). Co-transfection with PORCN WT significantly increased relative Wnt5a secretion compared to the no Wnt5a-control (14.6 ± 1.9%; $p < 0.001$). Without the co-transfection of PORCN WT, the Wnt5a secretion was limited to 67.5 ± 4.6% after inhibiting the enzymatic function of endogenous PORCN in HeLa cells ($p = 0.019$). Co-Expression of Wnt5a with PORCN S/D significantly reduced the relative Wnt5a secretion to 68.9 ± 8.6% in comparison with PORCN WT ($p = 0.045$). No significant difference in relative Wnt5a secretion was observed between cells co-expressing PORCN WT and those expressing the PORCN S/A mutant (99.3 ± 6.0%; $p > 0.999$). Examination of Wnt5a secretion in HeLa cells indicated that the PORCN S/A mutation did not affect the ability of PORCN to promote Wnt5a secretion under the tested conditions, while PORCN S/D co-expression reduced Wnt5a secretion.

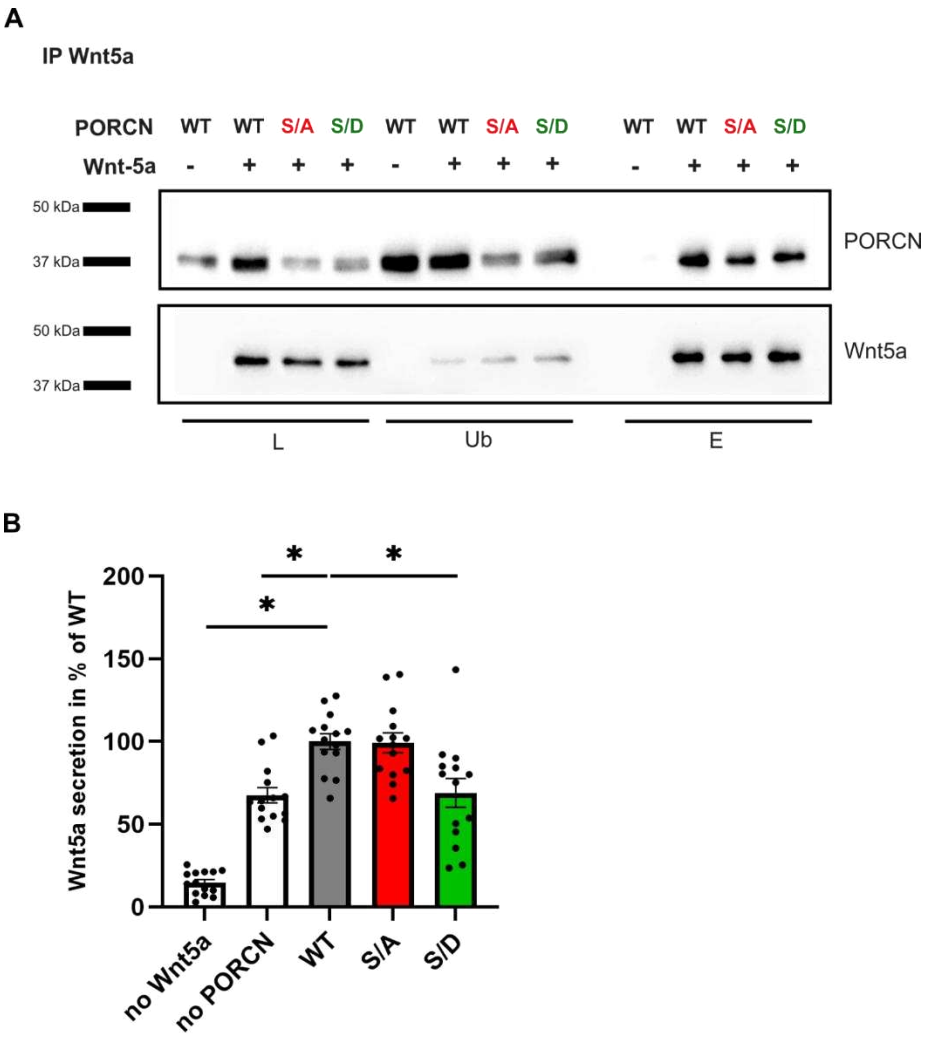


**Figure 9: PORCN S297D significantly reduces Wnt5a secretion in HeLa cells.**
**A:** Representative Western blot of co-IPs with V5(Wnt5a)-conjugated beads (n = 3). Samples consisted of HeLa cells overexpressing Flag-tagged PORCN WT (grey), PORCN S297A (red, S/A) or PORCN S297D (green, S/D) together with V5-tagged Wnt5a. PORCN WT alone served as a negative control, whereas co-expression of PORCN WT together with Wnt5a served as a positive control for co-IP. PORCN was detected at 38 kDa using an anti-FlagM2 mouse antibody and Wnt5a was detected at 42 kDa using a mouse anti-V5 antibody. All PORCN variants are detectable in the load fraction, with differences in the protein expression levels. Wnt5a expression is consistent across all samples. PORCN together with Wnt5a is detected in the eluate of each sample. PORCN WT and mutants interact with Wnt5a in a Wnt5a-related co-IP in HeLa cells. **B:** Relative Wnt5a secretion in HeLa cells overexpressing PORCN WT, PORCN S/A or PORCN S/D. Wnt5a secretion was quantified using a luminescence-based measurement approach. Wnt5a was fused with NanoLuc and detected in the supernatant of overexpressing HeLa cells following inhibition of endogenous PORCN by Wnt-C59. Control conditions included HeLa cells transfected with pcDNA3.1+ (lacking Wnt5a) and cells transfected with Wnt5a alone (lacking PORCN). Data were normalized and compared to Wnt5a secretion in WT-overexpressing cells (relative Wnt5a secretion = 100.0 ± 4.8%). The co-transfection of PORCN WT significantly increases relative Wnt5a secretion compared to no Wnt5a transfection at 14.6 ± 1.9% ($p < 0.001$) and no PORCN transfection at 67.5 ± 4.6% ($p = 0.019$). Co-transfection of PORCN S/D significantly reduces the relative Wnt5a secretion to 68.9 ± 8.6% compared to PORCN WT ($p = 0.045$). The relative Wnt5a secretion does not differ between PORCN WT and PORCN S/A (99.3 ± 6.0%; $p > 0.999$).
Data are presented as mean ± SEM and n = 14 for all data. Statistics: Kruskal-Wallis test + Dunn's test for multiple comparisons in comparison to the WT.
A = Alanine; D = Aspartic acid; E = Eluate; co-IP = co-Immunoprecipitation; kDa = Kilodalton; L = Load; PORCN = Porcupine; S = Serine; Ub = Unbound; WT = Wild type.

To summarize, neuronal outgrowth and glutamatergic synaptic transmission were reduced in hippocampal neurons overexpressing the phosphomimetic mutant PORCN S/D compared to neurons overexpressing PORCN WT or PORCN S/A. In HeLa cells, overexpression of PORCN S/D attenuated the decrease in relative GluA1 surface expression and reduced Wnt5a secretion compared to PORCN WT. These findings suggest that phosphorylation at serine 297 in PORCN may differentially regulate its functional roles.

## 3.3 Disease-Associated PORCN Mutant S297L Reduces Dendritic Length, in Contrast to the PORCN Mutant Lacking Enzymatic Activity

The rare disease FDH is a X-linked genetic disorder caused by mutations in the *PORCN* gene, disrupting Wnt signaling and leading to a broad spectrum of developmental abnormalities [46]. Two patients with FDH were identified for a mutation at amino acid 297 in *PORCN* where serine was mutated to leucine [92]. PORCN mutants resulting in FDH can be classified into three distinct categories: low expression, expression with low catalytic activity and wild type catalytic activity. The PORCN mutant S297L (S/L) falls into the second category, because it has been shown that this mutation reduces the enzymatic activity of PORCN while maintaining an expression level comparable to that of PORCN WT, resulting in reduced Wnt secretion [96]. The negative effect of PORCN S/L on Wnt secretion was also observed in previous experiments in HeLa cells conducted by the research group.

The S/L mutation targets the same serine residue (S297) as the phosphomimetic S/D variant, which was associated with changes in dendritic morphology and a reduction in AMPAR-mediated synaptic transmission. However, it remains unclear whether these effects result from altered phosphorylation-dependent regulation or from structural disruption at this position. Analysis of the S/L mutation, which substitutes serine with a non-phosphorylatable hydrophobic residue, was performed to determine whether modulation of AMPAR function by PORCN specifically depends on phosphorylation at S297 or on the residue itself as a critical element for PORCN's regulatory capacity. The effects of overexpressing PORCN S/L were investigated with regard to GluA1 surface expression in HeLa cells, as well as dendritic outgrowth and AMPAR-mediated synaptic transmission in hippocampal neurons.

Prior to further characterization, the expression of PORCN S/L and its potential impact on GluA1 protein levels were assessed. Whole-cell lysates were prepared from HeLa cells overexpressing either PORCN WT or the PORCN S/L mutant, in the presence or absence of GluA1 and subsequently analyzed (n = 5). Both PORCN WT and the disease-associated S/L mutant were comparably expressed and caused a reduction in total GluA1 protein levels in HeLa cells (Figure 10A). This suggests that the PORCN S/L mutant retains the ability to

modulate AMPAR expression similarly to the WT. To determine whether this effect extends to surface-localized receptors, GluA1 surface expression was subsequently assessed.

Relative to PORCN WT, the S/L mutation did not result in a detectable change in GluA1 surface expression (WT = 100 ± 4.1%; S/L = 96.7 ± 5.0%; p = 0.612) (Figure 10B).

Since no differences were observed between PORCN WT and PORCN S/L regarding their effects on total and surface GluA1 levels in HeLa cells, the next step focused on assessing the impact of PORCN S/L overexpression on neuronal morphology. This approach was further motivated by previous findings demonstrating that the S/L mutation impairs Wnt secretion – a process known to affect dendritic growth [80, 86].

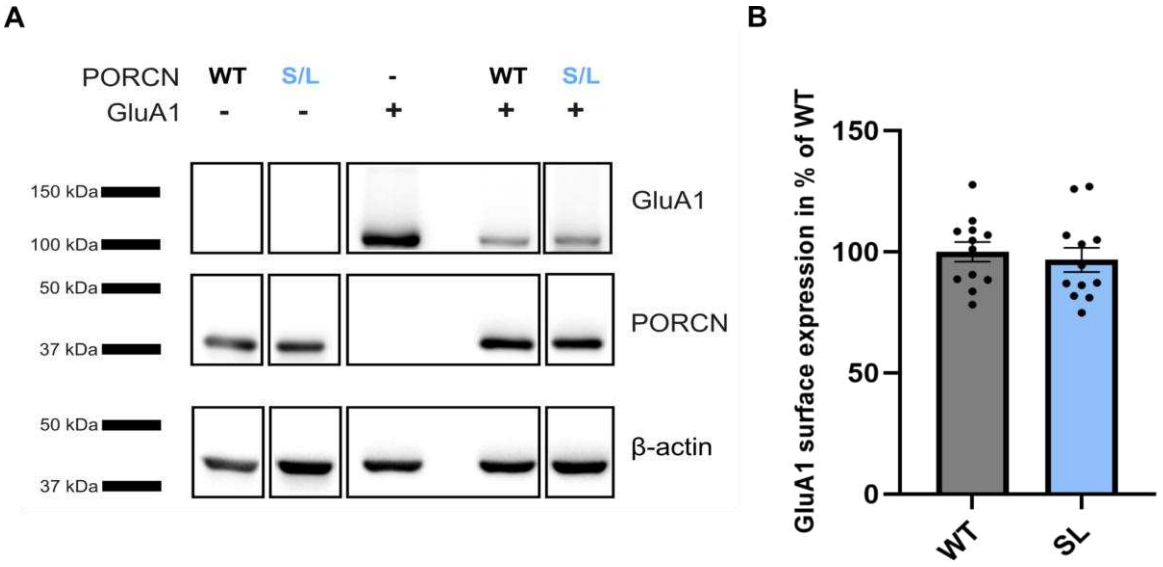


**Figure 10: Total and surface GluA1 expression in HeLa cells is not affected by PORCN S297L.**
**A:** Representative Western blot of whole-cell lysates of HeLa cells overexpressing PORCN WT (grey) or PORCN S297L (blue, S/L) without (-) or together (+) with GluA1 (n = 5). GluA1 alone served as a control. GluA1 was detected at 102 kDa using anti-GluA1 antibody. V5-tagged PORCN was detected at 38 kDa using mouse anti-V5 antibody and β-actin served as a loading control at 42 kDa. The overexpression of PORCN WT as well as PORCN S/L reduces total GluA1 levels in co-transfected HeLa cells. **B:** Surface expression of GluA1 in HeLa cells was assessed using a chemiluminescence-based assay, in which an extracellular HA-tag on GluA1 was detected using an anti-HA antibody. The resulting data were normalized to GluA1 co-transfected with PORCN WT. Relative to PORCN WT, the PORCN S/L mutation does not alter GluA1 surface expression (WT = 100 ± 4.12%; S/L = 96.7 ± 5.0%; p = 0.612).
See original full-length blots in supplementary (Figure 25). Data are presented as mean ± SEM with n = 12 for all data. Statistics: Unpaired t test.
GluA1 = Glutamate receptor ionotropic, AMPA 1; kDa = Kilodalton; L = Leucine; PORCN = Porcupine; S = Serine; WT = Wild type.

Dendritic length in hippocampal neurons overexpressing either PORCN WT or PORCN S/L was quantified by morphological reconstructions followed by Sholl analysis of both apical and basal dendrites. The overlay of all reconstructed neurons revealed a lower dendritic complexity in hippocampal neurons overexpressing PORCN S/L (n = 21) compared to PORCN WT (n = 20) (Figure 11A). Density plots confirmed that neurons transfected with

PORCN S/L showed a reduced distal dendritic span and decreased distal complexity compared to those expressing PORCN WT (Figure 11B). The quantification of dendritic length via Sholl analysis showed a significant decrease in the length of both apical and basal dendrites by pairwise comparison of PORCN S/L overexpressing neurons to PORCN WT overexpressing neurons ($p_{(apical)}$ = 0.003 ; $p_{(basal)}$ < 0.001) (Figure 11 C/D). The average total dendritic length was significantly decreased in neurons overexpressing PORCN S/L compared to those overexpressing WT (WT = 84.4 ± 4.5 µm; S/L = 46.3 ± 2.5 µm; p = 0.012). Thus, the disease-associated mutant PORCN S/L affected neuronal morphology with an overall reduced dendritic length.

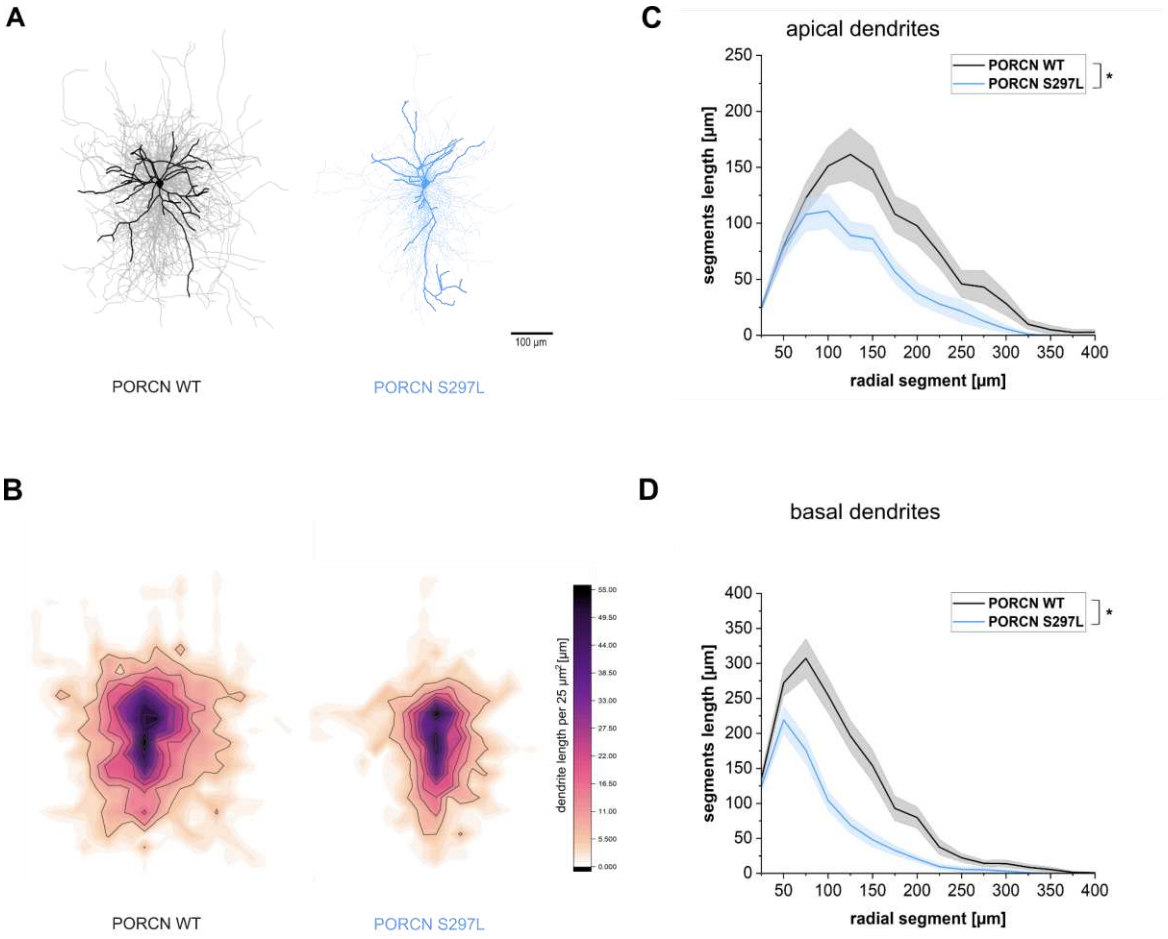


**Figure 11: Overexpression of PORCN S297L reduces the length of apical and basal dendrites in hippocampal neurons.**
**A:** Overlay of all manually reconstructed hippocampal neurons overexpressing PORCN WT (black, n = 20) or PORCN S297L (blue, S/L; n = 21). Overexpression of PORCN S/L decreases the size of the dendritic tree compared to PORCN WT. **B:** Density plots of hippocampal neurons overexpressing PORCN WT or PORCN S/L. The density was calculated based on the total number of reconstructed hippocampal neurons within 25 µm² squares. Overexpression of PORCN S/L results in a reduced dendritic span and lower distal dendritic complexity compared to neurons expressing PORCN WT. **C, D:** Sholl analysis of reconstructed hippocampal neurons. Overexpression of PORCN S/L significantly reduces the lengths of both apical and basal dendrites in 25 µm segments compared to PORCN WT-expressing neurons ($p_{(apical)}$ = 0.003; $p_{(basal)}$ < 0.001).
Data are shown as mean ± SEM. Statistics: Two-way RM ANOVA with Bonferroni correction; significance reported for group effect only. Density plots were created by Prof. Dr. Max Anstötz.
L = Leucine; PORCN = Porcupine; RM = repeated measures; WT = Wild type.

To examine whether the morphological alterations observed upon PORCN S/L overexpression are accompanied by changes in synaptic function, AMPAR-mediated mEPSCs were recorded by Kelvin Tofan.

For the PORCN S/L variant, mEPSC frequency did not significantly differ from PORCN WT (4.4 ± 0.7 Hz vs. 5.4 ± 1.0 Hz; n = 48; p = 0.489) (Figure 12B). Similarly, no significant differences in mEPSC amplitude were observed between PORCN S/L (10.6 ± 0.5 pA) and PORCN WT (11.5 ± 0.5 pA; p = 0.184) (Figure 12C). The mean rise time (10% to 90%) was comparable between PORCN S/L (3.7 ± 0.2 ms) and PORCN WT (3.9 ± 0.2 ms; p = 0.542), and CVs of rise time were equally unaffected (WT = 0.13 ± 0.01; S/L = 0.12 ± 0.004; p = 0.170) (Figure 12D). The decay time constant (WT = 10.7 ± 0.5 ms; S/L = 10.4 ± 0.5 ms; p = 0.639), and its CV (WT = 0.20 ± 0.01; S/L =0.20 ± 0.01; p = 0.906) also did not differ between groups (Figure 12E).

Overexpression of the PORCN S/L mutant in hippocampal neurons did not lead to significant alterations in AMPAR-mediated mEPSCs when compared to PORCN WT. Frequency, amplitude, rise time and decay time constant, as well as the respective CVs, remained unchanged between the two groups. These findings indicate that the PORCN S/L mutant does not affect AMPAR-mediated synaptic transmission or receptor kinetics under the conditions tested.

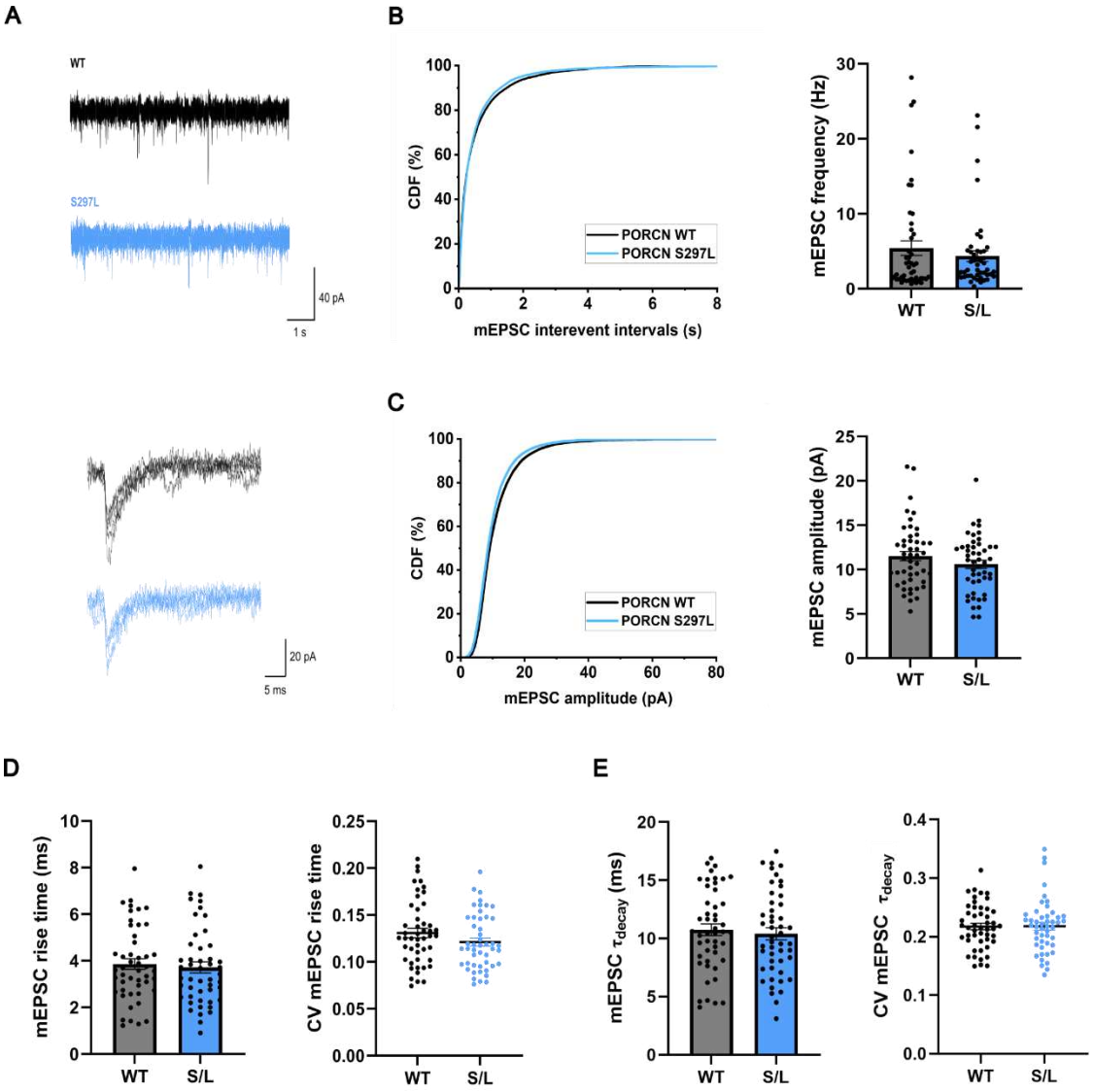


**Figure 12: Overexpression of PORCN S297L does not affect synaptic transmission of hippocampal neurons**.
**A:** Sample traces of AMPAR-mediated mEPSCs are displayed, with an overlay of five individual mEPSCs for each experimental condition. **B:** Frequency in hippocampal neurons overexpressing PORCN WT (grey) or PORCN S297L (blue, S/L) presented in cumulative distribution functions (CDFs) and bar graphs with mean ± SEM. The frequency remains unchanged in PORCN S/L-overexpressing neurons at 4.4 ± 0.7 Hz compared to PORCN WT (5.4 ± 1.0 Hz; p = 0.450). **C:** CDFs and bar graphs of the amplitude of hippocampal neurons overexpressing PORCN WT or PORCN S/L. No differences in amplitude were observed between PORCN WT (11.5 ± 0.5 pA) and S/L-overexpressing neurons (10.6 ± 0.5 pA; p = 0.184). **D:** Mean rise time (10% to 90%) and coefficient of variation (CV) of the rise time of hippocampal neurons transfected with PORCN WT or PORCN S/L. Neither the rise time at 3.7 ± 0.2 ms nor its variability at 0.13 ± 0.01 is affected by PORCN S/L overexpression compared to the PORCN WT with a mean rise time at 3.9 ± 0.2 ms and a CV at 0.12 ± 0.004 ($p_{(rise\ time)}$ = 0.542; $p_{(CV)}$ = 0.170). **E:** Decay time constant ($\tau_{decay}$) and CV of $\tau_{decay}$ in hippocampal neurons overexpressing PORCN WT or PORCN S/L. The $\tau_{decay}$ of PORCN WT-transfected neurons (10.7 ± 0.5 ms) remains unchanged upon PORCN S/L transfection (10.4 ± 0.5 ms), with no differences in variability detected between PORCN WT (0.2 ± 0.01) and PORCN S/L (0.2 ± 0.01) ($p_{(\tau decay)}$ = 0.639; $p_{(CV)}$ = 0.906).
Data are shown as mean ± SEM and n = 48 for all data. Statistics: Unpaired t-test (amplitude + $\tau_{decay}$) or Mann-Whitney U test (rest).
L = Leucine; mEPSCs = Miniature excitatory postsynaptic currents; PORCN = Porcupine; S = Serine; WT = Wild type.

In order to ascertain whether the negative effect of PORCN S/D and PORCN S/L mutants on the length of dendrites is related to an impaired Wnt secretion, the overexpression of the mutant PORCN H341D (H/D) was investigated. The mutation is located in the active center of PORCN and has been demonstrated to impair the enzymatic activity of the protein, thus preventing the palmitoylation and subsequent secretion of Wnt [55]. This allowed assessment of whether the dendritic phenotype of PORCN S/L overexpressing neurons resulted from disrupted Wnt signaling rather than Wnt-independent modulation of AMPARs by PORCN.

The morphology of hippocampal neurons overexpressing PORCN H/D was analyzed as described above, with a total of 20 reconstructed cells per group. Reconstructions were performed by Jordana Martinez Vilela (Institute of Neuro- and Sensory Physiology, Heinrich Heine University Düsseldorf). The overlay of all manually reconstructed neurons revealed no difference in the complexity of the dendritic tree between PORCN WT and PORCN H/D overexpressing neurons (Figure 13A). The length of apical and basal dendrites was quantified using Sholl analysis. The analyses showed no difference in the length of apical and basal dendrites by pairwise comparison of PORCN WT and PORCN H/D overexpressing neurons ($p_{(apical)} = 0.451$; $p_{(basal)} = 0.342$) (Figure 13B/C). Neurons overexpressing PORCN H/D showed no significant difference in total dendritic length compared to WT neurons (WT = 112.5 ± 5.8 µm; H/D = 102.2 ± 8.9 µm; p = 0.067).

Overexpression of the catalytically inactive PORCN H/D did not affect neuronal morphology compared to PORCN WT, whereas overexpression of PORCN S/D and PORCN S/L led to significant morphological changes.

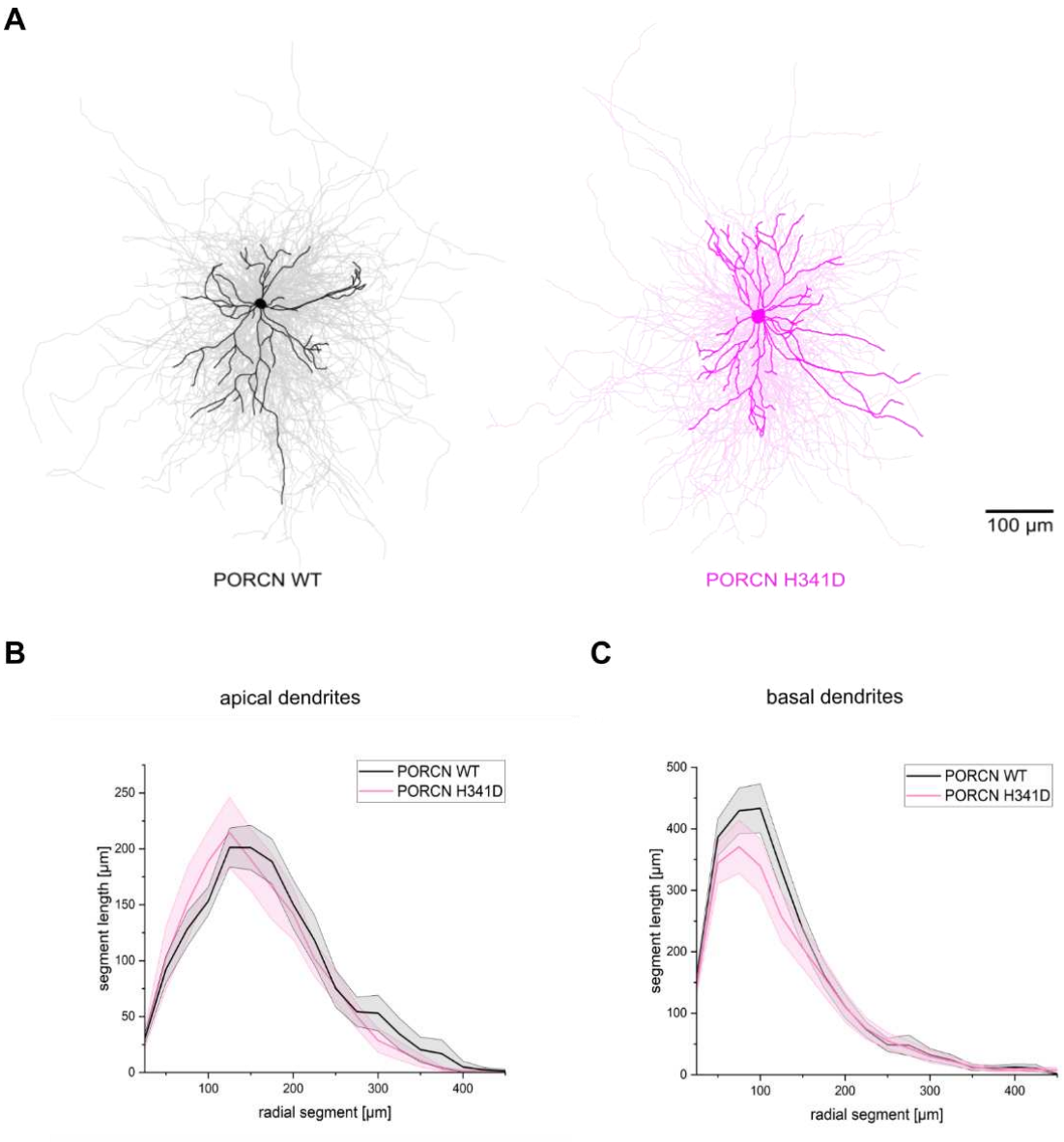


**Figure 13: Inhibition of PORCN enzymatic activity does not affect neuronal morphology.**
**A:** Overlay of all manually reconstructed neurons. Hippocampal neurons were transfected with V5-tagged PORCN WT and PORCN H341D stained with antibodies against V5 and MAP2. The complexity of the dendritic tree remains unchanged between neurons overexpressing PORCN WT (black) and PORCN H341D (pink, H/D). **B, C:** Sholl analysis of apical and basal dendrites in hippocampal neurons overexpressing PORCN WT or PORCN H/D. Neither the length of the apical dendrites nor the length of the basal dendrites is affected by PORCN H/D overexpression compared to PORCN WT overexpression ($p_{(apical)}$ = 0.451; $p_{(basal)}$ = 0.342).
Data are shown as mean ± SEM with n = 20 for all data. Statistics: Two-way RM ANOVA + Bonferroni correction; significance reported for group effect only.
D = Aspartic acid; H = Histidine; PORCN = Porcupine; RM = repeated measures; WT = Wild type.

## 3.4 C-Terminal Mutations in PORCN Impair Dendritic Growth, Indicating a Location-Specific Role

Beside serine 297, also tyrosine 430 was identified as a possible phosphorylation site in PORCN. The site is also known as a mutation site in FDH, where the tyrosine is mutated to

a stop codon. Like the patients with the S/L mutation, the patient with a Y430* mutation did not deal with neurological disorders.

Initial immunofluorescence staining revealed differences in the morphology of hippocampal neurons between PORCN WT and the phosphodeficient mutant PORCN Y430F (Y/F) as well as the phosphomimetic mutant PORCN Y430E (Y/E). To follow up on these observations, neuronal morphology was quantified through reconstruction of hippocampal neurons overexpressing the respective variants. Reconstructions were performed by Jordana Martinez Vilela.

The overlay of all reconstructed hippocampal neurons revealed a slightly reduced dendritic complexity of hippocampal neurons overexpressing PORCN Y/F (n = 21) and PORCN Y/E (n = 20) variants compared to the PORCN WT (n = 26) (Figure 14A). Sholl analysis resulted in no differences between the length of apical dendrites of hippocampal neurons overexpressing PORCN WT, PORCN Y/F and PORCN Y/E ($p_{(WT\_Y/F)}$ = 0.530; $p_{(WT\_Y/E)}$ > 0.999; $p_{(Y/F\_Y/E)}$ > 0.999) (Figure 14B). Investigating the length of basal dendrites, a reduction in dendritic length was observed between PORCN WT and PORCN Y/F as well as PORCN WT and PORCN Y/E overexpressing neurons ($p_{(WT\_Y/F)}$ < 0.001; $p_{(WT\_Y/E)}$ < 0.001) (Figure 14C). There was no significant difference in basal dendritic length between PORCN Y/F and PORCN Y/E overexpressing neurons (p = 0.227) (Figure 14C). The mean total dendritic length of neurons overexpressing PORCN Y/F or Y/E was not significantly reduced compared to PORCN WT and no significant difference was observed between the two mutants (WT = 107.2 ± 5.1 µm; Y/F = 87.38 ± 5.4 µm; Y/E = 88.4 ± 7.4 µm; $p_{(WT\_Y/F)}$ = 0.058; $p_{(WT\_Y/E)}$ = 0.059; $p_{(Y/F\_Y/E)}$ > 0.999).

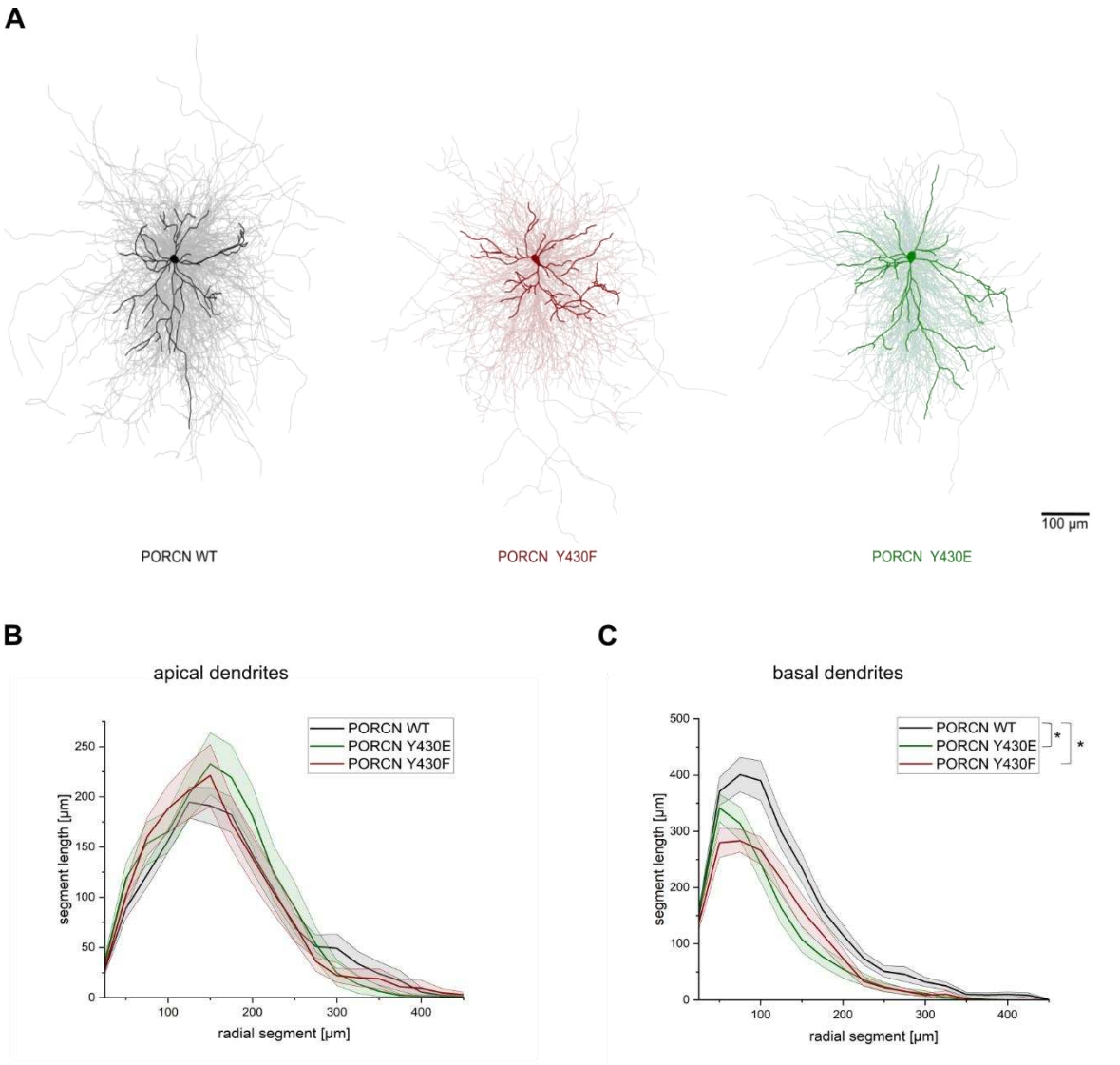


**Figure 14: C-terminal mutation at PORCN Y430X affects neuronal morphology.**
**A:** Visualization of manually reconstructed neurons. Hippocampal neurons were transfected with PORCN WT (black, n = 26), PORCN Y430F (red, Y/F; n = 21) and PORCN Y430E (green, Y/E; n = 20) and stained with mouse anti-V5 antibody and anti-MAP2 antibody. The complexity of the dendritic tree is reduced in neurons overexpressing PORCN Y/F and PORCN Y/E compared to PORCN WT. **B, C:** Sholl analysis of apical and basal dendrites in hippocampal neurons expressing PORCN WT, PORCN Y/F or PORCN Y/E. Overexpression of both PORCN Y/F and PORCN Y/E leads to a significant reduction in the length of basal dendrites compared to PORCN WT ($p_{(WT\_Y/F)} < 0.001$; $p_{(WT\_Y/E)} < 0.001$), while the length of apical dendrites remains unaffected ($p_{(WT\_Y/F)} = 0.530$; $p_{(WT\_Y/E)} > 0.999$). Neither the lengths of apical dendrites nor basal dendrites differ between PORCN Y/F and PORCN Y/E overexpressing neurons ($p_{(apical)} > 0.999$; $p_{(basal)} = 0.227$).
Date are presented as mean ± SEM. Statistics: Two-way RM ANOVA + Bonferroni; group-level comparisons only (no single-radius analysis).
E = Glutamic acid; F = Phenylalanine; PORCN = Porcupine; RM = repeated measures; WT = Wild type; Y = Tyrosine.

Since both PORCN Y430F and Y430E mutants similarly reduced basal dendritic length, their potential impact on AMPAR regulation was subsequently assessed. To investigate whether these morphological alterations were accompanied by changes in AMPA receptor expression, GluA1 protein levels in HeLa cells were quantified in relation to the respective PORCN mutants (n = 2).

PORCN WT and both Y430X mutants were expressed at comparable levels in HeLa cells. In all three conditions, total GluA1 protein levels were similarly reduced, indicating that the Y430X mutations did not differentially affect total GluA1 levels (Figure 15A).

Preliminary experiments from the research group indicated that the phosphomimetic mutant PORCN Y/E inhibits Wnt secretion. To investigate whether this effect resulted from altered interaction between PORCN and Wnt5a, co-IPs were performed in HeLa cells (n = 2). The known interaction between Wnt5a and PORCN WT served as a positive control for the interaction of the proteins. The phosphomimetic mutant PORCN Y/E as well as the phosphodeficient mutant PORCN Y/F mutants were able to interact with Wnt5a like PORCN WT (Figure 15B).

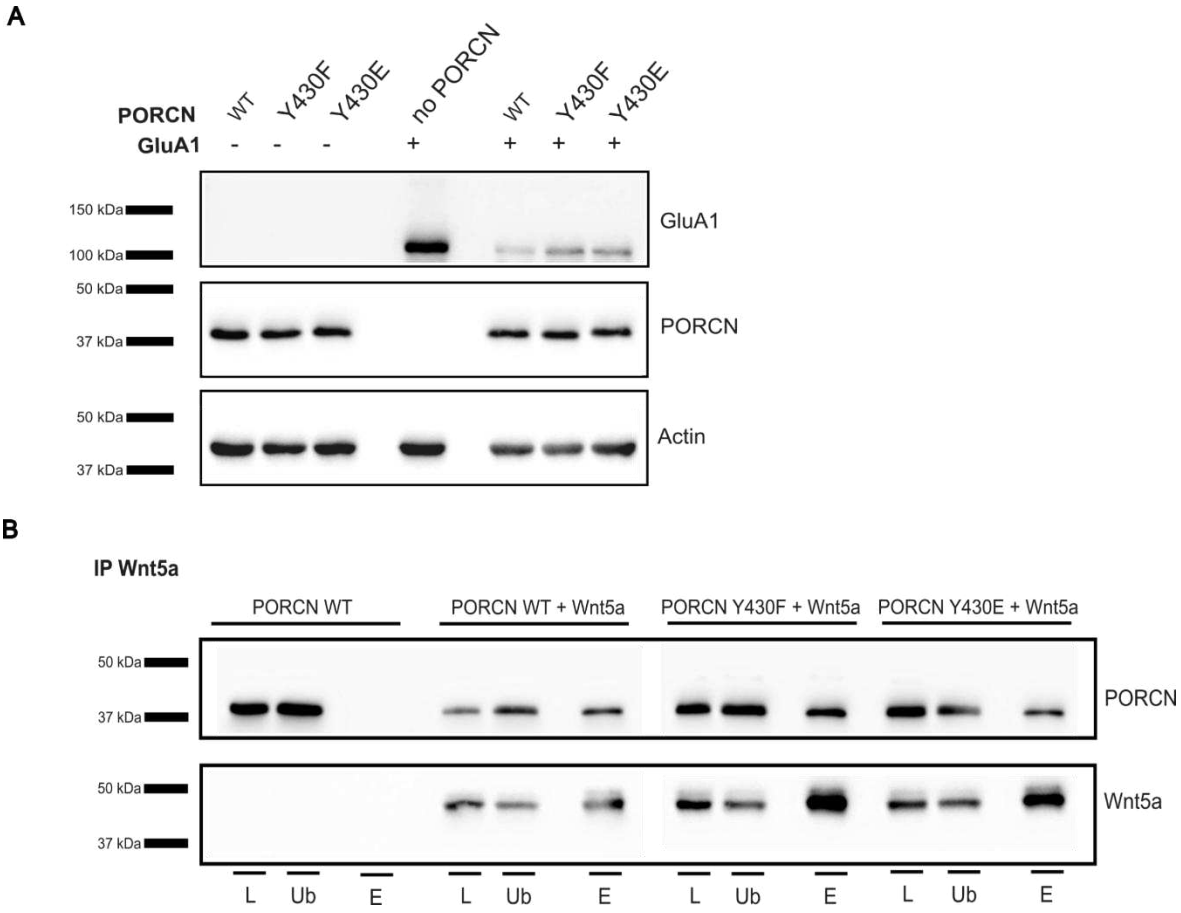


**Figure 15: PORCN Y430F and PORCN Y430E mutants reduce whole-cell GluA1 levels and interact with Wnt5a in HeLa cells.**
**A:** Representative Western blot of whole-cell lysates of HeLa cells transfected with PORCN WT, PORCN Y430F or PORCN Y430E together (+) or without (-) GluA1 (n = 2). GluA1 was detected at 102 kDa using anti-GluA1 antibody. V5-tagged PORCN was detected at 38 kDa using mouse anti-V5 antibody. As a loading control, β-actin was detected at 42 kDa. PORCN WT and PORCN mutants are equally expressed in all samples. The whole-cell GluA1 levels are reduced in HeLa cells co-transfected with PORCN WT or PORCN Y430X mutants. **B:** Representative Western blot of co-IPs with V5(Wnt5a)-conjugated beads (n =2). PORCN WT alone served as a negative control, whereas PORCN WT co-transfected with Wnt5a served as a positive control for co-IP. All PORCN variants are able to interact with Wnt5a in a Wnt5a-dependent co-IP.

E = Glutamic acid/Eluate; F = Phenylalanine; GluA1 = Glutamate receptor ionotropic, AMPA1; co-IP = Co-immunoprecipitation; kDa = Kilodalton; L = Load; PORCN = Porcupine; Ub = Unbound; WT = Wild type; Y = Tyrosine.

## 3.5 Inhibition of Enzymatic Activity Increases Total AMPAR Levels in Hippocampal Neurons While Overexpression of PORCN WT Has No Effect

PORCN enzymatic activity could not only be inhibited by introducing the mutation H341D, but also pharmacologically using the small-molecule inhibitor Wnt-C59 [79, 97-99]. By preventing the palmitoylation of Wnt, inhibition of PORCN enzymatic activity causes their retention in the ER and thereby disrupts Wnt secretion [56]. In addition, inhibition of PORCN leads to a decrease in dendritic complexity [80]. To investigate how this reduction in dendritic arborization affects AMPAR expression, GluA1 levels in membrane fractions of hippocampal neurons were analyzed following Wnt-C59 treatment.

In comparison to the control, the inhibition of PORCN via Wnt-C59 elevated the GluA1 levels and the Wnt5a levels in membrane fractions of hippocampal neurons after 48 hours (n = 3) (Figure 16A). Quantification of the mean band intensity in ImageJ revealed a significant increase in the GluA1 protein levels to 159.2 ± 11.55% compared to the control (100.0 ± 14.5%; n = 3; p = 0.033) (Figure 16B).

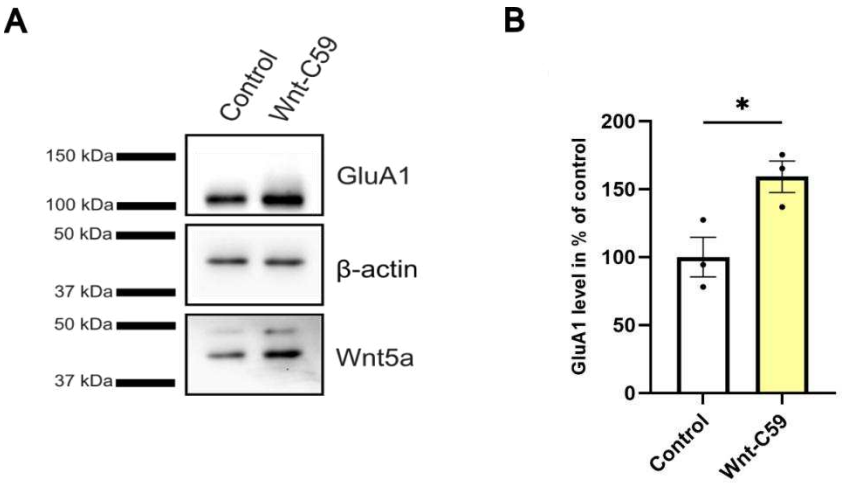


**Figure 16: Inhibition of the enzymatic activity of PORCN increases total GluA1 protein in membrane fractions of hippocampal neurons.**
**A:** Representative Western blot of membrane fractions of hippocampal neurons treated with the PORCN inhibitor Wnt-C59 for 48 hours (100 nM) (n = 3). The control is hippocampal neurons treated with the same amount of DMSO without inhibitor. GluA1 was detected at 102 kDa using anti-GluA1 antibody, Wnt5a was detected at 42 kDa using anti-Wnt5a antibody and β-actin served as a loading control for normalization (42 kDa). The GluA1 level is higher in Wnt-C59-treated neurons compared to the control. **B:** Quantitative analysis of the GluA1 levels in membrane fractions of hippocampal neurons treated with 100 nm Wnt-C59. The data are normalized to the respective β-actin levels and the relative GluA1 levels of the control (100.0 ± 14.5%). The inhibition of PORCN by Wnt-C59 significantly increases the relative GluA1 levels in the membrane fraction of hippocampal neurons by the factor 1.59 (159.2 ± 11.55%; p = 0.033).
Data are shown as mean ± SEM and n = 3 for all data. Statistics: Unpaired t-test.

GluA1 = Glutamate receptor ionotropic, AMPA 1; kDa = Kilodalton.

To further explore the mechanisms behind the observed increase in GluA1 levels in hippocampal neurons, this effect was considered to arise either from Wnt accumulation in the ER due to impaired secretion or from a larger pool of unbound PORCN available to modulate AMPARs. In the physiological context, the majority of endogenous PORCN is thought to be occupied by Wnt binding, thereby limiting its availability for potential Wnt-independent functions. However, under overexpression conditions, the amount of PORCN may exceed the capacity of endogenous Wnt to bind, resulting in a surplus of unbound PORCN. This excess could then engage in alternative interactions, such as the modulation of AMPAR surface expression.

To test this hypothesis and assess whether increased PORCN availability alone could influence GluA1 levels, SFV-mediated overexpression of PORCN WT was employed in primary hippocampal neurons. In membrane fractions of hippocampal neurons, GluA1 protein levels were comparable between cells overexpressing GFP and those overexpressing wild type PORCN (n = 4) (Figure 17A). Western blot quantification revealed that GluA1 levels in PORCN WT-overexpressing neurons were 96.1 ± 10.3% relative to control cells (100.0 ± 9.5%; n = 4; p = 0.788) (Figure 17B).

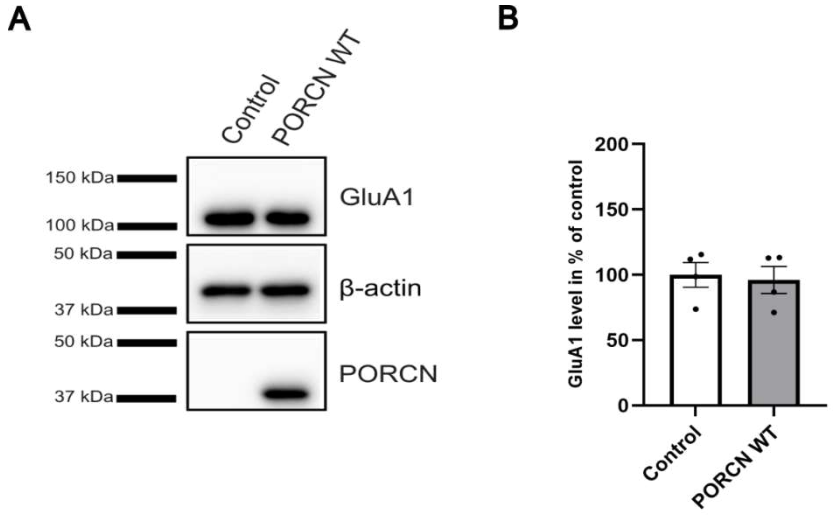


**Figure 17: Overexpression of PORCN WT does not affect GluA1 levels of hippocampal neurons.**
**A:** Representative Western blot of membrane fractions of hippocampal neurons transduced with GFP (control) or PORCN WT SFV (n = 4). Neurons were harvested 24 hours after transduction. GluA1 levels of PORCN WT overexpressing neurons do not show any differences compared to the control cells. **B:** Quantitative analysis of the GluA1 levels in hippocampal neurons overexpressing PORCN WT. Samples are normalized to the respective β-actin levels and the GluA1 expression levels of the control (100.0 ± 9.5%). GluA1 levels remained unchanged upon PORCN WT overexpression via SFV transduction (96.1 ± 10.3%; p = 0.788).
Date are presented as mean ± SEM and n = 4 for all data. Statistics: Unpaired t-test.
GluA1 = Glutamate receptor ionotropic, AMPA 1; kDa = Kilodalton; PORCN = porcupine; WT = Wild type.

Thus, the availability of Wnt-free PORCN, presumed to increase upon overexpression, does not appear to alter membrane-associated GluA1 levels.

## 3.6 PORCN Ability to Strongly Reduce AMPAR Levels Is Preserved Across Species and Unaffected by FDH-Associated Mutation

To date, it remains unclear which structural regions of PORCN are responsible for its modulatory function on AMPARs. To identify these molecular determinants, comparative analyses using PORCN homologs and FDH-linked variants were performed.

To verify the expression of PORCN homologs from *M. musculus* (Mus), *C. elegans* (Cel) and *D. melanogaster* (Dro) and to assess their impact on GluA1 protein levels, Western blot analyses of whole-cell lysates were performed (n = 2). Both PORCN homologs from *M. musculus* and *D. melanogaster* were equally expressed and found to reduce GluA1 levels (Figure 18A). An overexpression of the PORCN homolog from *C. elegans* could not be achieved in HeLa cells. These findings indicate that PORCN homologs from both invertebrates and vertebrates are capable of reducing total GluA1 levels in HeLa cells. To determine whether this effect extends to GluA1 surface expression, a cell-based surface expression assay was conducted.

The relative surface expression of GluA1 in HeLa cells co-transfected with the respective PORCN homologs was significantly reduced from 100.0 ± 9.7% in the control (without PORCN) to 1.8 ± 0.8% in cells expressing PORCN *M. musculus* and further to 2.8 ± 0.9% in cells expressing PORCN *D. melanogaster* (n = 9; $p_{(Control\_Mus)} < 0.001$; $p_{(Control\_Dro)} = 0.002$) (Figure 18B). The relative GluA1 surface expression did not change between both PORCN homologs ($p > 0.999$). The pronounced decrease in whole-cell and surface GluA1 levels in the presence of PORCN was conserved across both vertebrates and invertebrates. Nonetheless, this observation does not yet allow conclusions about the domains mediating PORCN's AMPAR-modulating function. To address this, additional PORCN mutants were examined in HeLa cells.

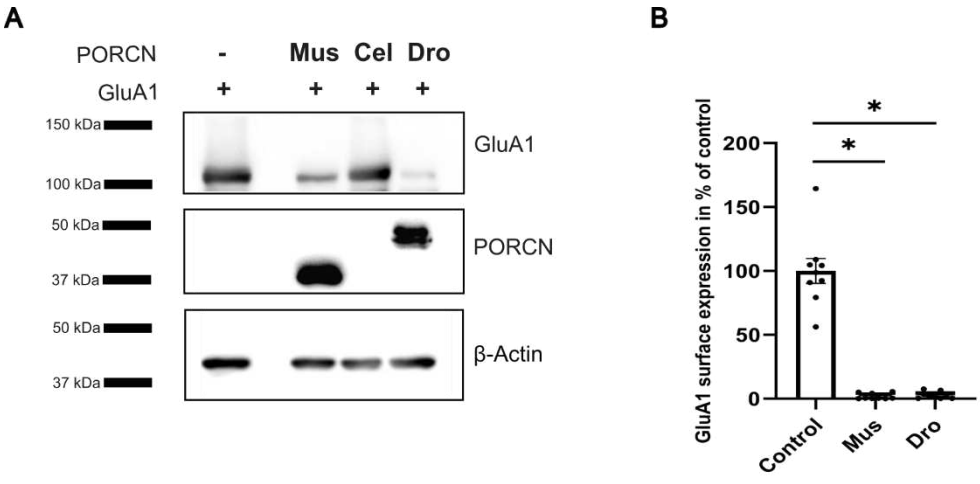


**Figure 18: The negative impact of PORCN co-expression on total and surface GluA1 is observed to be consistent across vertebrates and invertebrates.**
**A:** Representative Western blot of whole-cell lysates of HeLa cells expressing GluA1 alone or together with PORCN from Mus, Cel und Dro (n = 2). GluA1 was detected at 102 kDa using a GluA1-

specific antibody. Flag-tagged PORCN was detected at 38 kDa (Mus) or 48 kDa (Dro) using a FlagM2 antibody. The loading control was β-actin (42 kDa). PORCN protein from *C. elegans* is not expressed in HeLa cells whereas PORCN Mus and PORCN Dro both reduce total GluA1 levels. **B:** Quantification of GluA1 surface expression using a luminescence-measurement approach in HeLa cells transfected with GluA1 alone (control) or together with Mus and Dro. Samples were normalized to the control group without PORCN (relative GluA1 surface expression = 100.0 ± 9.7%). Both Mus and Dro decrease relative GluA1 surface expression significantly (Mus = 1.8 ± 0.8%; $p_{(Control\_Mus)} < 0.001$; Dro = 2.8 ± 0.9%; $p_{(Control\_Dro)} = 0.002$). No significant difference between Mus and Dro can be detected ($p > 0.999$).
Data are shown as mean ± SEM with n = 9 for all data. Statistics: Kruskal-Wallis test + Dunn's multiple comparisons test.
Cel = Caenorhabditis elegans; Dro = Drosophila melanogaster; GluA1 = Glutamate receptor ionotropic, AMPA 1; kDa = Kilodalton; Mus = Mus musculus; PORCN = Porcupine.

To identify regions in PORCN that are necessary for PORCNs moonlighting function, mutations in PORCN from patients that suffer from FDH were analyzed in regard to their ability to affect the GluA1 levels in HeLa cells. Four different FDH mutation sites were investigated, three of them were from patients with neurological deficits and one mutation which is known to not affect Wnt secretion (Figure 19A). To assess the expression of PORCN variants and their effect on GluA1 levels in HeLa cells, whole-cell lysates were analyzed by Western blot (n = 3). All PORCN variants were expressed, with minor differences in expression levels and all strongly reduced GluA1 levels, similar to the WT (Figure 19B).

Although whole protein levels of GluA1 were not affected by these mutations, they could still have an effect on GluA1 surface expression. Thus, a luminescence measurement approach was used to determine the effect of PORCN mutants on the relative GluA1 surface expression in HeLa cells. The GluA1 surface level of PORCN mutants was normalized and compared to PORCN WT-dependent relative GluA1 surface expression at 100.0 ± 2.2% (n = 9) (Figure 19B). There were no significant differences in relative GluA1 surface expression between PORCN WT, PORCN S136F (116.9 ± 17.5%; p = 0.680), PORCN D283H (110.6 ± 7.2%; p = 0.274), PORCN ∆285 (115.6 ± 5.7%; p = 0.070) and PORCN R228C (113.2 ± 5.8%; p = 0.127) detectable. The identified PORCN mutation sites in FDH patients with neurological disorders and the mutation site in FDH that did not affect Wnt secretion, showed no differential effect on AMPAR total and surface expression in HeLa cells compared to PORCN WT.

**A**

**FDH related mutations with neurological findings**

| Mutation | Epilepsy | Microcephaly | Developmental Delay | Intellectual disability | Brain defects | Reference |
|---|---|---|---|---|---|---|
| S136F | NR | + | NR | NR | + | Bornholdt et al. 2009 |
| D283H | + | + | + | - | NR | Arlt et al. 2022 |
| Δ285 | NR | + | NR | NR | NR | Peters et al. 2014 |

**FDH related mutation regular wnt secretion**

| Mutation | Effect | Reference |
|---|---|---|
| R228C | no loss of enzymatic function | Leoyklang et al. 2008 |

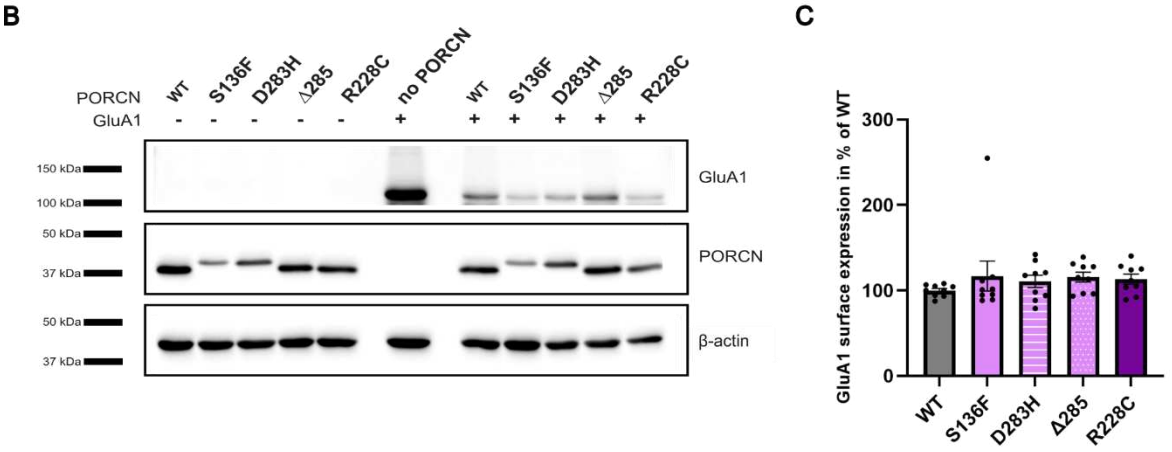


**Figure 19: FDH-associated PORCN mutations do not influence the PORCN-specific reduction of GluA1 in HeLa cells.**
**A:** Overview of FDH-related PORCN mutations investigated for their effects on AMPAR. The mutations were categorized into two groups: patients with neurological findings (+) and a mutation that does not cause a loss of function **B:** Representative Western blot of whole-cell lysates of HeLa cells overexpressing PORCN WT or mutants alongside GluA1 (+) or without GluA1 (-) (n = 3). GluA1 was detected at 102 kDa using an anti-GluA1 antibody and V5- or Flag-tagged PORCN was detected at 38–40 kDa using anti-FlagM2 and mouse anti-V5 tag antibody. The loading control was β-actin, detected at 42 kDa. Both PORCN WT and mutants drastically reduce total AMPAR levels in HeLa cells. **C:** Quantification of relative GluA1 surface expression of HeLa cells expressing extracellularly HA-tagged GluA1 together with PORCN WT or mutants. The samples were normalized to the relative GluA1 surface expression levels of HeLa cells co-transfected with GluA1 and PORCN WT. No differences were detected between PORCN WT related relative GluA1 surface expression with 100.0 ± 2.2% and mutants PORCN S136F (116.9 ± 17.5%; p > 0.999), PORCN D283H (110.6 ± 7.2%; p > 0.999), PORCN Δ285 (115.6 ± 5.7%; p = 0.280) and PORCN R228C (113.2 ± 5.8%; p = 0.509).
Data are shown as mean ± SEM and n = 9 for all data. Statistics: Kruskal-Wallis test + Dunn's multiple comparisons test.
C = Cysteine; F = Phenylalanine; FDH = Focal dermal hypoplasia; GluA1 = Glutamate receptor ionotropic, AMPA 1; H = Histidine; kDa = Kilodalton; NR = Not reported; PORCN = Porcupine; R = Arginine; S = Serine; WT = Wild type.

## 3.7 Wnt5a Interacts with AMPARs in Hippocampal Neurons, Lightly Reducing their Levels, while Drastically Decreasing Whole-Cell and Surface GluA1 Expression in HeLa Cells

Experimental data from the research group showed that Wnt5a overexpression leads to a reduction in total and surface GluA1 levels in HeLa cells, independent of PORCN expression. To investigate if Wnt5a and GluA1 can bind directly to each other or if PORCN is needed as a linker, a Wnt5a mutant that was supposed to not bind to PORCN anymore

was engineered within the working group. The mutation site C240A in Wnt5a was chosen based on established mutation sites in Wnt3a that impair PORCN interaction [100]. To verify whether the Wnt mutant is able to interact with PORCN, co-IPs were performed with HeLa cells transfected with PORCN alone (negative control) or together with Wnt5a WT and Wnt5a C240A (C/A) mutant (n = 3). An interaction was observed between Wnt5a WT and PORCN, whereas Wnt5a C/A failed to interact with PORCN (Figure 20). The Wnt5a C/A mutant was used further in this study.

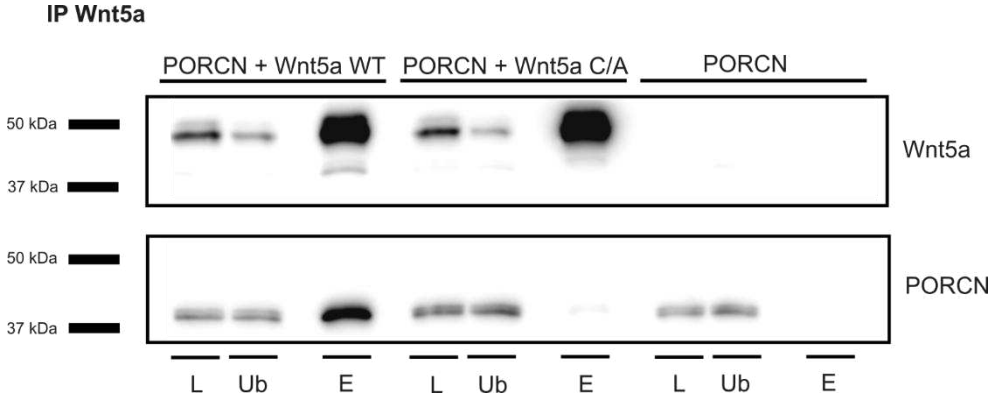


**Figure 20: Mutant Wnt5a C240A is no longer able to interact with PORCN.**
Representative Western blot of co-IPs with V5(Wnt5a)-conjugated beads in HeLa cells (n = 3). Cells were transfected with PORCN together with either Wnt5a WT or Wnt5a C240A mutant (C/A) or with PORCN alone (negative control). V5-tagged Wnt5a was detected at 48 kDa using mouse anti-V5 antibody, while Flag-tagged PORCN was detected at 38 kDa using anti-Flag antibody. PORCN and Wnt5a WT interact with each other in a Wnt5a-related co-IP. The mutant Wnt5a C/A is no longer able to interact with PORCN.
A = Alanine; C = Cysteine; co-IP = Co-immunoprecipitation; E = Eluate; kDa = Kilodalton; L = Load; Ub = Unbound; WT = Wild type.

To investigate a potential PORCN-independent interaction between Wnt5a-V5 and GluA1 in HeLa cells, co-IPs were performed using both GluA1-conjugated and V5-conjugated beads (n = 3). Wnt5a-V5 directly binds to GluA1 and downregulates its total protein expression in HeLa cells (Figure 21A).

Following the identification of a direct interaction between Wnt5a and GluA1, the effects of Wnt5a WT and Wnt5a C/A on GluA1 surface expression in HeLa cells were investigated. While total GluA1 levels reflect overall expression and protein stability, surface expression is critical for evaluating synaptic availability and the functional incorporation of AMPARs into the plasma membrane. The effect of Wnt5a on the relative surface expression of GluA1 in HeLa cells was investigated by the luminescence-based surface expression assay. GluA1 co-transfected with pcDNA3.1+ served as the control for relative GluA1 surface expression (100.0 ± 1.8%; n = 9) (Figure 21B). Wnt5a WT significantly reduced the relative GluA1 surface expression levels to 4.5 ± 0.8% ($p < 0.001$). Relative GluA1 surface expression was reduced by the Wnt5a C/A mutant to a similar extent as by Wnt5a WT co-expression (5.0 ± 1.1%; $p < 0.001$).

To determine whether the Wnt5a-induced reduction in GluA1 levels was specific to AMPARs, the effect of Wnt5a overexpression on additional ion channels – GluK2, NMDAR and HCN2 – was examined by Western blot analysis of whole-cell lysates from HeLa cells (n = 4). This approach allowed for the assessment of potential broader effects of Wnt5a on glutamatergic and non-glutamatergic ion channels. A decrease in whole-cell levels of GluA1, GluK2 and NMDAR was observed upon co-expression with Wnt5a WT (Figure 21C). However, the whole-cell levels of the HCN2 channels remained unaffected by the co-expression of Wnt5a WT in HeLa cells.

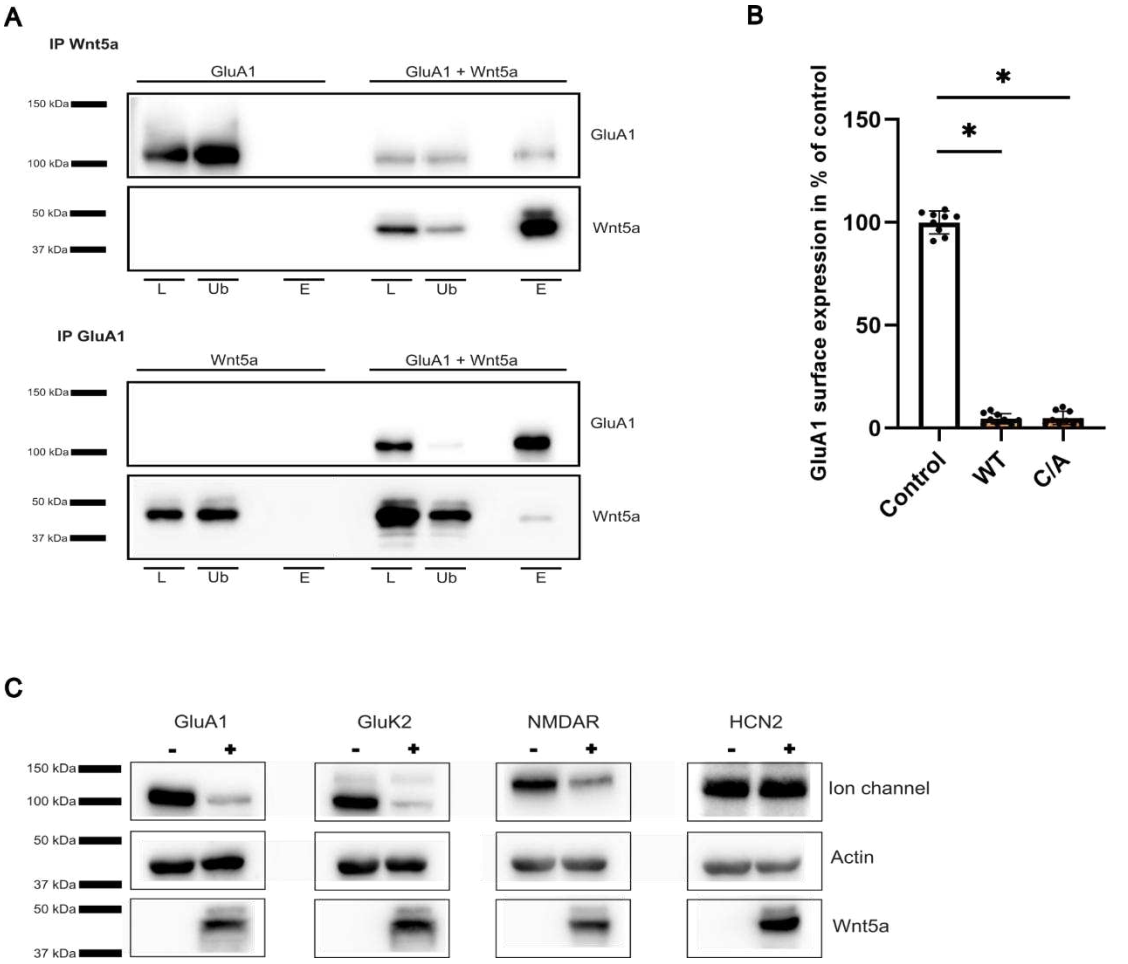


**Figure 21: In HeLa cells, Wnt5a co-expression reduces the overall levels of glutamate receptors, as well as the levels of GluA1 present at the cell surface.**
**A:** Representative Western blot of V5(Wnt5a)- and GluA1- co-IPs in HeLa cells (n =3). GluA1 was detected at 102 kDa using anti-GluA1 antibody, while V5-tagged Wnt5a was detected at 45 kDa using mouse anti-V5 tag antibody. In HeLa cells, GluA1 and Wnt-5a interact with each other. **B:** Quantification of GluA1 surface expression of HeLa cells expressing extracellularly HA-tagged GluA1 alone or together with Wnt5a WT or Wnt5a C240A (C/A). Samples were normalized and compared to the control group expressing GluA1 alone (relative GluA1 surface expression = 100.0 ± 1.8%). Co-expression of Wnt5a WT and C/A significantly reduces the relative surface levels of GluA1 to 4.5 ± 0.8% and 5.0 ± 1.1%, respectively ($p_{(Control\_WT)} < 0.001$; $p_{(Control\_C/A)} < 0.001$). The similar effects of WT and C/A suggest that GluA1 and Wnt5a interact within the ER. **C:** Representative Western blot of whole-cell lysates from HeLa cells expressing various ion channels alone (-) or together with Wnt5a WT (+) (n = 4). GluA1 was detected at 102 kDa using anti-GluA1 antibody, Flag-tagged GluK2 at 102 kDa using anti-FlagM2 antibody, NMDAR at 120 kDa using anti-NMDAR1 antibody and HCN2 at 120 kDa using anti-HCN2 antibody. V5-tagged Wnt5a was observed at 45 kDa using a mouse anti-V5 antibody and β-actin was detected at 42 kDa as loading control. Co-expression of Wnt5a WT reduces the total levels of glutamate receptors GluA1, GluK2 and NMDAR, while having no effect on

the expression of the HCN2 ion channel. These results indicate that the effect of Wnt5a is specific to glutamate receptors.
Data are presented as mean ± SEM and n = 9 for all data. Statistics: Kruskal-Wallis test + Dunn's multiple comparisons test in comparison to the control.
A = Alanine; C = Cysteine; E = Eluate; GluA1 = Glutamate receptor ionotropic, AMPA 1; GluK2 = Glutamate receptor ionotropic, kainite 2; HCN2 = Hyperpolarization-activated cyclic nucleotide-gated channel 2; co-IP = Co-immunoprecipitation; kDa = Kilodalton; L = Load; NMDAR = N-methyl-D-aspartate receptor; Ub = Unbound; WT = Wild type.

These findings indicate an effect of Wnt5a on GluA1 by decreasing GluA1 whole-cell and surface expression in HeLa cells. The effect of Wnt5a WT on the whole-cell receptor levels is not AMPAR-specific. Wnt5a also lowered the expression of the glutamate receptors GluK2 and NMDAR in HeLa cells.

Given the observed downregulation of total and surface GluA1 levels in HeLa cells following Wnt5a overexpression, its impact on AMPA receptor regulation was subsequently examined in primary hippocampal neurons. To confirm the overexpression of Wnt5a WT, hippocampal neurons were transduced with different amounts of virus. The lentiviral transduction of hippocampal neurons led to an overexpression of Wnt5a in nearly every neuron (Figure 22A).

To confirm that the overexpressed Wnt5a was not only present intracellularly but also secreted in a physiologically relevant manner, its secretion efficiency was subsequently evaluated. The relative Wnt5a secretion was detected in the supernatant of secreting cells by a luminescence measurement approach. GFP transduced hippocampal neurons served as a negative control. Relative Wnt5a secretion in neurons overexpressing Wnt5a WT reached 100.0 ± 7.5%, whereas the control remained at 0.1 ± 0.02%, confirming efficient secretion of Wnt5a WT by the transduced cells ($n = 7$; $p < 0.001$) (Figure 22B). The overexpression of the mutant Wnt5a C/A significantly decreased Wnt5a secretion compared to Wnt5a WT overexpression (C/A = 30.3 ± 5.7%; $p < 0.001$). Overexpressed Wnt5a was secreted in hippocampal neurons.

To verify the expression of overexpressed Wnt5a at the protein level in hippocampal neurons and to assess its subcellular distribution, soluble and membrane fractions were isolated and analyzed by Western blotting (n = 1). The results demonstrated that Wnt5a was enriched in the membrane fraction of hippocampal neurons (Figure 22C). These findings indicate that Wnt5a remained associated with intracellular membranes, consistent with its maturation and trafficking through the secretory pathway prior to extracellular release.

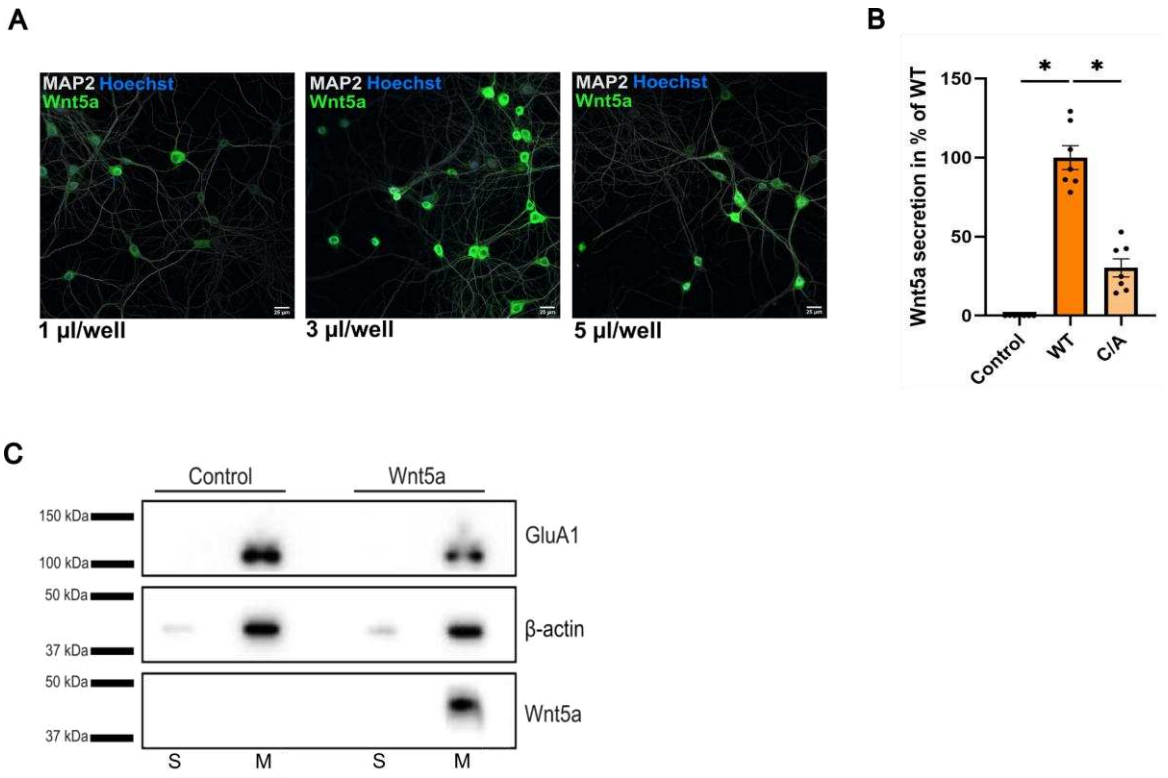


**Figure 22: Lentiviral Wnt5a overexpression is achieved in hippocampal neurons.**
**A:** Immunofluorescence staining of hippocampal neurons transduced with different concentration of Wnt5a WT lentivirus. Lentiviral overexpression of Wnt5a was successfully achieved. The bar represents 25 µm. **B:** Quantification of Wnt5a secretion by hippocampal neurons using a luminescence-based measurement approach. Samples were normalized and compared to Wnt5a WT secretion (relative Wnt5a secretion = 100.0 ± 7.5%). GFP-transduced hippocampal neurons served as a negative control with a relative Wnt5a secretion of 0.1 ± 0.0% ($p < 0.0001$). The relative Wnt5a secretion is reduced to 30.3 ± 5.7% in hippocampal neurons overexpressing the Wnt5a C240A (C/A) mutant ($p < 0.001$). Overexpression of NanoLuc-merged Wnt5a WT and Wnt5a C/A, as well as correct Wnt secretion, was achieved through lentiviral transduction of hippocampal neurons. **C:** Western blot analysis of soluble (S) and membrane (M) fractions of hippocampal neurons without (control) or with Wnt5a overexpression (n = 1). Hippocampal neurons were transduced with Wnt5a WT lentivirus and subjected to membrane preparation. GluA1 was detected at 102 kDa using anti-GluA1 antibody, while V5-tagged Wnt5a was detected at 45 kDa using mouse anti-V5 antibody. As a loading control, β-actin was detected at 42 kDa. Wnt5a predominantly localizes to the membrane fraction of hippocampal neurons.
Data are presented as mean ± SEM with n = 7 for all data. Statistics: One-way ANOVA + Dunnett's multiple comparison test.
A = Alanine; C = Cysteine; E = Eluate: GluA1 = Glutamate receptor ionotropic, AMPA 1; kDa = Kilodalton; L = Load; MAP2 = Microtubule-associated protein 2; Ub = Unbound; WT = Wild type.

Taken together, the data indicate that overexpressed Wnt5a is properly processed and secreted in hippocampal neurons.

After confirming proper overexpression and secretion of Wnt5a via lentiviral transduction in hippocampal neurons, the interaction of Wnt5a WT and C/A with AMPARs was examined by co-IP using lysates from neurons overexpressing either variant (n = 3) (Figure 23A). Both GluA1 and GluA2 were found to interact with Wnt5a WT and Wnt5a C/A in a GluA1-dependent co-IP (Figure 23A). The co-IP was effective, as Wnt5a variants were not detectable in the unbound fraction of the co-IP.

Given the interaction between Wnt5a and AMPARs in hippocampal neurons and prior findings in HeLa cells showing that Wnt5a overexpression reduces both total and surface GluA1 levels, we next examined whether Wnt5a overexpression similarly affects total GluA1 expression in neurons.

Although Wnt5a WT overexpression appeared to reduce GluA1 levels in hippocampal neurons (Figure 23B), this decrease was not statistically significant when compared to control (100.0 ± 13.8% vs. 71.3 ± 14.9%; n = 6; p = 0.188) (Figure 23C).

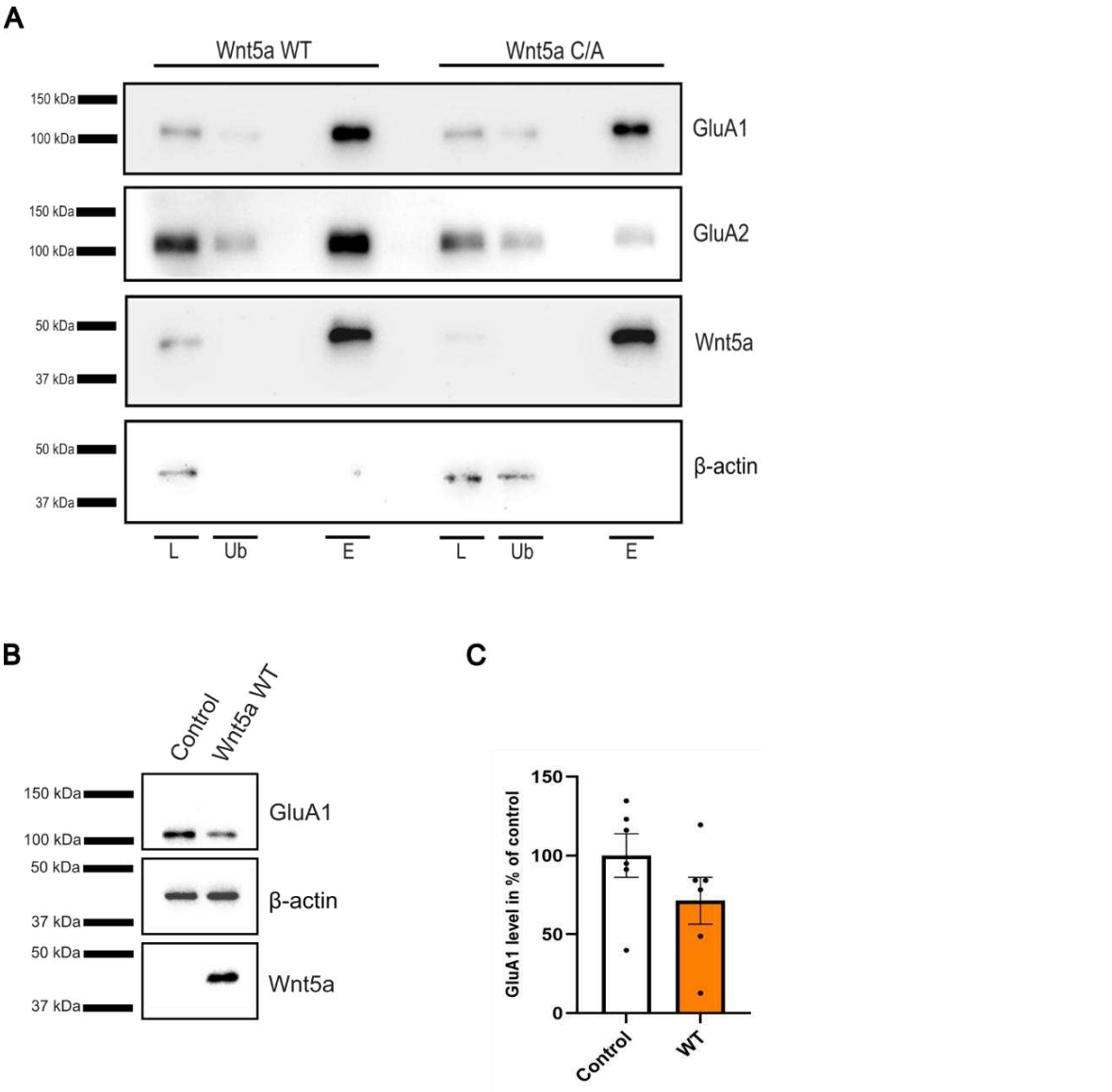


**Figure 23: AMPARs bind to Wn5a WT and Wnt5a C240A in hippocampal neurons.**
**A:** Representative Western blot of GluA1-dependent co-IPs of hippocampal neurons transduced with Wnt5a WT and Wnt5a C240A (C/A) lentivirus (n = 3). GluA1 and GluA2 were detected at 102 kDa using specific antibodies while V5-tagged Wnt5a was detected at 45 kDa using mouse anti-V5 antibody. As a loading control, β-actin was detected at 42 kDa. Both Wnt5a WT and Wnt5a C/A interact with GluA1 and GluA2 in hippocampal neurons. **B:** Representative Western blot of membrane fractions of hippocampal neurons overexpressing GFP (control) or Wnt5a WT (n=6). Overexpression was achieved by lentivirus transduction. GluA1 was detected at 102 kDa using an anti-GluA1 antibody while V5-tagged Wnt5a was detected at 45 kDa using mouse anti-V5 antibody. The loading control was β-actin, detected at 42 kDa. Wnt5a WT overexpression lowers the GluA1

levels in hippocampal neurons compared to the control (GFP-transduced cells). **C:** Quantitative analysis of GluA1 levels in hippocampal neurons overexpressing Wnt5a WT. Samples were normalized to the corresponding β-actin levels and to the GluA1 expression levels of the control (set to 100.0 ± 13.8%). Overexpression of Wnt5a WT via lentivirus transduction does not significantly affect GluA1 levels (71.3 ± 14.9%; p = 0.188).
Date are presented as mean ± SEM with n = 6 for all data. Statistics: Unpaired t test.
A = Alanine; C = Cysteine; co-IP = Co-immunoprecipitation; E = Eluate: GluA1 = Glutamate receptor ionotropic, AMPA 1; GluA2 = Glutamate receptor ionotropic, AMPA 2; kDa = Kilodalton; L = Load; Ub = Unbound; WT = Wild type.

In summary, the results suggest that Wnt5a functions as a PORCN-independent modulator of GluA1. In HeLa cells, overexpression of Wnt5a reduced both total and surface GluA1 levels. In hippocampal neurons, GluA1 levels significantly increased when Wnt secretion from the ER was inhibited, whereas overexpression of Wnt5a WT caused a slight, non-significant reduction in GluA1 levels.

# 4 Discussion

Auxiliary and associated proteins are key regulators of AMPAR biogenesis, trafficking and function, critically shaping glutamate-mediated excitatory transmission in the central nervous system. PORCN, a component of the Wnt signaling pathway, has been shown to possess a secondary, moonlighting function in AMPAR regulation. As demonstrated by Erlenhardt et al., PORCN regulates GluA1 surface expression independently of its enzymatic activity [59], pointing to a regulatory role beyond Wnt palmitoylation. To address this, a key objective of the present study was to investigate how the multifunctional roles of PORCN are regulated. The study showed that PORCN's structural integrity and potential phosphorylation critically influence its non-canonical role in AMPAR physiology. C-terminal mutations affected dendritic architecture, while its interaction with AMPARs was evolutionarily conserved. Additionally, Wnt5a modulated AMPAR expression in a manner dependent on subcellular context, highlighting the importance of spatial regulation in synaptic signaling.

## 4.1 Mutation in the AMPAR-Associated Protein PORCN Reduces Neuronal Outgrowth and Synaptic Transmission

In this study, phosphorylation of PORCN as a potential PTM regulating its non-canonical functions was investigated. PORCN point mutants mimicking phosphorylated (S/D) and dephosphorylated (S/A) states, a disease-associated mutation (S/L) and a catalytically inactive mutant (H/D) were used. Neuronal morphology (via Sholl analysis) and AMPAR function (via mEPSC recordings) were assessed in primary neurons, while GluA1 surface levels, protein–protein interactions and Wnt secretion were analyzed in HeLa cells.

### 4.1.1 Serine 297 as a Molecular Switch in PORCN Function

Summarizing the effects of PORCN WT and its mutants on both Wnt signaling and AMPAR-related processes revealed distinct functional profiles that highlight the mechanistic diversity and specialization of individual PORCN variants (Table 38).

**Table 38: PORCN mutant characterization: PORCN S297X and PORCN H341D versus PORCN WT.**

| | PORCN | | | |
|---|---|---|---|---|
| | **S297A** | **S297D** | **S297L** | **H341D** |
| Variant | phosphodeficient | phosphomimetic | FDH-associated | no enzymatic function |
| ER localized | - | - | - | NT |
| Dendritic length | - | ↓ | ↓ | - |
| Neuronal transmission | - | ↓ | - | NT |
| GluA1 surface level | - | ↑ | - | -* |
| Wnt secretion | - | ↓ | ↓* | ↓* |
| TARPγ8 interaction | - | - | - | NT |
| Wnt5a interaction | - | - | - | NT |

- = No difference; ↓ = Decrease; ↑ = Increase; * = Unpublished results from working group members; A= Alanine; D = Aspartic acid; ER = Endoplasmic reticulum; GluA1 = Glutamate receptor ionotropic, AMPA 1; H = Histidine; L = Leucine; S = Serine; NT = Not tested; PORCN = Porcupine; TARPγ8 = Transmembrane AMPAR regulatory protein γ8; WT = Wild type.

This study focused on serine 297, as phosphodeficient PORCN S/A and phosphomimetic PORCN S/D mutants exert differential effects on dendritic arborization. All variants localized to the ER, but downstream effects on dendritic morphology, GluA1 surface expression and Wnt secretion differed. PORCN WT and S297X mutants reduced whole-cell and surface GluA1 in HeLa cells, whereas in HEK293T cells, PORCN WT increased overall AMPAR expression but reduced surface levels, as reported by Erlenhardt et al. and Wei et al. [59, 60]. This suggests PORCN's regulatory influence on AMPARs is context-dependent but consistent within each system.

Interestingly, PORCN S/D overexpression in HeLa cells attenuated the GluA1 surface expression decrease while reducing Wnt secretion, compared to PORCN WT and PORCN S/A. This indicates that S297 phosphorylation may act as a molecular switch, selectively uncoupling PORCN's enzymatic activity from its AMPAR-regulatory function, enabling cell type-specific modulation of synaptic plasticity while preserving canonical Wnt signaling. Analogously, phosphorylation of AMPAR-associated proteins such as stargazin is a well-established mechanism of receptor modulation [101, 102], raising the possibility that PORCN phosphorylation represents a parallel mode of fine-tuning AMPAR regulation.

Reconstructed hippocampal neurons were selected based on morphological resemblance to pyramidal neurons. Dendritic arborization differs between apical and basal dendrites, which is critical for signal processing [103-109]. PORCN may shape region-specific dendritic arbors by regulating AMPARs within the dendritic ER, linking morphology to synaptic function. While axon–dendrite polarity is relatively well understood [110], the mechanisms underlying the formation and maintenance of distinct dendritic compartments remain less clear [111]. Basal dendrites are shorter and emerge directly from the soma, while apical and basal dendrites normally occupy distinct layers of the hippocampus, with clear dendritic polarity established from 4 DIV onward [103-105]. PORCN S/D reduced both apical and basal dendritic lengths, whereas PORCN S/A selectively affected apical dendrites. The impairment of dendritic complexity is important, as it reflects the functional capacity of neurons [93], and is a hallmark of neurodegenerative diseases such as Alzheimer's, where dendritic degeneration closely correlates with characteristic functional deficits [112]. Apical dendrites may be more sensitive due to cable properties or network organization, though variability in primary culture must be considered, since pyramidal neurons form arbors resembling *in vivo* cells but may function differently in the absence of tissue-specific organization [104, 106]. Total dendritic length in PORCN S/A overexpressing neurons remained similar to PORCN WT, suggesting intact basic signal transmission.

Dendrites serve as the principal sites for synaptic input [111]. Excitatory signals are filtered by distance-dependent attenuation [108, 113-117], compensated by increased synaptic strength at distal sites [109, 118-120] and higher spine density proximally [109, 121]. Neurons overexpressing PORCN S/D exhibited reduced dendritic complexity and decreased AMPAR-mediated mEPSC frequency. This likely reflects a lower number of functional synapses due to the reduced dendritic length. Moreover, mEPSC amplitude was reduced, suggesting a possible decrease in the availability of AMPARs at the synapse. Alterations due to TARPγ8 depletion from the AMPAR complexes, as reported under PORCN KD conditions [59], may be excluded in this context as the confirmed interaction between PORCN mutants and TARPγ8 in HeLa cells suggested that TARPγ8-mediated regulation of AMPAR function remained intact. This suggests that the observed changes in AMPAR function are likely mediated within the ER, affecting receptor assembly or trafficking.

Coherent with the unchanged total dendritic length in PORCN S/A overexpressing neurons the frequency of mEPSCs remained the same as in PORCN WT overexpressing neurons. Nevertheless, changes in the mEPSC amplitude and kinetics indicated that the contributing synapses were likely located distally and that the expected compensatory mechanisms were not sufficiently engaged. The pronounced variability in rise time further reflected the heterogeneity of primary hippocampal neurons in culture. PORCN S/L overexpression reduced dendritic length similar to PORCN S/D without affecting synaptic transmission. This decouples morphological deficits from functional output and aligns with the fact that patients carrying the PORCN S/L mutation showed no obvious neurological abnormalities [92], which is why no further neurological testing was conducted. Nevertheless, both frequency and amplitude are shaped by multiple pre- and postsynaptic factors, including release probability, receptor sensitivity, synapse location, vesicle content and membrane properties [122]. Therefore, mEPSC data must be interpreted carefully, considering the complexity of underlying mechanisms [122]. Comparison of PORCN S/A and PORCN S/D shows that phosphomimetic substitution induces both morphological and functional impairments, likely via altered AMPAR maturation, trafficking or surface expression. These findings suggest that a possible phosphorylation at S297 dynamically modulates PORCN multifunctionality.

### 4.1.2 Wnt Signaling vs. AMPAR Regulation in Morphological Changes

The distinct morphological and functional phenotypes induced by different PORCN mutants in hippocampal neurons prompted further investigation into the underlying mechanisms, particularly to determine whether these changes result from altered Wnt signaling or AMPAR regulation.

Wnt signaling also contributes to dendritic development. Decreased Wnt5a signaling in PORCN S/D and PORCN S/L mutants may explain reduced arborization, in concordance

with the fact, that Wnt5a KD impaired dendritic growth and neuronal differentiation [86, 87]. However, catalytically inactive PORCN H/D did not alter dendritic architecture, suggesting that reduced Wnt secretion alone cannot account for morphological changes. In hippocampal neurons, endogenous PORCN may still support Wnt palmitoylation within the ER independently of the overexpressed palmitoylation-deficient PORCN mutant, allowing Wnt secretion and physiological function to remain largely intact. While this raises the question of why catalytically inactive PORCN variants exert morphological effects despite intact Wnt signaling, the observed phenotypes point to the involvement of Wnt-independent or moonlighting functions of PORCN. Alternative mechanisms, such as direct AMPAR modulation, are therefore likely to mediate these dendritic phenotypes. Supporting this, overexpression of GluA1 and GluA2 in cortical neurons increases dendritic length and complexity, while GluA1 overexpression in spinal motor neurons enhances both dendritic length and complexity and GluA2 selectively increases length [95, 123]. Conversely, chronic stress reduces synaptosomal AMPAR levels and dendritic complexity [124], highlighting a general role for AMPARs in shaping dendritic architecture across neuronal types. Hence, PORCN mutants could impair AMPAR expression and thereby impair dendritic arborization.

These findings demonstrate that specific PORCN mutations induce both morphological and AMPAR-specific functional effects. Phosphorylation under basal conditions remains undetected and upstream activation pathways are unknown. Given that PORCN KD drastically reduces AMPAR levels in hippocampal neurons [59], mutations likely interfere with AMPAR-stabilizing function, emphasizing the importance of intact AMPAR-associated proteins. FRRS1L KD similarly reduces GluA1 surface expression and synaptic transmission [30, 125], illustrating how disruptions at different regulatory levels converge functionally [27].

### 4.1.3 Conclusion: Structural Integrity of AMPAR Regulators Is Essential for Synaptic Function

Even a single amino acid substitution (S297D) disrupted AMPAR function and morphology despite preserved protein–protein interactions, indicating that PORCN's multifunctionality is governed by structural features and potentially by phosphorylation. Maintaining PORCN integrity is essential for proper synaptic function and neuronal architecture and genetic mutations or altered regulation can impair AMPAR biogenesis and signaling. Taken together, these findings suggest that the observed morphological and synaptic alterations are more likely attributable to changes in AMPAR regulation rather than Wnt signaling. The S297D mutation may selectively impair receptor processing or local trafficking within the ER, thereby directly influencing dendritic structure and synaptic output, independent of canonical Wnt pathways.

## 4.2 Structural Uncertainty and Its Potential Role in PORCN Multifunctionality

A central aim of this study was to use PORCN mutants to identify structural domains or motifs required for its interaction with AMPA receptors. Although an interaction between PORCN and AMPARs has been previously reported [59, 60], the precise nature of this interaction remains unknown. Understanding these structural features may provide insight into the molecular mechanisms underlying PORCN's non-canonical function in AMPAR physiology. Uncertainty about PORCN's membrane topology, particularly the number of TMDs and the orientation of its N- and C-termini, complicates functional characterization.

### 4.2.1 Structural Determinants of PORCN Function in AMPAR Regulation

In this study, a C-terminal mutation at Y430 did not produce phospho-specific effects on neuronal morphology, though a general reduction in basal dendritic complexity was observed. Both phosphodeficient and phosphomimetic mutants reduced GluA1 protein levels comparable to PORCN WT and retained the ability to interact with Wnt5a in HeLa cells. This suggests that the spatial positioning of Y430 within the protein, rather than its phosphorylation status, may be critical for its functional impact.

Previous work from the group showed that the phosphomimetic PORCN Y/E mutant inhibited Wnt secretion in HeLa cells. In contrast, neuronal reconstructions with the catalytically inactive PORCN H/D mutant revealed that, despite reduced Wnt signaling, dendritic morphology in hippocampal neurons remained unchanged. This indicates that the basal dendritic length reduction observed in Y430X-overexpressing neurons likely reflects altered AMPAR modulation by PORCN rather than impaired Wnt secretion. Notably, Y430X mutants had no additional effect on AMPAR function compared to PORCN WT in HeLa cells. Although mean dendritic length was slightly lower in Y430X mutants, the difference was not statistically significant, which may explain the lack of detectable effects in HeLa cells. Furthermore, because PORCN strongly reduced total and surface AMPAR expression in this system, it is difficult to isolate the contribution of a single point mutation.

Taken together, these findings suggest that PORCN's influence on dendritic morphology in neurons is largely independent of Wnt secretion and likely reflects direct modulation of AMPAR function.

Interpretation of PORCN's structural features has been challenging due to divergent models reported in the literature (as seen in Figure 2). A comparative analysis of published PORCN structural models underscores its uncertainty (Table 39). For MBOAT proteins, the family to which PORCN belongs, electron microscopy studies have identified a conserved MBOAT core composed of eight transmembrane helices, with divergent N- and C-termini [47]. This core includes two re-entrant loops (between TMDs 3/4 and 5/6) [47]. The catalytically active histidine residue, which is essential for acyltransferase activity, is located within

transmembrane segment 6 (H341 in PORCN) [55, 126]. In addition, an asparagine, aspartic acid or histidine residue within re-entrant loop 2 is required for catalytic function [126, 127].

Various studies have proposed divergent models of PORCN topology. Bornholdt et al. reported a topology with eight TMDs and both termini located in the cytoplasm based on Uniprot prediction [46], which aligns with the model proposed by Nile and Hannoush, although they identified ten TMDs [128]. Rios-Esteves et al. suggested eleven TMDs, featuring a cytoplasmic N-terminus and a luminal C-terminus [100]. In contrast, Lee et al. experimentally identified ten TMDs with both termini in the cytoplasm [54]. Galli et al. proposed a model with nine TMDs and two re-entrant loops, placing the N-terminus in the lumen and the C-terminus in the cytoplasm [53]. Yu et al. described a model with ten TMDs and a cytoplasmic orientation of both termini [129]. Most recently, Liu et al. resolved a cryo-electron microscopy structure of human PORCN showing eleven TMDs, with the N-terminus in the lumen and the C-terminus in the cytoplasm [48].

**Table 39: Comparison of PORCN topology described in the literature.**

| Reference | TMDs | N-Terminus | C-Terminus | Y430 |
|---|---|---|---|---|
| Bornholdt et al. (2009) | 8 | Cytoplasm | Cytoplasm | Cytoplasm |
| Rios-Esteves et al. (2014) | 11 | Cytoplasm | Lumen | Cytoplasm |
| Nile and Hannoush (2016) | 10 | Cytoplasm | Cytoplasm | Lumen |
| Lee et al. (2019) | 10 | Cytoplasm | Cytoplasm | Lumen |
| Galli et al. (2021) | 9 | Lumen | Cytoplasm | Lumen |
| Yu et al. (2021) | 10 | Cytoplasm | Cytoplasm | NR |
| Liu et al. (2022) | 11 | Lumen | Cytoplasm | NR |

NR = Not reported; TMD = Transmembrane domain; Y = Tyrosine.

These models vary between eight and eleven TMDs and show inconsistencies regarding the orientation of the terminal domains. Compared with other AMPAR-associated proteins, the structure of PORCN is relatively complex, particularly with regard to the number of TMDs and the configuration of its loops [26]. Due to these uncertainties, it remains unresolved whether Y430 is cytoplasmic or luminal. If Y430 is luminal, its function as a phosphorylation site would be unlikely, as phosphorylation typically occurs in the cytoplasmic compartment. Interestingly, the phosphorylation-independent effect on neuronal outgrowth supports the hypothesis that Y430 may indeed be luminally localized, possibly influencing local ER-mediated AMPAR assembly or trafficking.

Together, these findings suggest that the C-terminal region of PORCN contributes specifically to its moonlighting activity, analogous to its role in catalytic function [100].

### 4.2.2 Evolutionary Perspective on PORCN's Moonlighting Function

To investigate the evolutionary conservation of PORCN's moonlighting function, structural elements critical for AMPAR modulation were analyzed by assessing the effects of PORCN homologs from *M. musculus* and *D. melanogaster* and *C. elegans* on GluA1 in HeLa cells. As moonlighting functions are thought to have evolved after a protein's canonical role [130],

often reflected in lower evolutionary conservation, regions mediating AMPAR-related activity may be less conserved than those required for Wnt signaling. Proteins with moonlighting functions may use either shared or distinct domains to fulfil their separate roles. In the case of PORCN, this concept is paralleled by other multifunctional proteins such as CNIHs, which serve as ER cargo exporters for soluble growth factors, while also acting as AMPAR modulators by regulating receptor trafficking and channel properties [131].

The investigation of PORCN homologs from *M. musculus*, *C. elegans*, and *D. melanogaster* revealed a consistent negative impact of PORCN overexpression on GluA1 whole-cell and surface levels in both invertebrates and vertebrates, whereas overexpression of PORCN *C. elegans* could not be achieved in HeLa cells. The present findings demonstrate that PORCN's AMPAR-modulating function is evolutionarily conserved across both vertebrate and invertebrate species, similar to its enzymatic activity, which is also preserved through evolution [51]. This unexpected degree of conservation raises the possibility that PORCN's moonlighting role emerged earlier in evolution than previously anticipated. Such functional preservation across distant taxa underscores the biological significance of PORCN in regulating AMPAR physiology and suggests that its non-canonical activity may confer an evolutionary advantage [132, 133]. Moreover, the data imply that overlapping structural elements may facilitate both its canonical role in Wnt signaling and its interaction with AMPARs. Taken together, these observations support the notion that the AMPAR-modulating function is not a secondary or incidental feature, but rather an inherent aspect of PORCN's molecular identity.

### 4.2.3 Functional Analysis of Patient-Associated PORCN Mutations

To further identify regions in PORCN that may determine PORCN moonlighting function, PORCN variants carrying mutations reported in FDH patients with neurological deficits (S136F, D283H, and Δ285), as well as a variant associated with unaltered Wnt secretion (R228C), were tested regarding their ability to modulate expression of AMPARs in HeLa cells.

All PORCN variants, similar to the WT, were able to reduce GluA1 whole-cell and surface levels in HeLa cells. These results suggest that the respective residues are no critical molecular determinants for the functional modulation of AMPARs by PORCN. It is possible that a broader amino acid region must be mutated or deleted to identify the specific interaction domain within PORCN. One challenge in identifying the interaction domains is the ongoing discussion regarding the topology of PORCN. Larger deletions or other targeted mutations within PORCN may help to identify functionally relevant regions.

### 4.2.4 Conclusion: Structural Determinants of PORCN's Multifunctionality

Taken together, the findings suggest that the PORCN C-terminus may contribute to AMPAR modulation independently of Wnt signaling and influence neuronal morphology, underscoring the need for further structural investigation. Moreover, evolutionary comparisons and patient-associated mutations suggest that the AMPAR-modulating function is conserved and functionally relevant. It is conceivable that specific C-terminal motifs in PORCN mediate direct interactions with AMPARs. Beyond AMPAR regulation, PORCN has been proposed to exert an additional moonlighting function in cancer cell growth that is also independent of Wnt signaling. This raises the possibility that PORCN employs similar structural domains for diverse non-canonical functions in different cell types. A precise understanding of PORCN's membrane topology and identification of key functional motifs will therefore be critical for defining the structural basis of its multifunctionality across different cellular contexts.

## 4.3 Subcellular Localization of Wnt5a Determines Its Regulatory Role on AMPARs

Interaction studies involving PORCN, AMPAR and Wnt conducted in the research group revealed a novel PORCN-independent interaction between Wnt and AMPARs in HeLa cells. Wnt and their associated signaling components represent a highly conserved pathway implicated in a wide range of developmental processes and pathological conditions. While Wnt signaling has often been studied in the context of its effects on neuronal morphology and synaptic plasticity, a direct effect of Wnt on AMPARs has not yet been sufficiently characterized.

### 4.3.1 Differential Effects of Wnt5a in Heterologous vs. Neuronal Systems

In HeLa cells, both Wnt5a WT and the palmitoylation-deficient mutant Wnt5a C/A interacted with GluA1 and reduced its whole-cell and surface levels. Wnt5a C/A cannot interact with PORCN and remains unpalmitoylated in the ER. Yet it lowered GluA1 levels similarly to Wnt5a WT. This suggests that the Wnt5a-GluA1 interaction occurs in the ER, independent of Wnt5a secretion. The strong reduction in GluA1 levels may result from the high availability of Wnt5a in the ER due to overexpression. This could interfere with AMPAR biogenesis or receptor folding. The mechanism underlying this PORCN-independent effect of Wnt5a on GluA1 in HeLa cells remains unclear. It is possible that ER quality-control mechanisms retain AMPARs and target them for degradation [134-136].

The negative effect of Wnt5a on GluA1 expression also extended to other glutamate receptors, as co-expression of Wnt5a WT with GluK2 and NMDAR similarly reduced their expression levels, while the HCN2 channel remained unaffected. Wnt modulate synaptic plasticity through canonical and non-canonical signaling pathways. These pathways

influence glutamate receptor trafficking and surface delivery [81, 137]. Wnt7a and its postsynaptic receptor Fz7 regulate AMPAR localization and function. Their loss impairs LTP-dependent potentiation, dendritic spine growth and AMPAR distribution [84]. Wnt5a enhances postsynaptic organization by upregulating the GluN2B subunit of NMDA receptors [138]. Synaptic Wnt3a release triggered by NMDA receptor activation strengthens β-catenin-dependent signaling and hippocampal LTP [139]. HCN2, in contrast, is a hyperpolarization-activated ion channel contributing to rhythmic activity in specific neurons and cardiomyocytes [140, 141]. To date, no primary or secondary effects of Wnt on HCN2 have been reported. These findings suggest that Wnt5a may regulate glutamate receptor homeostasis, fine-tuning excitatory neurotransmission and synaptic plasticity.

Protein–protein interactions in heterologous systems may differ from those in primary neurons. As observed with PORCN, overexpression in HEK293T cells reduced glutamate-evoked currents, whereas in neurons, PORCN overexpression did not affect AMPAR-mediated currents [59]. Therefore, Wnt5a-induced effects in primary hippocampal neurons were tested for physiological relevance.

Using lentiviral vectors, Wnt5a was overexpressed in primary hippocampal neurons, with successful secretion confirmed. Notably, secretion of the palmitoylation-deficient mutant Wnt5a C/A was significantly reduced compared to Wnt5a WT, but remained higher than in the GFP control condition. It is possible that lentiviral transduction of Wnt5a C/A increased neuronal death, contributing to higher Wnt levels in the supernatant. Wnt5a C/A may also undergo partial palmitoylation. Additional immunofluorescence co-staining of Wnt5a WT and Wnt5a C/A with the ER marker Calnexin could clarify ER localization of these proteins. Furthermore, cell viability/cytotoxicity may be conducted in parallel to continuously assess neuronal survival and cell death.

Both Wnt5a WT and C/A interacted with endogenous GluA1 and GluA2 in hippocampal neurons. This suggests that the interaction occurs within the ER. Unlike HeLa cells, Wnt5a WT overexpression did not significantly change GluA1 protein levels in hippocampal neurons. This may reflect neuron-specific mechanisms that maintain AMPAR levels. While the intracellular effects of Wnt5a on AMPARs remain unexplored, extracellular Wnt5a has shown inconsistent effects on AMPAR-mediated mEPSCs. In hippocampal slices, extracellular application of Wnt5a exerted differential effects: One study indicated an increase in AMPAR-mediated currents following extracellular Wnt5a treatment [130], whereas another did not [131]. The discrepancy might be explained by prolonged lack of stimulation after baseline in the previous study, which can induce homeostatic potentiation of AMPAR and NMDAR currents [142, 143]. In cultured hippocampal neurons, exposure to Wnt5a-conditioned medium significantly increased the amplitude of AMPAR-mediated mEPSCs [88]. Wnt5a promoted the functional maturation of silent synapses by triggering

the insertion of AMPA receptors into the postsynaptic membrane [144]. This AMPAR recruitment contributed to synapse unsilencing and enhanced excitatory transmission during early circuit development [144]. Also, the Wnt5a/JNK pathway modulated postsynaptic regions by regulating the clustering and distribution of PSD-95 [85]. *CaMKII-Wnt5a*$^{fl/fl}$ mice showed a decrease in CaMKII-mediated phosphorylation resulting in a decrease of phospho-S831-GluA1, a modified GluA1 subunit that is functionally linked to synaptic plasticity [19, 86, 145]. In hippocampal neurons, 12% to 50% of GluA1 subunits were phosphorylated, highlighting the relevance of phosphorylation in synaptic plasticity [146]. Overall, higher extracellular Wnt availability appears to enhance AMPAR function, whereas lower availability reduces it. These results suggest that Wnt5a's impact on AMPAR function depends on its localization and availability, with ER accumulation and extracellular signaling exerting distinct effects on synaptic maturation and plasticity. During overexpression, it remains unclear whether Wnt is rapidly palmitoylated and secreted or accumulate in the ER. To mimic ER accumulation, the PORCN inhibitor Wnt-C59 was applied.

### 4.3.2 Palmitoylation Inhibition and Wnt-Dependent AMPAR Regulation

Wnt-C59 treatment increased GluA1 expression in hippocampal neurons and caused Wnt5a accumulation in membrane fractions. Overexpression of PORCN alone did not alter AMPAR levels. These findings suggest that the observed increase in GluA1 levels following inhibition of Wnt secretion is more likely due to Wnt-specific effects in the ER rather than to increased PORCN-mediated AMPAR modulation. Given the fact that the incubation of hippocampal neurons with Wnt-C59 reduced the complexity of the dendritic tree [80], the observed increase in GluA1 expression after Wnt-C59 treatment may reflect a short-term compensatory response to reduced dendritic complexity, aimed at preserving synaptic function [147]. Longer exposure could clarify the long-term effects of Wnt-C59 on AMPAR levels. Interestingly, *Wnt5a* KO did not alter GluA1 levels in hippocampal neurons, nor did it affect dendritic morphology after three months [86]. These findings indicate that Wnt may exert primary effects on AMPAR expression in the ER independent of PORCN. Increased ER-retained, non-palmitoylated Wnt may regulate AMPAR expression independently of canonical Wnt signaling pathways. Palmitoylation was inhibited for all Wnt proteins, so contributions from other ligands cannot be excluded. Extracellular application of Wnt7a was shown to increase GluA1 and GluA2 levels in dendritic spines, thereby promoting the synaptic localization of AMPARs in hippocampal neurons [84].

Future experiments could test whether extracellular Wnt rescues Wnt-C59–induced GluA1 upregulation, given that Wnt signaling not only supports dendritic structure but has been shown to restore neuronal morphology following disruption [80]. For this purpose, a previously published experimental approach may be applied: Wnt ligands can be produced

by transiently transfected HEK293 cells, which subsequently secrete them into Neurobasal media [82]. Surface biotinylation assays could distinguish between ER and plasma membrane GluA1 accumulation.

### 4.3.3 Conclusion: Toward a Primary Role of Wnt in AMPAR Biogenesis

The drastic GluA1 reduction seen in HeLa cells was not observed in primary neurons. This highlights differences between heterologous and neuronal systems. Neuron-specific factors such as GluA isoform expression, auxiliary proteins, signaling pathways and ER quality control may account for these differences. In conclusion, ER accumulation of Wnt5a in hippocampal neurons was associated with increased GluA1 in membrane fractions. This suggests a direct effect of Wnt5a on GluA1 within the ER. Further studies are needed to clarify the underlying mechanism, which is a promising target given the role of Wnt in neuronal development and function.

## 4.4 Conclusion

This study was designed to investigate the multifunctionality of PORCN, particularly its role as a non-canonical regulator of AMPAR physiology. A major goal was to dissect how structural features and potential PTMs contribute to PORCN's interaction with AMPARs. In parallel, the study aimed to provide new insights into the interplay between AMPARs and Wnt.

Overall, the findings highlight PORCN as a critical multifunctional protein involved in AMPAR regulation, extending beyond its established enzymatic role in Wnt palmitoylation. While palmitoylation remains the only well-characterized PTM of PORCN, the data suggest that phosphorylation may serve as a regulatory switch modulating its non-canonical functions. The sensitivity of AMPAR physiology not only to KD of PORCN, but also to subtle alterations in PORCN structure, such as single-residue substitutions demonstrated in this study, underscores the importance of maintaining structural integrity and precise molecular regulation. Mutation at the C-terminus of PORCN negatively affects neuronal morphology, suggesting that this region could also serve as a potential interaction site for PORCN and AMPARs. While the exact regions mediating PORCN's moonlighting role in AMPAR modulation remain unresolved, its function is conserved across vertebrates and invertebrates, highlighting the evolutionary and biological significance of the PORCN–AMPAR interaction.

Furthermore, these results demonstrate that Wnt5a's impact on AMPAR expression is highly dependent on cellular context and subcellular compartmentalization, emphasizing the need to investigate such regulatory mechanisms in physiologically relevant cell systems. This highlights the critical role of spatial regulation in Wnt-mediated signaling and its implications for synaptic receptor dynamics.

In conclusion, the findings underscore the importance of preserving AMPAR-associated proteins in their native, mutation-free state to ensure proper AMPAR biogenesis, trafficking and function. Additionally, the results support previous evidence that Wnt5a can exert PORCN-independent effects on AMPARs.

Future studies aiming to resolve the full membrane topology of PORCN and identify its key functional domains will be critical to fully elucidate the molecular basis of its multifunctionality. Additionally, investigating the molecular basis of Wnt and AMPAR interaction in the ER will be essential to clarify how this interaction regulates AMPAR function.

# 5 Literature


1. Wisden, W. and P.H. Seeburg, *Mammalian ionotropic glutamate receptors.* Curr Opin Neurobiol, 1993. **3**(3): p. 291-8.
2. Bredt, D.S. and R.A. Nicoll, *AMPA receptor trafficking at excitatory synapses.* Neuron, 2003. **40**(2): p. 361-79.
3. Meldrum, B.S., *Glutamate as a neurotransmitter in the brain: review of physiology and pathology.* J Nutr, 2000. **130**(4S Suppl): p. 1007S-15S.
4. Bissen, D., F. Foss, and A. Acker-Palmer, *AMPA receptors and their minions: auxiliary proteins in AMPA receptor trafficking.* Cell Mol Life Sci, 2019. **76**(11): p. 2133-2169.
5. Bear, M.F. and R.C. Malenka, *Synaptic plasticity: LTP and LTD.* Curr Opin Neurobiol, 1994. **4**(3): p. 389-99.
6. Malenka, R.C. and R.A. Nicoll, *Long-term potentiation--a decade of progress?* Science, 1999. **285**(5435): p. 1870-4.
7. Malinow, R. and R.C. Malenka, *AMPA receptor trafficking and synaptic plasticity.* Annu Rev Neurosci, 2002. **25**: p. 103-26.
8. Chang, E.H., et al., *AMPA receptor downscaling at the onset of Alzheimer's disease pathology in double knockin mice.* Proc Natl Acad Sci U S A, 2006. **103**(9): p. 3410-5.
9. Zhang, J. and J.M. Abdullah, *The role of GluA1 in central nervous system disorders.* Rev Neurosci, 2013. **24**(5): p. 499-505.
10. Traynelis, S.F., et al., *Glutamate receptor ion channels: structure, regulation, and function.* Pharmacol Rev, 2010. **62**(3): p. 405-96.
11. Greger, I.H., J.F. Watson, and S.G. Cull-Candy, *Structural and Functional Architecture of AMPA-Type Glutamate Receptors and Their Auxiliary Proteins.* Neuron, 2017. **94**(4): p. 713-730.
12. Stern-Bach, Y., et al., *Agonist selectivity of glutamate receptors is specified by two domains structurally related to bacterial amino acid-binding proteins.* Neuron, 1994. **13**(6): p. 1345-57.
13. Wo, Z.G. and R.E. Oswald, *Unraveling the modular design of glutamate-gated ion channels.* Trends Neurosci, 1995. **18**(4): p. 161-8.
14. Armstrong, N., et al., *Measurement of conformational changes accompanying desensitization in an ionotropic glutamate receptor.* Cell, 2006. **127**(1): p. 85-97.
15. Lomeli, H., et al., *Control of kinetic properties of AMPA receptor channels by nuclear RNA editing.* Science, 1994. **266**(5191): p. 1709-13.
16. Mosbacher, J., et al., *A molecular determinant for submillisecond desensitization in glutamate receptors.* Science, 1994. **266**(5187): p. 1059-62.
17. Greger, I.H., et al., *Developmentally regulated, combinatorial RNA processing modulates AMPA receptor biogenesis.* Neuron, 2006. **51**(1): p. 85-97.
18. Coleman, S.K., et al., *Isoform-specific early trafficking of AMPA receptor flip and flop variants.* J Neurosci, 2006. **26**(43): p. 11220-9.
19. Lee, H.K., et al., *Phosphorylation of the AMPA receptor GluR1 subunit is required for synaptic plasticity and retention of spatial memory.* Cell, 2003. **112**(5): p. 631-43.
20. Sommer, B., et al., *Flip and flop: a cell-specific functional switch in glutamate-operated channels of the CNS.* Science, 1990. **249**(4976): p. 1580-5.
21. Partin, K.M., D. Bowie, and M.L. Mayer, *Structural determinants of allosteric regulation in alternatively spliced AMPA receptors.* Neuron, 1995. **14**(4): p. 833-43.
22. Partin, K.M., M.W. Fleck, and M.L. Mayer, *AMPA receptor flip/flop mutants affecting deactivation, desensitization, and modulation by cyclothiazide, aniracetam, and thiocyanate.* J Neurosci, 1996. **16**(21): p. 6634-47.
23. Shepherd, J.D. and R.L. Huganir, *The cell biology of synaptic plasticity: AMPA receptor trafficking.* Annu Rev Cell Dev Biol, 2007. **23**: p. 613-43.
24. Greger, I.H., et al., *AMPA receptor tetramerization is mediated by Q/R editing.* Neuron, 2003. **40**(4): p. 763-74.

25. Schwenk, J., et al., *Regional diversity and developmental dynamics of the AMPA-receptor proteome in the mammalian brain.* Neuron, 2014. **84**(1): p. 41-54.
26. Schwenk, J., et al., *High-resolution proteomics unravel architecture and molecular diversity of native AMPA receptor complexes.* Neuron, 2012. **74**(4): p. 621-33.
27. Brechet, A., et al., *AMPA-receptor specific biogenesis complexes control synaptic transmission and intellectual ability.* Nat Commun, 2017. **8**: p. 15910.
28. Schwenk, J., et al., *An ER Assembly Line of AMPA-Receptors Controls Excitatory Neurotransmission and Its Plasticity.* Neuron, 2019. **104**(4): p. 680-692 e9.
29. Wu, X. and T.A. Rapoport, *Mechanistic insights into ER-associated protein degradation.* Curr Opin Cell Biol, 2018. **53**: p. 22-28.
30. Schwenk, J. and B. Fakler, *Building of AMPA-type glutamate receptors in the endoplasmic reticulum and its implication for excitatory neurotransmission.* J Physiol, 2021. **599**(10): p. 2639-2653.
31. Coombs, I.D. and S.G. Cull-Candy, *Transmembrane AMPA receptor regulatory proteins and AMPA receptor function in the cerebellum.* Neuroscience, 2009. **162**(3): p. 656-65.
32. Kato, A.S., et al., *TARPs differentially decorate AMPA receptors to specify neuropharmacology.* Trends Neurosci, 2010. **33**(5): p. 241-8.
33. Tomita, S., et al., *Functional studies and distribution define a family of transmembrane AMPA receptor regulatory proteins.* J Cell Biol, 2003. **161**(4): p. 805-16.
34. Rouach, N., et al., *TARP gamma-8 controls hippocampal AMPA receptor number, distribution and synaptic plasticity.* Nat Neurosci, 2005. **8**(11): p. 1525-33.
35. Schwenk, J., et al., *Functional proteomics identify cornichon proteins as auxiliary subunits of AMPA receptors.* Science, 2009. **323**(5919): p. 1313-9.
36. Harmel, N., et al., *AMPA receptors commandeer an ancient cargo exporter for use as an auxiliary subunit for signaling.* PLoS One, 2012. **7**(1): p. e30681.
37. Boudkkazi, S., et al., *Cornichon2 dictates the time course of excitatory transmission at individual hippocampal synapses.* Neuron, 2014. **82**(4): p. 848-58.
38. Herring, B.E., et al., *Cornichon proteins determine the subunit composition of synaptic AMPA receptors.* Neuron, 2013. **77**(6): p. 1083-96.
39. Gill, M.B., et al., *Cornichon-2 modulates AMPA receptor-transmembrane AMPA receptor regulatory protein assembly to dictate gating and pharmacology.* J Neurosci, 2011. **31**(18): p. 6928-38.
40. Gill, M.B., et al., *AMPA receptor modulation by cornichon-2 dictated by transmembrane AMPA receptor regulatory protein isoform.* Eur J Neurosci, 2012. **35**(2): p. 182-94.
41. Shanks, N.F., et al., *Molecular dissection of the interaction between the AMPA receptor and cornichon homolog-3.* J Neurosci, 2014. **34**(36): p. 12104-20.
42. Shanks, N.F., et al., *Differences in AMPA and kainate receptor interactomes facilitate identification of AMPA receptor auxiliary subunit GSG1L.* Cell Rep, 2012. **1**(6): p. 590-8.
43. Gu, X., et al., *GSG1L suppresses AMPA receptor-mediated synaptic transmission and uniquely modulates AMPA receptor kinetics in hippocampal neurons.* Nat Commun, 2016. **7**: p. 10873.
44. Kadowaki, T., et al., *The segment polarity gene porcupine encodes a putative multitransmembrane protein involved in Wingless processing.* Genes Dev, 1996. **10**(24): p. 3116-28.
45. Hofmann, K., *A superfamily of membrane-bound O-acyltransferases with implications for wnt signaling.* Trends Biochem Sci, 2000. **25**(3): p. 111-2.
46. Bornholdt, D., et al., *PORCN mutations in focal dermal hypoplasia: coping with lethality.* Hum Mutat, 2009. **30**(5): p. E618-28.
47. Coupland, C.E., et al., *Rocking the MBOAT: Structural insights into the membrane bound O-acyltransferase family.* Curr Opin Struct Biol, 2023. **80**: p. 102589.
48. Liu, Y., et al., *Mechanisms and inhibition of Porcupine-mediated Wnt acylation.* Nature, 2022. **607**(7920): p. 816-822.

49. Coupland, C.E., et al., *Structure, mechanism, and inhibition of Hedgehog acyltransferase.* Mol Cell, 2021. **81**(24): p. 5025-5038 e10.
50. Campana, M.B., et al., *The ghrelin O-acyltransferase structure reveals a catalytic channel for transmembrane hormone acylation.* J Biol Chem, 2019. **294**(39): p. 14166-14174.
51. Tanaka, K., et al., *The evolutionarily conserved porcupine gene family is involved in the processing of the Wnt family.* Eur J Biochem, 2000. **267**(13): p. 4300-11.
52. Caricasole, A., et al., *Molecular cloning and initial characterization of the MG61/PORC gene, the human homologue of the Drosophila segment polarity gene Porcupine.* Gene, 2002. **288**(1-2): p. 147-57.
53. Galli, L.M., et al., *Determination of the membrane topology of PORCN, an O-acyl transferase that modifies Wnt signalling proteins.* Open Biol, 2021. **11**(6): p. 200400.
54. Lee, C.J., et al., *In vitro reconstitution of Wnt acylation reveals structural determinants of substrate recognition by the acyltransferase human Porcupine.* J Biol Chem, 2019. **294**(1): p. 231-245.
55. Galli, L.M., et al., *Porcupine-mediated lipid-modification regulates the activity and distribution of Wnt proteins in the chick neural tube.* Development, 2007. **134**(18): p. 3339-48.
56. Takada, R., et al., *Monounsaturated fatty acid modification of Wnt protein: its role in Wnt secretion.* Dev Cell, 2006. **11**(6): p. 791-801.
57. Gao, X. and R.N. Hannoush, *Single-cell imaging of Wnt palmitoylation by the acyltransferase porcupine.* Nat Chem Biol, 2014. **10**(1): p. 61-8.
58. Covey, T.M., et al., *PORCN moonlights in a Wnt-independent pathway that regulates cancer cell proliferation.* PLoS One, 2012. **7**(4): p. e34532.
59. Erlenhardt, N., et al., *Porcupine Controls Hippocampal AMPAR Levels, Composition, and Synaptic Transmission.* Cell Rep, 2016. **14**(4): p. 782-794.
60. Wei, M., et al., *PORCN Negatively Regulates AMPAR Function Independently of Subunit Composition and the Amino-Terminal and Carboxy-Terminal Domains of AMPARs.* Front Cell Dev Biol, 2020. **8**: p. 829.
61. Grzeschik, K.H., et al., *Deficiency of PORCN, a regulator of Wnt signaling, is associated with focal dermal hypoplasia.* Nat Genet, 2007. **39**(7): p. 833-5.
62. Bostwick, B., et al., *Phenotypic and molecular characterization of focal dermal hypoplasia in 18 individuals.* Am J Med Genet C Semin Med Genet, 2016. **172C**(1): p. 9-20.
63. Kanemura, H., et al., *Epilepsy in a patient with focal dermal hypoplasia.* Pediatr Neurol, 2011. **44**(2): p. 135-8.
64. Peters, T., R. Perrier, and R.M. Haber, *Focal dermal hypoplasia: report of a case with myelomeningocele, Arnold-Chiari malformation and hydrocephalus with a review of neurologic manifestations of Goltz syndrome.* Pediatr Dermatol, 2014. **31**(2): p. 220-4.
65. Arlt, A., et al., *Novel insights into PORCN mutations, associated phenotypes and pathophysiological aspects.* Orphanet Journal of Rare Diseases, 2022. **17**(1).
66. Nusslein-Volhard, C. and E. Wieschaus, *Mutations affecting segment number and polarity in Drosophila.* Nature, 1980. **287**(5785): p. 795-801.
67. Torres, V.I., J.A. Godoy, and N.C. Inestrosa, *Modulating Wnt signaling at the root: Porcupine and Wnt acylation.* Pharmacol Ther, 2019. **198**: p. 34-45.
68. Banziger, C., et al., *Wntless, a conserved membrane protein dedicated to the secretion of Wnt proteins from signaling cells.* Cell, 2006. **125**(3): p. 509-22.
69. Gordon, M.D. and R. Nusse, *Wnt signaling: multiple pathways, multiple receptors, and multiple transcription factors.* J Biol Chem, 2006. **281**(32): p. 22429-33.
70. Alkailani, M.I., M. Aittaleb, and F. Tissir, *WNT signaling at the intersection between neurogenesis and brain tumorigenesis.* Front Mol Neurosci, 2022. **15**: p. 1017568.
71. Veeman, M.T., J.D. Axelrod, and R.T. Moon, *A second canon. Functions and mechanisms of beta-catenin-independent Wnt signaling.* Dev Cell, 2003. **5**(3): p. 367-77.
72. Nusse, R., *Wnt signaling.* Cold Spring Harb Perspect Biol, 2012. **4**(5).

73. Mason, J.O., J. Kitajewski, and H.E. Varmus, *Mutational analysis of mouse Wnt-1 identifies two temperature-sensitive alleles and attributes of Wnt-1 protein essential for transformation of a mammary cell line.* Mol Biol Cell, 1992. **3**(5): p. 521-33.
74. Komekado, H., et al., *Glycosylation and palmitoylation of Wnt-3a are coupled to produce an active form of Wnt-3a.* Genes Cells, 2007. **12**(4): p. 521-34.
75. Kurayoshi, M., et al., *Post-translational palmitoylation and glycosylation of Wnt-5a are necessary for its signalling.* Biochem J, 2007. **402**(3): p. 515-23.
76. Schatoff, E.M., B.I. Leach, and L.E. Dow, *Wnt Signaling and Colorectal Cancer.* Curr Colorectal Cancer Rep, 2017. **13**(2): p. 101-110.
77. Inestrosa, N.C., C. Montecinos-Oliva, and M. Fuenzalida, *Wnt signaling: role in Alzheimer disease and schizophrenia.* J Neuroimmune Pharmacol, 2012. **7**(4): p. 788-807.
78. Li, B., et al., *WNT5A Signaling Contributes to Aβ-Induced Neuroinflammation and Neurotoxicity.* PLoS ONE, 2011. **6**(8): p. e22920.
79. Proffitt, K.D., et al., *Pharmacological inhibition of the Wnt acyltransferase PORCN prevents growth of WNT-driven mammary cancer.* Cancer Res, 2013. **73**(2): p. 502-7.
80. Godoy, J.A., J. Espinoza-Caicedo, and N.C. Inestrosa, *Morphological neurite changes induced by porcupine inhibition are rescued by Wnt ligands.* Cell Communication and Signaling, 2021. **19**(1).
81. McLeod, F. and P.C. Salinas, *Wnt proteins as modulators of synaptic plasticity.* Curr Opin Neurobiol, 2018. **53**: p. 90-95.
82. Cerpa, W., et al., *Wnt-7a modulates the synaptic vesicle cycle and synaptic transmission in hippocampal neurons.* J Biol Chem, 2008. **283**(9): p. 5918-27.
83. Ciani, L., et al., *Wnt7a signaling promotes dendritic spine growth and synaptic strength through Ca(2)(+)/Calmodulin-dependent protein kinase II.* Proc Natl Acad Sci U S A, 2011. **108**(26): p. 10732-7.
84. McLeod, F., et al., *Wnt Signaling Mediates LTP-Dependent Spine Plasticity and AMPAR Localization through Frizzled-7 Receptors.* Cell Rep, 2018. **23**(4): p. 1060-1071.
85. Farias, G.G., et al., *Wnt-5a/JNK signaling promotes the clustering of PSD-95 in hippocampal neurons.* J Biol Chem, 2009. **284**(23): p. 15857-66.
86. Chen, C.M., et al., *Wnt5a is essential for hippocampal dendritic maintenance and spatial learning and memory in adult mice.* Proc Natl Acad Sci U S A, 2017. **114**(4): p. E619-E628.
87. Arredondo, S.B., et al., *Wnt5a promotes differentiation and development of adult-born neurons in the hippocampus by noncanonical Wnt signaling.* Stem Cells, 2020. **38**(3): p. 422-436.
88. Varela-Nallar, L., et al., *Wingless-type family member 5A (Wnt-5a) stimulates synaptic differentiation and function of glutamatergic synapses.* Proc Natl Acad Sci U S A, 2010. **107**(49): p. 21164-9.
89. Schroeter, A., et al., *Depletion of the AMPAR reserve pool impairs synaptic plasticity in a model of hepatic encephalopathy.* Mol Cell Neurosci, 2015. **68**: p. 331-9.
90. Lum, L. and H. Clevers, *Cell biology. The unusual case of Porcupine.* Science, 2012. **337**(6097): p. 922-3.
91. Ramazi, S. and J. Zahiri, *Posttranslational modifications in proteins: resources, tools and prediction methods.* Database (Oxford), 2021. **2021**.
92. Maas, S.M., et al., *Phenotype and genotype in 17 patients with Goltz-Gorlin syndrome.* J Med Genet, 2009. **46**(10): p. 716-20.
93. Komendantov, A.O. and G.A. Ascoli, *Dendritic excitability and neuronal morphology as determinants of synaptic efficacy.* J Neurophysiol, 2009. **101**(4): p. 1847-66.
94. Haas, K., J. Li, and H.T. Cline, *AMPA receptors regulate experience-dependent dendritic arbor growth in vivo.* Proc Natl Acad Sci U S A, 2006. **103**(32): p. 12127-31.
95. Chen, W., et al., *AMPA glutamate receptor subunits 1 and 2 regulate dendrite complexity and spine motility in neurons of the developing neocortex.* Neuroscience, 2009. **159**(1): p. 172-82.

96. Proffitt, K.D. and D.M. Virshup, *Precise regulation of porcupine activity is required for physiological Wnt signaling.* J Biol Chem, 2012. **287**(41): p. 34167-78.
97. Ayers, M., et al., *Inhibiting Wnt Signaling Reduces Cholestatic Injury by Disrupting the Inflammatory Axis.* Cell Mol Gastroenterol Hepatol, 2023. **16**(6): p. 895-921.
98. Guo, T., et al., *Isolation and identification of patient-derived liver cancer stem cells and development of personalized treatment strategies.* J Transl Med, 2024. **22**(1): p. 1036.
99. Paul, M.A., et al., *Short-Term Oral Administration of the Porcupine Inhibitor, Wnt-c59, Improves the Structural and Functional Features of Experimental HFpEF.* Pharmacol Res Perspect, 2025. **13**(1): p. e70054.
100. Rios-Esteves, J., B. Haugen, and M.D. Resh, *Identification of key residues and regions important for porcupine-mediated Wnt acylation.* J Biol Chem, 2014. **289**(24): p. 17009-19.
101. Sumioka, A., D. Yan, and S. Tomita, *TARP phosphorylation regulates synaptic AMPA receptors through lipid bilayers.* Neuron, 2010. **66**(5): p. 755-67.
102. Tomita, S., et al., *Bidirectional synaptic plasticity regulated by phosphorylation of stargazin-like TARPs.* Neuron, 2005. **45**(2): p. 269-77.
103. Mihaljević, B., et al., *Comparing basal dendrite branches in human and mouse hippocampal CA1 pyramidal neurons with Bayesian networks.* Scientific Reports, 2020. **10**(1): p. 1-13.
104. Wu, Y.K., K. Fujishima, and M. Kengaku, *Differentiation of apical and basal dendrites in pyramidal cells and granule cells in dissociated hippocampal cultures.* PLoS One, 2015. **10**(2): p. e0118482.
105. Spruston, N., *Pyramidal neurons: dendritic structure and synaptic integration.* Nat Rev Neurosci, 2008. **9**(3): p. 206-21.
106. Horton, A.C., J.J. Yi, and M.D. Ehlers, *Cell type-specific dendritic polarity in the absence of spatially organized external cues.* Brain Cell Biology, 2007. **35**(1): p. 29-38.
107. Bittner, K.C., B.K. Andrasfalvy, and J.C. Magee, *Ion channel gradients in the apical tuft region of CA1 pyramidal neurons.* PLoS One, 2012. **7**(10): p. e46652.
108. Branco, T. and M. Hausser, *The single dendritic branch as a fundamental functional unit in the nervous system.* Curr Opin Neurobiol, 2010. **20**(4): p. 494-502.
109. Menon, V., et al., *Balanced synaptic impact via distance-dependent synapse distribution and complementary expression of AMPARs and NMDARs in hippocampal dendrites.* Neuron, 2013. **80**(6): p. 1451-63.
110. de Anda, F.C., et al., *Centrosome localization determines neuronal polarity.* Nature, 2005. **436**(7051): p. 704-8.
111. Yuan, Y., et al., *Differential regulation of apical-basolateral dendrite outgrowth by activity in hippocampal neurons.* Front Cell Neurosci, 2015. **9**: p. 314.
112. Siskova, Z., et al., *Dendritic structural degeneration is functionally linked to cellular hyperexcitability in a mouse model of Alzheimer's disease.* Neuron, 2014. **84**(5): p. 1023-33.
113. Rall, W., *Theory of physiological properties of dendrites.* Ann N Y Acad Sci, 1962. **96**: p. 1071-92.
114. Rall, W., et al., *Matching dendritic neuron models to experimental data.* Physiol Rev, 1992. **72**(4 Suppl): p. S159-86.
115. Magee, J.C., *Dendritic integration of excitatory synaptic input.* Nat Rev Neurosci, 2000. **1**(3): p. 181-90.
116. Williams, S.R. and G.J. Stuart, *Role of dendritic synapse location in the control of action potential output.* Trends Neurosci, 2003. **26**(3): p. 147-54.
117. Golding, N.L., et al., *Factors mediating powerful voltage attenuation along CA1 pyramidal neuron dendrites.* J Physiol, 2005. **568**(Pt 1): p. 69-82.
118. Nicholson, D.A. and Y. Geinisman, *Axospinous synaptic subtype-specific differences in structure, size, ionotropic receptor expression, and connectivity in apical dendritic regions of rat hippocampal CA1 pyramidal neurons.* J Comp Neurol, 2009. **512**(3): p. 399-418.

119. Nicholson, D.A., et al., *Distance-dependent differences in synapse number and AMPA receptor expression in hippocampal CA1 pyramidal neurons.* Neuron, 2006. **50**(3): p. 431-42.
120. Magee, J.C. and E.P. Cook, *Somatic EPSP amplitude is independent of synapse location in hippocampal pyramidal neurons.* Nat Neurosci, 2000. **3**(9): p. 895-903.
121. Katz, Y., et al., *Synapse distribution suggests a two-stage model of dendritic integration in CA1 pyramidal neurons.* Neuron, 2009. **63**(2): p. 171-7.
122. Greger, I.H. and J.F. Watson, *'Mini analysis' is an unreliable reporter of synaptic changes.* 2024.
123. Prithviraj, R., et al., *Differential regulation of dendrite complexity by AMPA receptor subunits GluR1 and GluR2 in motor neurons.* Dev Neurobiol, 2008. **68**(2): p. 247-64.
124. Ma, H., et al., *Amygdala-hippocampal innervation modulates stress-induced depressive-like behaviors through AMPA receptors.* Proc Natl Acad Sci U S A, 2021. **118**(6).
125. Han, W., et al., *Ferric Chelate Reductase 1 Like Protein (FRRS1L) Associates with Dynein Vesicles and Regulates Glutamatergic Synaptic Transmission.* Front Mol Neurosci, 2017. **10**: p. 402.
126. Buglino, J.A. and M.D. Resh, *Identification of conserved regions and residues within Hedgehog acyltransferase critical for palmitoylation of Sonic Hedgehog.* PLoS One, 2010. **5**(6): p. e11195.
127. Ansell, T.B., et al., *Mapping structural and dynamic divergence across the MBOAT family.* Structure, 2024. **32**(7): p. 1011-1022 e3.
128. Nile, A.H. and R.N. Hannoush, *Fatty acylation of Wnt proteins.* Nat Chem Biol, 2016. **12**(2): p. 60-9.
129. Yu, J., et al., *Structural model of human PORCN illuminates disease-associated variants and drug-binding sites.* Journal of Cell Science, 2021. **134**(24).
130. Huberts, D.H. and I.J. van der Klei, *Moonlighting proteins: an intriguing mode of multitasking.* Biochim Biophys Acta, 2010. **1803**(4): p. 520-5.
131. Bokel, C., et al., *Drosophila Cornichon acts as cargo receptor for ER export of the TGFalpha-like growth factor Gurken.* Development, 2006. **133**(3): p. 459-70.
132. Sharir-Ivry, A. and Y. Xia, *Quantifying evolutionary importance of protein sites: A Tale of two measures.* PLoS Genet, 2021. **17**(4): p. e1009476.
133. Malhis, N., S.J.M. Jones, and J. Gsponer, *Improved measures for evolutionary conservation that exploit taxonomy distances.* Nat Commun, 2019. **10**(1): p. 1556.
134. Coleman, S.K., et al., *Aggregation Limits Surface Expression of Homomeric GluA3 Receptors.* J Biol Chem, 2016. **291**(16): p. 8784-94.
135. Mah, S.J., et al., *Glutamate receptor trafficking: endoplasmic reticulum quality control involves ligand binding and receptor function.* J Neurosci, 2005. **25**(9): p. 2215-25.
136. Hebert, D.N. and M. Molinari, *In and out of the ER: protein folding, quality control, degradation, and related human diseases.* Physiol Rev, 2007. **87**(4): p. 1377-408.
137. Oliva, C.A., J.Y. Vargas, and N.C. Inestrosa, *Wnts in adult brain: from synaptic plasticity to cognitive deficiencies.* Front Cell Neurosci, 2013. **7**: p. 224.
138. Ramos-Fernandez, E., et al., *Wnt5a promotes hippocampal postsynaptic development and GluN2B-induced expression via the eIF2alpha HRI kinase.* Sci Rep, 2021. **11**(1): p. 7395.
139. Chen, J., C.S. Park, and S.J. Tang, *Activity-dependent synaptic Wnt release regulates hippocampal long term potentiation.* J Biol Chem, 2006. **281**(17): p. 11910-6.
140. Biel, M., et al., *Hyperpolarization-activated cation channels: from genes to function.* Physiol Rev, 2009. **89**(3): p. 847-85.
141. Wahl-Schott, C. and M. Biel, *HCN channels: structure, cellular regulation and physiological function.* Cell Mol Life Sci, 2009. **66**(3): p. 470-94.
142. Gambrill, A.C. and A. Barria, *NMDA receptor subunit composition controls synaptogenesis and synapse stabilization.* Proc Natl Acad Sci U S A, 2011. **108**(14): p. 5855-60.

143. Cerpa, W., et al., *Regulation of NMDA-receptor synaptic transmission by Wnt signaling.* J Neurosci, 2011. **31**(26): p. 9466-71.
144. Alvarez-Ferradas, C., et al., *Wnt-5a induces the conversion of silent to functional synapses in the hippocampus.* Front Mol Neurosci, 2022. **15**: p. 1024034.
145. Derkach, V., A. Barria, and T.R. Soderling, *Ca2+/calmodulin-kinase II enhances channel conductance of alpha-amino-3-hydroxy-5-methyl-4-isoxazolepropionate type glutamate receptors.* Proc Natl Acad Sci U S A, 1999. **96**(6): p. 3269-74.
146. Diering, G.H., et al., *Extensive phosphorylation of AMPA receptors in neurons.* Proc Natl Acad Sci U S A, 2016. **113**(33): p. E4920-7.
147. Wang, G., et al., *Non-scaling regulation of AMPA receptors in homeostatic synaptic plasticity.* Neuropharmacology, 2019. **158**: p. 107700.

# 6 Supplementary

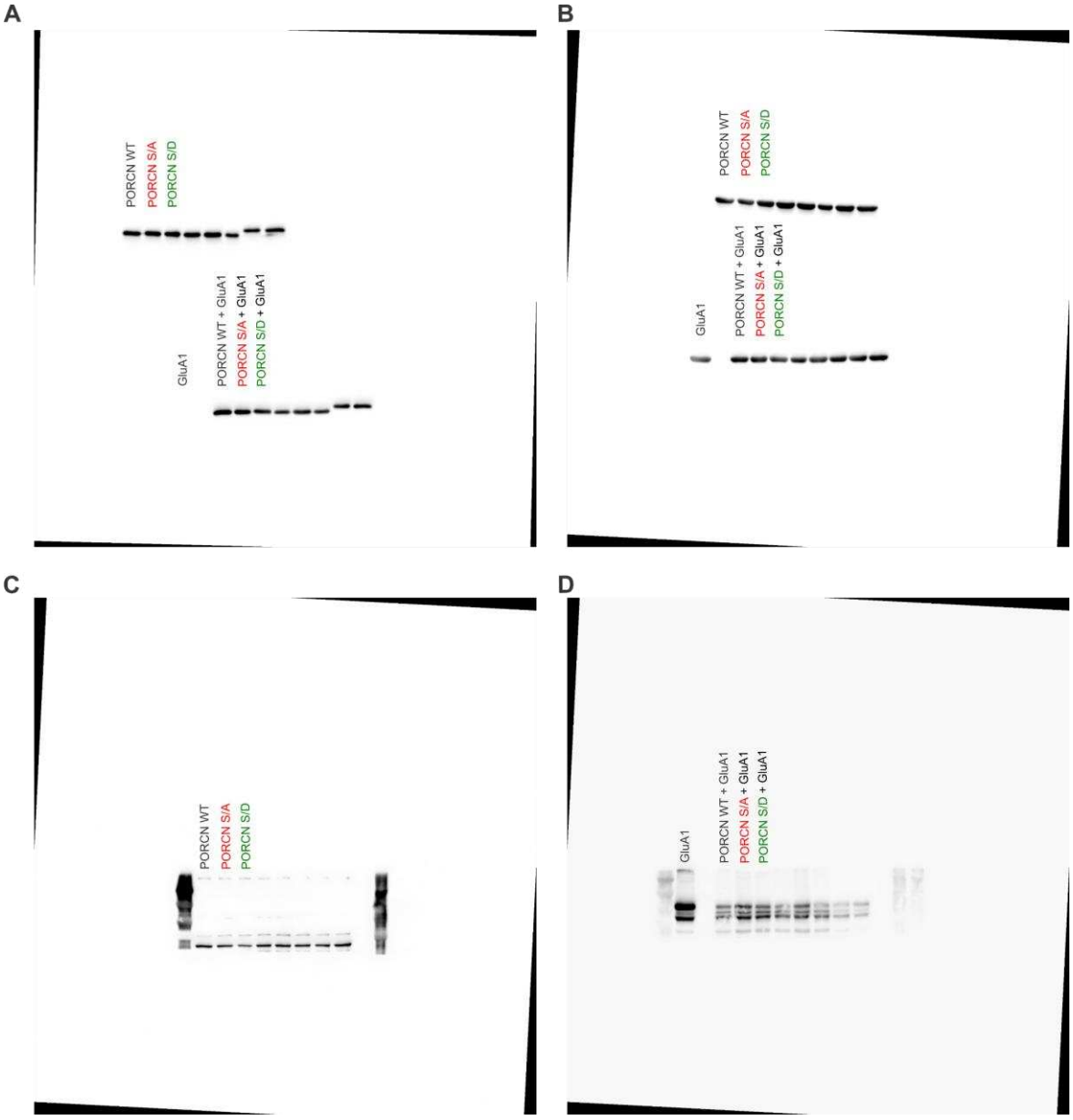


**Figure 24: Original full-length Western blots corresponding to Figure 8A.**
**A:** Detection using a mixture of V5 and FlagM2 antibodies. **B:** β-actin antibody as loading control. **C, D:** Detection with GluA1 antibody.

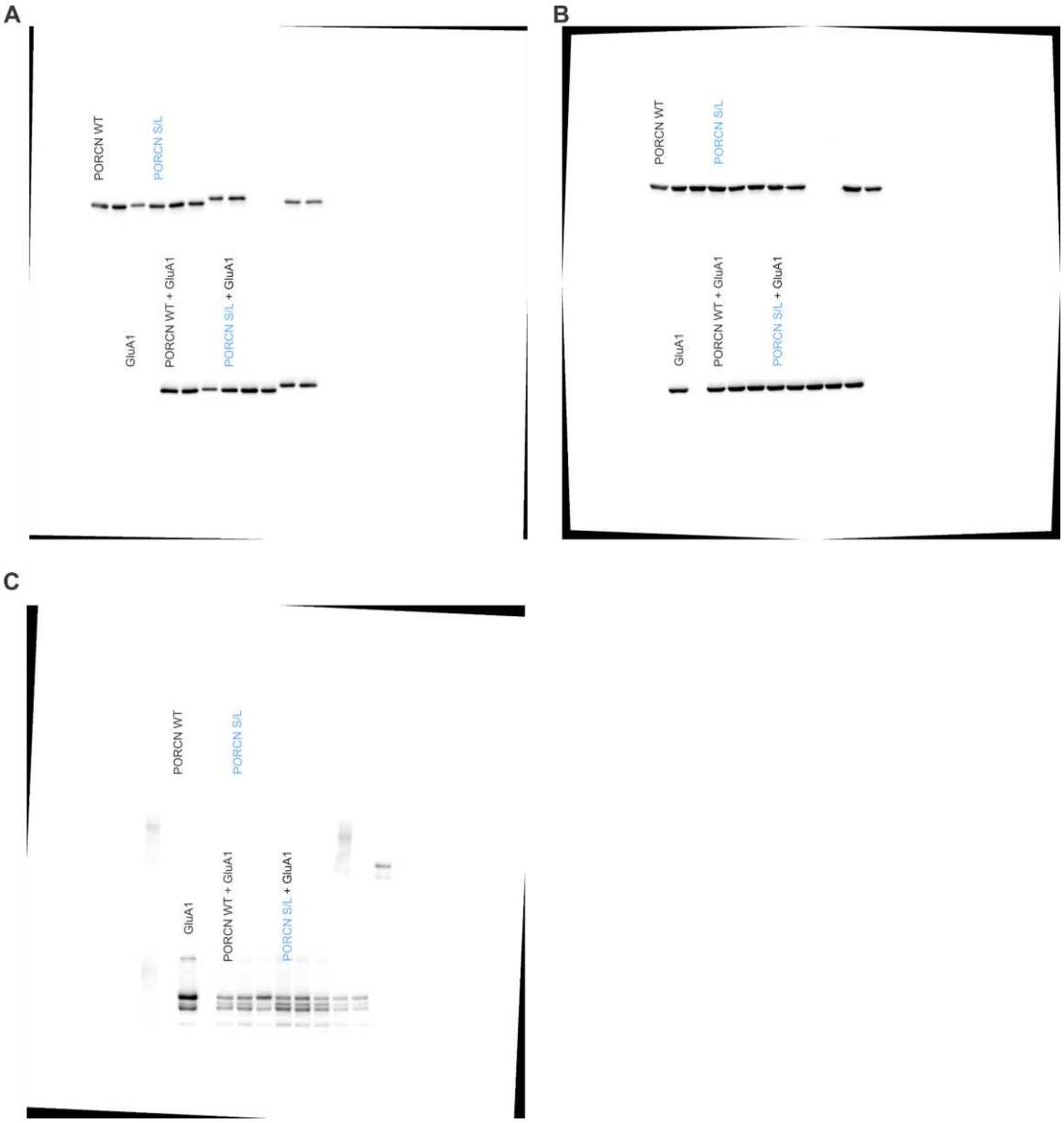


**Figure 25: Original full-length Western blots corresponding to Figure 10A.**
**A:** Detection using a mixture of V5 and FlagM2 antibodies. **B:** β-actin antibody as loading control. **C:** Detection with GluA1 antibody.

## Acknowledgements

I would like to sincerely thank all members of the Institute for Neuro- and Sensory Physiology, led by Prof. Dr. Klöcker. Working with you has been a truly enjoyable and enriching experience.

In addition, I would like to thank Prof. Dr. Max Anstötz and Kelvin Tofan for their (methodological) support during my research.

My deepest gratitude goes to Jun.-Prof. Dr. Nadine Erlenhardt. You have always supported me with valuable advice, helped me solve problems and gave me the opportunity to work in a research field that continues to fascinate me. Over the past few years, I was able to learn so much, surpass myself and develop both personally and professionally. Thank you for your trust in my work.

Esin, you are truly the backbone of the institute and a steady source of support for me in every aspect, both professionally and personally. Whether in moments of triumph or setbacks, your presence has been a constant comfort and I can't thank you enough for always being there.

Julia and Julia, thank you for your support in the lab and for always being there to listen. Your help has been incredibly valuable.

Marten and Mathias, sharing the office with you these past months has brought me not only laughter and great memories but also strength and invaluable advice. Your positive energy and kindness have made this time truly special.

I am especially grateful to my friends. Your encouragement has meant more to me than words can say. Beyond your unwavering support, thank you for the countless laughs, the unforgettable memories and for always being there for me.

My siblings, Cosima, Salome and Enno, you mean everything to me. Each one of you gives me something unique and together you make me whole. Your unconditional support and unwavering belief in me are the support system I need. I'm deeply grateful to walk through life with you by my side.

Mama and Papa, you have given me the freedom and support to discover who I am, to pursue what I love and to find my own path in life. You are my greatest role models – your drive, strength and resilience continue to amaze and inspire me every single day. I love you.

Max, I dedicated this thesis to you. Your unwavering belief in me has always given me the strength to keep going and to believe in myself. You celebrate my victories as if they are your own, you face every challenge by my side and you lift me up when I fall. I know I can always count on you. Thank you from the bottom of my heart, my love.